Revealing neural representations of movements and skill using multi voxel pattern analysis

Tobias Wiestler

University College London

PhD Supervisor: Jörn Diedrichsen

Declaration

I, Tobias Wiestler, confirm that the work presented in this thesis is my own. Where information has been derived from other sources, I confirm that this has been indicated in the thesis.

Signed:

Date:

Acknowledgements

I wish to thank a number of people who supported the work of this thesis. I first and foremost would like to thank my primary supervisor, Jörn Diedrichsen. His invaluable guidance and encouragement during all my projects allowed me to go quickly beyond traditional fMRI analysis. I am especially thankful for our regular meetings that most often educated me in a new statistical method or data analysis technique. I am also grateful for his habit of asking the right questions, which enabled me to develop experiments that optimally answered my research interest.

Special thanks go to Winfried Ilg and Martin Giese, who introduced me to Jörn Diedrichsen. Without their help I would not have considered a PhD in the motor control lab.

My thanks go also to my colleagues at Bangor University. I appreciate the enthusiasm and advise of Paul Downing and Steve Tipper during my first PhD committee meetings. Bangor is also the place where I first met Nikolaas Oosterhof. It was very fortunate that we both made our first experiences with multi voxel pattern analysis at the same time, and I like to thank him for the great discussions that we had during that period.

For the warm welcome and helpful advice, I would like to thank my dear colleagues at the ICN and the FIL. My office mates Slava, Hauke, Nahid, Pradheep and Sheena and the members of the motor control lab as well as Eva and Mathias were always supportive and made my time at Queen Square enjoyable beyond my scientific research.

I am especially grateful for the support by Sheena, Daniela, Jing, and Nada who spend endless hours of proofreading this thesis and polishing my English.

I also would like to thank my parents Bernhardt and Beatrix and my sister Isabell for their patience and support during ups and downs of my studies.

Above all, I would like to thank my partner Daniela for moving with me to the UK and for her unconditional encouragement at every moment during my PhD.

Contributions

In this section I would like to clarify the contributions of my collaborators to the presented work.

Chapter 2

The with surface based searchlight (Section 2.2.2) was developed in cooperation with Nikolaas Oosterhof, Jörn Diedrichsen and myself. Nikolaas Oosterhof implemented the algorithm for freesurfer surfaces and I programmed the same routines for caret surfaces. We validated the method with the experimental data from Chapter 3. The method has been published as a research paper (Oosterhof et al., 2010).

In collaboration, Jörn and I developed a method to measure the dimensionality of representations (Section 2.4). The theoretical concept was developed by Jörn Diedrichsen. I validated and tested the method on generated and experimental data (Chapter 4).

In Section 2.5, I present a technique to decompose activity patterns into different pattern components. Jörn Diedrichsen is responsible for the mathematical concept, algorithm development and implementation (Diedrichsen et al., 2011). The method was further extended by Karl Friston and Ged Ridgway. With the experimental data set in Chapter 3, this novel technique was validated and employed by myself in Chapter 3 and 5.

Chapter 3

Jörn Diedrichsen supervised this experiment in all stages and was involved in the data collection, interpretation of the results and writing the manuscript. David McGonigle contributed in interpreting and publishing the results: T Wiestler, D J McGonigle and J Diedrichsen. Integration of sensory and motor representations of single fingers in the human cerebellum. *J Neurophysiol*, 105(6):3042-3053, 2011.

Chapter 4

The experiment was designed, conducted together with Jörn Diedrichsen.

Chapter 5

This is a collaborative project with Jörn Diedrichsen and Sheena Waters-Metenier. Sheena Waters-Metenier collected the behavioural data. The imaging data were acquired together with Jörn Diedrichsen and Sheena Waters-Metenier.

For all other parts, not mentioned here, this thesis reflects my own work.

Contents

List of Figures

List of Tables

Abstract

One of the main functions of the human brain is to process information, such that we can interact efficiently with our environment by moving our body. *Neuronal representations* of information pertaining to the movement is fundamental for control.

Using functional magnetic resonance imaging, researchers have studied brain areas that are responsible for motor control based on *overall* neuronal signal changes. It is assumed that the amount of overall activity indicates how much an area is *involved* in the control of movements. In this thesis, I start from the approach that the representation of critical variables describing the movements, rather than the overall activation, is the most relevant factor for a region to be important in the control of an action.

Representations in three major fields of motor control were studied in this thesis. First, the integration of sensory and motor information was analysed via finger representations in the cerebellum and the neocortex. The findings suggest that sensory and motor representations of fingers overlap spatially in the neocortex but are interdigitated in the cerebellum, suggesting neuronal differences in how information are integrated in the brain structures. Then, neuronal reorganisations of representations were studied during motor learning. The results showed that the neural representation of sequences becomes more distinct with training, while the overall activity does not change. Lastly, I studied effector specific and effector independent representations of sequential motor behaviours by investigating the similarity of neuronal representations for left and right hand performance.

Overall, this thesis demonstrates that the study of neural representations using multivariate methods in fMRI provides a new hypothesis-driven approach to the study of human motor control and learning of movements.

Chapter 1

Introduction

1.1 Activation vs. Representation

Since the beginning of functional imaging, researchers have studied how activation levels in regions of the brain change in response to experimental conditions. The extent to which a brain area is *involved* in a task is typically linked to the amount of its overall activity relative to baseline. Hence, if an area shows higher activity for an experimental condition X compared to an experimental condition Y, it is assumed that the area is more involved in the processing of condition X. This assumption, as reasonable as it may seem, becomes problematic under some circumstances, for example, when applied to neuronal changes of representation through learning.

Researchers have employed this assumption to explain how activity changes when a region learns to process a stimulus of category X (e.g. finger sequences or visual cues). The basic idea is that the activity of a brain area correlates with how well a learned stimulus category can be processed. Thus, if a region is highly skilled to process a stimulus category X, it shows high activity when X is processed. Putatively, this is because more neural units are *recruited* and

dedicated to process X (Karni et al., 1995). However a region could also show decreased activity after learning. Following the same argumentation, such decreases must be interpreted as a sign that a region becomes unimportant in processing X. However, there is an alternative explanation for such activity decreases. It is possible that an area becomes specialised and *efficient* in processing a stimulus category X. This suggests that fewer neuronal units are active while X is processed or that the same set of neurons is activated less. Given these two possibilities of how the brain changes with learning, analysis of overall signal changes can be ambiguous and can prevent meaningful interpretation.

One important type of learning is *motor learning*, which underpins many aspects of our daily lives, such as using a musical instrument, playing sports or typing. In traditional functional MRI analysis, researchers contrast the overall activity of trained and untrained motor behaviour with each other. In studies where participants learn a motor behaviour, higher brain activity has been found in motor cortices (Floyer-Lea and Matthews, 2005; Grafton et al., 1995; Hazeltine et al., 1997; Karni et al., 1998; Penhune and Doyon, 2002, 2005), premotor areas (Penhune and Doyon, 2002), and in the basal ganglia (Hazeltine et al., 1997; Lehericy et al., 2005). However, many other studies have shown decreases of brain activity with learning, mostly in the cerebellum (Penhune and Doyon, 2005), parietal and premotor regions (Poldrack et al., 2005) but also in the primary motor cortex (Jenkins et al., 1994; Toni et al., 1998; Ungerleider et al., 2002). Given these discrepancies, it is impossible to ascertain how the brain changes with learning, based on the overall signal changes. In the extreme case, two processes could occur at the same time: During learning of a motor task, a cortical region may recruit new neural units (leading to *signal increases*) while at the same time encoding the motor tasks more efficiently (leading to *signal decreases*). Thus, signal decreases partly

compensate for signal increases, possibly explaining some of the discrepancies in the literature. If both processes are occurring at once, this would render learning related processes invisible to traditional functional brain imaging.

In this thesis, I will focus on a different criterion that can tell us something about the neural processing in a region: the *representation* of certain stimulus dimensions. Neural activity can be said to represent states in the world (e.g. a stimulus, object, or a movement). Consider a region in which there is a representation of the orientation of visual stimuli. In such a region, we would expect to find neurons that vary their firing rate depending on the orientation of a visual cue. To test experimentally for this representation, four bars with different orientations could be used as visual test stimuli. Assume the level of activity of a single neuron depends on the orientation of a bar. With such a relationship, it would be possible to predict the orientation of a bar by examining the neuronal activity. In other words, *mutual information* exists between experimental stimuli and neuronal activity. In view of this, I will define that neurons that show an informative relationship between experimental stimuli and neuronal activity have a *representation* of the experimental conditions (Figure 1.1).

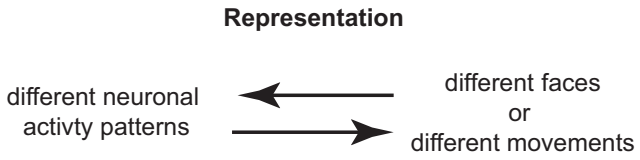

Figure 1.1: *Representation as an essential concept to interact with the environment*

The study of representation is widely used in neurophysiology. Usually, the activity changes of a single neuron are not sufficient to capture the whole

information in a region. For example, neurons in the motor cortex respond with maximum firing rate for a certain movement direction (Georgopoulos et al., 1982), thus implying that this neuron is tuned for a movement direction (Figure 1.2). Assume that there are three different movement directions (-90°, 0°, +90°) given, which are experimentally tested while the activity of a single neuron in the motor cortex is recorded. Say that this neuron is tuned to respond with maximal firing rate for 0° and that it fires moderately for the remaining movement directions (Figure 1.2). It is clear that a 0° movement can be predicted based on the neuronal response of this neuron. In contrast, there is no clear information contained in the neuronal activity changes that would allow distinction of the other two directions from each other (Figure 1.2). However, if a second neuron is recorded and this neuron is tuned for 90°, it becomes possible to differentiate all three movement directions from each other based on the combined neuronal firing rates, which can be referred to as the *population code* (Georgopoulos et al., 1999). In summary, the firing rate of a single neuron may tell us something about the current movement direction. However, when the information from multiple neurons is combined, each of which may respond maximally for a different direction, one can decode unambiguously the direction of movement.

In the fMRI literature on visual processing, the study of representations, rather than activation, has become commonplace (e.g. Cox and Savoy, 2003; Haxby et al., 2001; Haynes and Rees, 2005a; Kamitani and Tong, 2006; Kriegeskorte et al., 2008b; Swisher et al., 2010). These studies are motivated by the idea that the representations found in a region tell us something about the computational function. For instance, a region that is involved in recognising the identity of other people should show different activity patterns for different faces (Kriegeskorte et al., 2007; Nichols et al., 2010).

Similarly, representations are also essential for movement production.

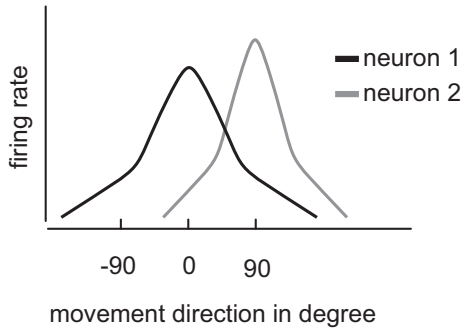

Figure 1.2: *Tuning curve of two neurons*
Illustrative firing rate of neurons under different movement directions. Neuron 1 is tuned to fire maximally for a direction with 0° and neuron 2 shows the highest response for +90°.

Brain areas that are in control of a movement have to show unique activity patterns for certain movements. This is because the output of a region that controls a particular behaviour must be dependent on a set of critical variables that describe the goal of the movement and the state of the controlled body part. Without such representation it would be, from a computational point of view, impossible to control movements. In contrast to vision, the idea of studying representation rather than activation is only starting to be applied to the field of functional imaging in motor control (Eisenberg et al., 2010).

1.2 Representations and functional MRI

Brain activation can refer to several different neuronal parameters depending on the modalities used for measurement. For instance, it can be acquired with EEG and reflect the cortical excitability, PET and reflect the radiolabeled metabolites or functional magnetic resonance imaging (fMRI) and reflect the blood-oxygen-level-dependent signal. Compared to the previous two methods fMRI has a high spatial resolution, making it especially suited to the study of representations that rely on different spatial pattern of activation.

MRI relies on the measurement of the nuclear spin, the synchronised

rotation of free protons around the main axis of the magnetic field, which is caused by a short radio frequency pulse. Functional MRI is based on the transverse relaxation decay, the time that it takes for nuclear spins to dephase. This relaxation time ($T2^*$) is highly influenced by local magnetic field inhomogeneities, which are usually induced by spin-spin interactions of neighbouring nuclei. Importantly, the level of local field inhomogeneity in brain tissue depends on the physiological state of the tissue and is predominantly influenced by the local change of the ratio of oxygenated to deoxygenated blood. Because deoxygenated haemoglobin is paramagnetic, it increases the local magnetic field inhomogeneity and therefore decreases $T2^*$. The local amount of deoxygenated haemoglobin depends on the demand of oxygen. Any increase of neural activity will lead to a higher demand of oxygen. Hence, the local amount of deoxygenated blood increases when neurons become more active. Because of the paramagnetic properties of deoxygenated blood, one would expect that neural activity is indicated through decreases in blood-oxygen-level-dependent (BOLD) signal. However, through focal increases of the capillaries, the blood flow to this region increases, overcompensating for increased oxygen consumption. This leads to an overall increase of the BOLD signal with enhanced neural activity. The physiological reasons for the overcompensation are still not fully understood (e.g. Mintun et al., 2001). However, the overcompensation is the critical factor that enables us to measure activity changes with MRI. Importantly, such overcompensations occur mainly in capillaries that are next to the active neuron (Iadecola et al., 1997). The overcompensation effect is therefore spatially limited to the location of the active neurons.

The greatest advantage of functional MRI is its high spatial specificity. With a resolution of 1-3mm^3, fMRI is currently the best non-invasive method for measuring spatial activity patterns in human brains. However, the majority

of fMRI studies focus only on overall BOLD signal increases or decreases, thereby ignoring the information of fine spatial variations in the BOLD activation pattern across voxels. In contrast, the work in this thesis is primarily based on the information of *voxel activity patterns*.

1.3 Understand and measure representations

This thesis focuses on neuronal representations. The neural activity patterns that are used to study these representations are activity patterns of multiple voxels. As mentioned previously, neurophysiologists speak of a representation if the firing rates of different neurons contain information about the variable of interest. Since fMRI has a high spatial resolution, voxel activity patterns can be used to study representations that are based on different spatial activity patterns. This means that it is possible to use voxel activity patterns to ascertain if a region has information about experimental conditions and therefore represents them.

Voxel activity patterns measured by fMRI can be very sensitive to variations of neuronal tuning functions on a small spatial scale. This has been demonstrated by Swisher et al. (2010) and colleagues, who studied spatial orientation columns in the primary visual cortex with fMRI. In the visual cortex, neurons with similar tuning to the orientation of a visual stimulus cluster together in columns of 0.3-0.5mm width. Thus, the variation of the neuronal activations with orientation is well below the spatial resolution of current fMRI methods. However, on the basis of voxel activity patterns it is still possible to reveal information from spatial orientation columns in the primary visual cortex. The key feature that has allowed such decoding is the unequal distribution and spatial clustering of dominance columns with similar tuning properties. A representation that shows this organisation will lead to

small biases in the activation of voxels. That is, one voxel will show slightly higher activity for a vertical orientated stimulus, whereas another voxel may for a diagonal stimulus. Thus multiple voxels will show a unique activation pattern for each stimulus orientation. It is the existence of these unique patterns that makes it possible to predict which orientation a visual stimulus has.

The study of representations on the basis of voxel activity patterns (*multi voxel pattern analysis* (MVPA)) has been proposed and implemented previously (Haxby et al., 2001; Cox and Savoy, 2003; Haynes and Rees, 2005a; Norman et al., 2006; R and Kriegeskorte, 2010; Kamitani and Tong, 2005; Kriegeskorte et al., 2006). The general premise is to determine whether and how much information a neural activity pattern contains about a variable or stimulus of interest. There are multiple methods available that can be used to approximate the amount of this information, such as *multivariate analysis of variance* (MANOVA), canonical correlation analysis (Friston et al., 2008) and decoding models, such as pattern classifiers. The basic idea of a pattern classifier is to map between an activity space, which in this case is defined by the voxel activity patterns space, and a feature space, which is here defined by different experimental conditions (Figure 1.3). Pattern classification techniques can be quite sensitive when approximating the amount of information in a group of voxels (Mur et al., 2009; Haynes and Rees, 2005b; Norman et al., 2006).

To map representations in the brain *pattern classification* can be combined with a searchlight approach (Section 2.2, Kriegeskorte et al., 2006). In a searchlight approach, the information content of groups of voxels, continuously selected from the brain, is calculated. The information content of each voxel is based on voxel activity patterns of the surrounding voxels. In my thesis, I applied and further developed these techniques.

Besides mapping the brain, representation can also be used to gain deeper

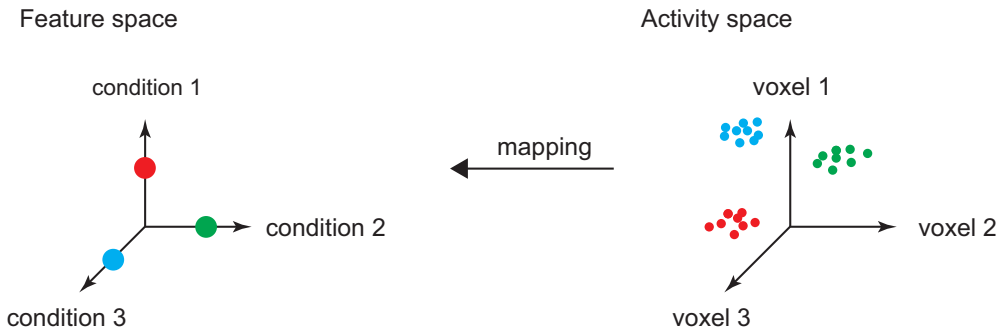

Figure 1.3: *Feature- and activity space*
On the left hand side is the feature space. In a decoding model, each axis of the feature space belongs to a certain class (blue, green, red experimental condition). On the right hand side is the activity space. In this space each axis corresponds to the activity of one voxel. The blue, green and red points are sample patterns of three experimental conditions. Single points in this space are characterised by certain voxel activity patterns. A decoding model aims to map patterns in the activity space to the correct experimental conditions in the feature space.

insight into how the brain processes information. In Chapter 3, for example, I will investigate the interaction between the sensory and motor representations in the cerebellum (Chapter 3). This thesis supports the idea that activity patterns of voxels provide an excellent basis to study neuronal processes in the field of motor control and beyond.

1.4 Overview

Using fMRI, brain areas that are involved in motor control of human behaviour have been mainly studied by overall BOLD signal changes. In this thesis, I applied the concept of representational analysis in fMRI to three fields of motor control: motor and sensory integration, learning related plasticity changes and motor representations of movements.

1.4.1 Motor and sensory integration

In my first study, I focus on sensory and motor representations of individual fingers in the cerebellum and compare them to neocortical representations. After identifying the areas that encode fingers in the cerebellum, I investigate how sensory and motor representations of fingers interact with each other.

1.4.2 Learning related plasticity changes

In the second empirical part of my thesis, I study finger sequence performance. A sequence includes each finger of a hand once and sequences differed only in the order of these five finger presses. These finger sequences are performed with high speed during fMRI scans. Hence, the decoding between voxel activity patterns of finger sequences was challenging.

To determine how training changes the underlying neural representation, skilled and unskilled representations of sequences, are studied. Because it is unknown how the overall BOLD signal is modulated when a region starts to represent a motor skill, the focus is placed on representations, to circumvent the ambiguity inherent in the interpretation of overall activity changes.

1.4.3 Motor representations of movements

In the third empirical part of my work, I characterise representations of sequences while they are performed with different hands. This allows me to study effector specific and effector independent representations of movements. Additionally I ask in what coordinate frame effector independent representations of sequential movements are encoded.

Chapter 2

Multivariate techniques

Abstract

This chapter gives a detailed overview of the multivariate techniques that I applied and developed during my doctoral studies. I established these methods with the aim of understanding motor representations in the human brain. In Section 2.1, I will outline the techniques used to identify regions that contain a representation of variables of interests. First, I derive the linear classifier that I am using to identify representational structures. Section 2.1.2 describes the cross validation method to test the classifier and discusses situations in which this method may fail. Section 2.2 lays out how classification performance maps are calculated and discusses the difference between a volume- and a surface-based searchlight approach. In Section 2.4, I deal with the problem of how to decide whether a representation that was established by the classification approach reflects a representation of the experimental variable, or whether it is caused by other behavioural differences between conditions. A principled treatment of such behavioural confounds is especially important in motor control studies, where the experimenter can never fully control the external stimulus (movement). The techniques in the last three Sections 2.5-2.7 aim to understand the structure of representations in more depth. I will demonstrate how correlations across different brain areas can be compared with each other. I will describe (Section 2.6) how the new method can be used to estimate a quantitative measure of the representational size. In the last Section (2.7), I explain how representations can be tested for topological arrangements.

2.1 Classification

The core idea of this thesis is to study neural representations of motor behaviours in the human brain. A brain area represents experimental conditions when it shows specific voxel activity patterns for each of them that allow us to differentiate between the experimental conditions. This also means that such voxel activity patterns contain *information* about the experimental conditions. The amount of information determines how well experimental conditions can be distinguished from each other. In order to approximate the amount of information *pattern classification* is used.

Imagine a space of voxel activity patterns in which each axis corresponds to the activity of a single voxel. A single point in this *activity space* characterises a specific voxel activity pattern. Points in this space are labelled with the experimental conditions that lead to a certain activity pattern. Additionally, there exists another space, the *feature space*, in which each point represents voxel patterns that have the same label (see Figure 1.3). A classifier maps an activity space to a feature space. Depending on the type of classifier this mapping can be linear or nonlinear. The amount of information between the activity space and the feature space determines the accuracy of this mapping. Our feature space is defined by experimental conditions and the voxels of the activity patterns span the activity space.

If activity patterns of experimental conditions can be separated easily from each other there will be a lot of information and therefore a clear mapping between the activity and the feature space. Brain areas that would show such activity patterns would represent the experimental conditions very well. In contrast, if voxels respond with similar activation patterns for different features, the activity patterns of the experimental conditions cannot be easily separated from each other. Thus, there would be insufficient information in

such activity patterns and a mapping from the activity space to the feature space would be difficult. Based on such patterns a classifier would perform poorly and one would conclude that a brain area does not represent the experimental conditions.

In summary, through the accuracy of the mapping it can be measured how distinctly or uniquely activity patterns represent the experimental conditions. Therefore, the classification accuracy is an approximation of the amount of information between voxel activity patterns and experimental conditions. Such information is correlated with the strength of a neuronal representation and reflects how strongly a brain region represents certain behavioural dimensions.

2.1.1 Classifier

In this section, I will explain in detail the classification approach that I used for decoding. In general, a classifier aims to find a *decision boundary* (Figure 2.1) that separates the activity patterns of different experimental conditions, for example different finger movements, from each other. Types of classifiers differ in their model assumptions and their ways of defining decision boundaries (for a review see Misaki et al., 2010). The decision boundary for linear classifiers is a hyperplane, whereas non-linear classifiers would allow nonplanar decision boundaries. After a decision boundary has been found, the performance of a classifier is tested on unknown activity patterns and the classifier has to predict to which class an unknown pattern belongs.

For illustration, imagine data clouds, which represent different classes. The clouds are arranged in a three-dimensional activity space. Each axis in this space corresponds to the activity of one voxel and each point in the space represents a sample from a class (Figure 1.3).

Assuming that the clouds are spaced far apart from each other (distinct

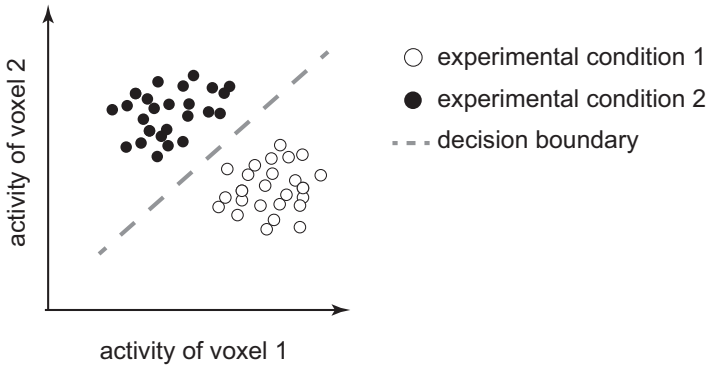

Figure 2.1: *Linear decision boundary between two experimental conditions in an activity space of two voxels*

representation), training a classifier on such data would result in decision boundaries that separate the training samples very well. Furthermore, new class samples, which have not been used to define the decision boundaries and are located within the cloud of their classes, would also be clearly separated from other classes by the decision boundaries. This means it would be possible to use this classifier to predict with a high probability to which experimental condition an unknown activity pattern belongs.

In contrast, if the clouds are moved closer together or even overlap completely, a linear classifier would be unable to define clear decision boundaries between the classes. Such a classifier would therefore show a reduced probability in assigning unknown patterns to the correct classes. In the extreme case (no information), a classifier would assign unknown data randomly to classes and operate at chance level. *Percent correct classification* of unknown patterns shows the quality of the classifier, but also reflects how distinct and dissimilar the different activity patterns of different classes are. In other words, the classifier is measuring the information between voxel activity patterns and their experimental conditions. Hence, the classifier indicates quantitatively how strong the representations of the experimental conditions are.

In my studies, I used *linear discriminant analysis (LDA)* because of its simplicity, theoretical tractability, and computational speed. The linear discriminant analysis defines a hyperplane and assumes a linear relationship between the space of voxel activity patterns and the space of the experimental conditions. Hence, it assumes that single voxels change their activity linearly to the experimental conditions. For illustration, imagine two experimental conditions: thumb movements and index finger movements. A voxel might respond to thumb presses with low activity and show higher activity for index finger presses (linear activity change, thumb $\rightarrow$ index). However, if the same voxel becomes more active if the thumb press exceeds a certain force level, its activity function would be non-linear (thumb (low force) $\rightarrow$ index (low and high force) $\rightarrow$ thumb (high force)). Such non-linear voxel responses are excluded by the model assumption. Furthermore, an LDA classifier assumes that the activity patterns of classes have a normal distribution. That means that the samples of each class (data cloud), from the example above, are assumed to have a multivariate normal distribution. Compared to a linear classifier, nonlinear classifiers overfit data easily. Therefore, known data can be distinguished very well between classes whereas unknown patterns are assigned incorrectly to a class. In general, a linear classifier is more robust against overfitting, because it is simpler and classes are separated with a hyperplane. In practice, an LDA is easy to derive and to implement. It is therefore possible to manipulate and to study the decoding directly in various ways (Section 2.4). Additionally, compared to support vector machines (SVMs) an LDA classifier is computationally efficient and makes whole brain classification with a searchlight (Section 2.2) feasible.

The exact form of the LDA classifier can be derived through Bayes rule (or as Baysian inference) from a simple generative model. This model assumes that the data have the following properties:

1. The activity patterns of any class i have multivariate normal distribution $\mathcal{N}(\mu_{c_i}, \Sigma)$.

2. The classes share the same covariance matrix Σ.

For an unknown voxel activity pattern $x \in \mathbb{R}^{N\times 1}$ the classifier calculates the likelihood that this pattern belongs to a certain class and assigns the pattern to the class that is most likely (maximising the likelihood). That means that it is necessary to calculate the likelihood $P(c_i|x)$ that pattern x belongs to a class c_i. This probability $P(c_i|x)$ can be reformulated with Bayes rule:

$$P(c_i|x) = \frac{P(c_i) \cdot P(x|c_i)}{P(x)} \tag{2.1}$$

Assuming the patterns of classes are multivariate Gaussian ($\mathcal{N}(\mu_{c_i}, \Sigma)$), we can express $P(x|c_i)$ by:

$$P(x|c_i) = \frac{1}{(2\pi)^{N/2}} \cdot \frac{1}{\sqrt{|\Sigma|}} \cdot e^{(-1/2(x-\mu_{c_i})^T \Sigma^{-1}(x-\mu_{c_i})} \tag{2.2}$$

Substituting $P(x|c_i)$ in 2.1 by 2.2 the log-likelihood $l_{c_i}(x) = ln(P(c_i|x))$ can be calculated. Note, the logarithm is a monotonic function and will therefore not change the optimisation value:

$$\begin{aligned} l_{c_i}(x) = & ln(p(c_i)) - ln(p(x)) \\ & - \frac{N}{2} ln(2\pi) - \frac{1}{2} ln(|\Sigma|) \\ & - \frac{1}{2}(x-\mu_{c_i})^T \Sigma^{-1}(x-\mu_{c_i}) \end{aligned}$$

This equation can be simplified by dropping all the constants ($\frac{N}{2} ln(2\pi)$, $\frac{1}{2} ln(|\Sigma|)$) and parts that do not depend on c_i ($ln(p(x))$), because they are

negligible when doing maximisation. We then obtain:

$$l_{c_i}(x) \propto ln(p(c_i)) - \frac{1}{2}(x - \mu_{c_i})^T \Sigma^{-1}(x - \mu_{c_i}) \tag{2.3}$$

Through expanding $(x - \mu_{c_i})^T \Sigma^{-1}(x - \mu_{c_i})$ we get:

$$(x - \mu_{c_i})^T \cdot \Sigma^{-1} \cdot (x - \mu_{c_i}) \tag{2.4}$$

$$\Leftrightarrow (x^T - \mu_{c_i}^T) \cdot \Sigma^{-1} \cdot (x - \mu_{c_i}) \tag{2.5}$$

$$\Leftrightarrow (x^T \Sigma^{-1} - \mu_{c_i}^T \Sigma^{-1}) \cdot (x - \mu_{c_i}) \tag{2.6}$$

$$\Leftrightarrow x^T \Sigma^{-1} x - x^T \Sigma^{-1} \mu_{c_i} - \mu_{c_i}^T \Sigma^{-1} x + \mu_{c_i}^T \Sigma^{-1} \mu_{c_i} \tag{2.7}$$

Because it is assumed that all the classes share the same covariance matrix and Σ^{-1} is by definition symmetric $\Rightarrow (\Sigma^T)^{-1} = (\Sigma^{-1})^T$ and $\mu_{c_i}^T \Sigma^{-1^T} x = (x^T \Sigma^{-1} \mu_{c_i})^T$, equation 2.4 simplifies to:

$$x^T \Sigma^{-1} x - 2x\Sigma^{-1} \mu_{c_i} + \mu_{c_i}^T \Sigma^{-1} \mu_{c_i} \tag{2.8}$$

Putting equation 2.8 back into equation 2.3 we get:

$$\begin{aligned} l_{c_i}(x) &\propto ln(p(c_i)) - \frac{1}{2}(x^T \Sigma^{-1} x - 2x\Sigma^{-1} \mu_{c_i} + \mu_{c_i}^T \Sigma^{-1} \mu_{c_i}) \\ &= ln(p(c_i)) - \frac{1}{2} x^T \Sigma^{-1} x + x\Sigma^{-1} \mu_{c_i} - \frac{1}{2} \mu_{c_i}^T \Sigma^{-1} \mu_{c_i} \end{aligned}$$

Similarly, because $\frac{1}{2} x^T \Sigma^{-1} x$ does not depend on class c_i, this term can be dropped and the final discrimination function is $g_{c_i}(x)$:

$$g_{c_i}(x) = ln(p(c_i)) - \frac{1}{2} \mu_{c_i}^T \Sigma^{-1} \mu_{c_i} + \mu_{c_i}^T \Sigma^{-1} x \tag{2.9}$$

Equations 2.9, expresses the log-likelihood that a pattern x belongs to class c_i. Finally, the input pattern x is assigned to the class that maximizes this log likelihood:

$$\hat{c} = \arg\max_{c_i}(g_{c_i}(x))$$

Note that the final equation is not a full likelihood because the normalisation factors are ignored.

In practice, to train the classifier one needs to estimate *class means* (μ_{c_i}) and the *within class covariance matrix* Σ from a training set of voxel activity patterns. In equation 2.9, the covariance matrix Σ needed to be inverted. However the true Σ is unknown and the covariance matrix from the data can only be approximated. Because there are more voxels than classes this matrix is ill conditioned and needs to be regularised. I regularise Σ by adding 1% of the diagonal mean to each diagonal element (Pereira et al., 2009). After the above steps, this classifier is then robust and efficient and can be used to measure the amount of information between activity patterns and experimental conditions.

2.1.2 Cross-validation

How can the performance of a classifier be validated for a given data set? Ultimately, we would like to have a test statistic that allows us to estimate how dissimilar voxel activity patterns of experimental conditions are. This dissimilarity would be an approximation of the information between voxel activity patterns and their experimental conditions. A statistical method that would test this information is a *multivariate analysis of variance* (MANOVA). However, the test statistic Wilks' lambda is only valid if the (*number of trials - number of conditions*) $\cdot \frac{1}{2} >$ *number of dependent variables*. Hence, it is not possible to use this test statistic because activity patterns consist of many

voxels (dependent variables) but only a small number of trials (scans). For higher dimensional patterns a close form solution for the test statistic does not exist.

A method to test a classifier against a known baseline is cross-validation. The basic idea is to split the data in a training set and a test set. The training set is used to estimate the parameters of the classifier (class means μ_{c_i} and shared covariance matrix Σ) and the test set is used to test the performance of the classifier. If the input patterns of classes do not show consistent differences, the trained classifier assigns unknown patterns randomly to classes and would perform at chance level. Hence, the baseline performance of the classifier is known. This baseline enables us to validate the performance of a classifier. For example, the chance level of a classifier with four different classes would be 25% correct classifications. A classifier that performs above its baseline must be based on voxel activity patterns that show systematic differences between classes. Hence, such a brain region would represent the experimental conditions.

How are test and training sets defined? One way is to leave out one single pattern and train the classifier on the remaining patterns. When we repeat this procedure until every pattern has been used as test pattern, we know how often the classifier predicted the correct class (classification performance). Surprisingly, when this procedure is applied to random data ($\mathcal{N}(0, \Sigma)$) the classifier will perform, on average, below chance level (Figure 2.2). However, as stated before, it is expected to get chance-level performance for random input data. A classification performance below chance means that there exists a systematic bias in the cross-validation procedure.

The reason for this unexpected pitfall is the following: When a single pattern of class i is left out for testing, the remaining training set consists of $n - 1$ patterns for this class, and n patterns for all other classes. Hence,

the variance of the estimator for the class mean (μ_{c_i}) for the left-out class is $\sigma^2/n - 1$, whereas the variance of the estimator of the class mean for the remaining classes is σ^2/n. The unknown test pattern, which will be on average somewhere around zero (the origin), is therefore more likely to be further away from the estimated μ_{c_i}. As a result, the test pattern will be less likely assigned to its true class. In machine learning such a cross-validation is called *unbalanced cross-validation*. In general it is advisable to avoid unbalanced cross-validation.

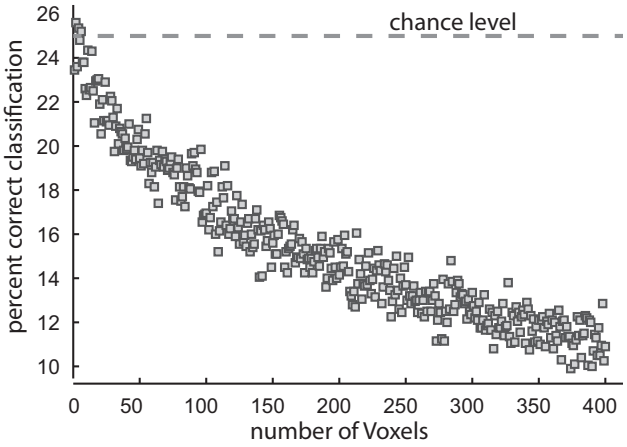

Figure 2.2: *Unbalanced cross-validation leads to under chance classification accuracy.*
The classification accuracy for a classifier with four different classes should have a chance level of 25%. However if the cross-validation is unbiased, the classifier is biased to predict unknown classes wrongly. With increasing number of voxels, this effect becomes even stronger.

The classification performance in this thesis is therefore based on a *balanced cross-validation*. To train a classifier, a complete run of a scan was excluded from the full data set. The test set consists therefore of one voxel activity pattern of each experimental condition. With this procedure, I can estimate the unbiased percent correct classification accuracy. The resultant classification accuracy shows how distinct the activity patterns of different experimental conditions are and reflects the information between the voxel activation patterns and the experimental conditions.

2.2 Voxel selection

In Section 2.1, I described the classification method that is used to calculate the strength of a neural representation on the basis of voxel activity patterns. So far, I have not yet defined which groups of voxels should be used for the classification analysis. Early studies used all voxels of the functional images and correlated or classified between experimental conditions (see Norman et al., 2006, for a review). This global approach makes it impossible to gain deeper understanding of the functional specialisation of different brain regions. Alternatively one can pre-define *regions of interest (ROI)* and test for task-relevant representations in these areas (e.g. Haxby et al., 2001; Kamitani and Tong, 2005; Haynes and Rees, 2005a). However, with this approach potential representations in an area may be missed where no ROI is defined. Additionally, depending on the criteria used to select local ROIs, there is the danger of making circular inferences (Kriegeskorte et al., 2009). Finally, as different ROIs contain different numbers of voxels, it is hard to compare the findings fairly across different regions. In this Section, I will therefore describe a map-wise approach to find all representations in the brain to avoid those problems.

2.2.1 Volume-based search light

Kriegeskorte et al. (2006) proposed the idea of *whole brain information-based-mapping*. Such maps are obtained with a *searchlight procedure*. A single voxel in the volume is chosen as the current centre-voxel. Neighbouring voxels are selected as a sphere around this centre-voxel. Based on the activity patterns of these voxels a classifier is trained and tested. Note that the size of the input patterns depends on the radius of the sphere. The result of this local classifier is then assigned to the centre voxel. After

that, the searchlight moves to a new location in the brain and the process starts again. By moving the searchlight to every single voxel in the brain, an information-based map is estimated. Such a map shows where task-relevant information is represented. Since my central measure is classification accuracy, I will refer to the information-based maps as *classification accuracy maps*. In this thesis, I used a volume-based searchlight to map sensory and motor representations of fingers in the cerebellum (Chapter 3).

2.2.2 Surface-based search light

The volume-based searchlight allows us to explore which parts of the brain represent a variable of interest. However, such a searchlight approach can be problematic if the aim is to study anatomically separate representations that are close together in the volume. Isometric finger presses have a sensory and a motor component. Hence, one would expect to find two separate representations, one in the primary somatosensory cortex and another in the motor cortex. These two areas are anatomically far apart from each other and spatially separated by the central sulcus. However, a volume searchlight ignores the anatomical characteristics of the brain and a sphere may include voxels from both sides of a sulcus (Figure 2.3a). It is therefore impossible to distinguish finger representations in the sensory cortex from those in the motor cortex. To solve this problem, the searchlight needs to take into account the anatomical folding of the brain.

Together with Oosterhof et al. (2010) I developed a new searchlight approach to address this problem. The novel idea is to perform the searchlight not in the volume, but on the surface of subjects brain. Using the surface of the brain to define the searchlight will preserve the anatomical distance in different searchlights and therefore improve the spatial specificity of the

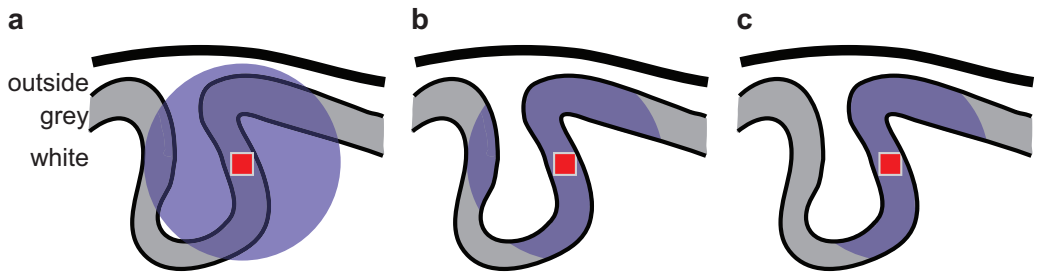

Figure 2.3: *Voxels can be selected by different methods.*
The illustrative brain slice **(a)** shows how voxels are selected with a sphere around a centre vertex (red). In **(b)** white matter voxels are excluded to improve the voxel selection. The surface based voxel selection **(c)** considers anatomical properties and increases the spatial selectivity of the voxel selection.

classification accuracy maps. For obvious reasons this technique is called *surface-based information mapping*. This method was published (Oosterhof et al., 2010) and was made public in a freely available Matlab toolbox (http://surfing.sourceforge.net/Welcome.html).

Surface-based techniques have been used in traditional univariate fMRI studies (Dale et al., 1999; Van Essen and Drury, 1997; Van Essen et al., 2001; Van Essen and Dierker, 2007) and became popular with the software packages Freesurfer (http://surfer.nmr.mgh.harvard.edu/) and Caret (http://brainvis.wustl.edu/wiki/index.php/Caret). The main advantages of surface-based analyses are a better normalisation across subjects (Fischl et al., 1999) and an easier visualisation of the results. The ability to inflate the otherwise highly folded cortical surface is an especially powerful tool to visualise different brain areas. Furthermore, a surface-based analysis includes only cortical grey matter voxels and reduces the search area, thus reducing the noise for the statistical inference. To perform surface-based information mapping, a surface needs to be constructed, which is a closed surface with no boundaries. A 3-dimensional grid defines such surfaces through two types of information, the coordinates of vertices in the grid and the connections among those vertices (topology). The inner surface separating grey and white

matters and the outer surface defined by the pial layer of the brain are created by Freesurfer using the high-resolution anatomical image of a participant (T1-weighted images). Importantly, these surfaces have the same topology so an intermediate surface can be estimated by taking the mean between the coordinates of the outer and inner surface.

To select the voxels of a single searchlight, one vertex on the intermediate surface is chosen as the centre vertex. Starting from there, adjacent vertices within a pre-defined searchlight radius are selected. To estimate the geodesic distances along the intermediate surface the Matlab toolbox created by (Peyre, 2008) has been used, which adopts Kimmel and Sethian (1998)s algorithm to efficiently calculate the distance along a surface. After finding the neighbouring vertices along the intermediate surface, the corresponding voxels are selected using the following procedure: For each vertex in the searchlight, a line between corresponding inner and outer vertex is specified. Note that the length of the line corresponds to the local thickness of the cortical area. Along this line 10 equally spaced points are defined. The voxels that are covering these points are included into the searchlight. The voxel activity patterns of the searchlight are then used as input patterns for the classifier. The resultant cross-validated classification accuracy is assigned to the centre vertex of the surface searchlight. Similar to the volume-based searchlight the surface-based information map is calculated for the whole brain and each vertex serves as a centre vertex.

This new way of estimating information maps takes into account the subject specific folding of the brain and increases the spatial specificity of informative mapping. Furthermore, only voxels between the inner and outer cortical surfaces are considered and thus the searchlights include only adjacent grey matter voxels (Figure 2.3c).

To demonstrate that surface-based information maps improve, the spatial specificity and classification performance of three different types of information

maps were compared (Oosterhof et al., 2010): the volume-based search light (Figure 2.3a), the volume-based searchlight combined with a grey matter mask (Figure 2.3b), and the surface-based searchlight (Figure 2.3c). It was important to study the volume-based with grey matter masking, because differences between the volume-based and surface-based search lights could be explained by the exclusion of uninformative white matter voxels. Because these searchlights will select different numbers of voxels for an identical searchlight radius, information maps with 4, 6, 8, 10 and 12mm radius were produced for the volume-based searchlights and 4, 6, 8, 10 and 22mm radius for the surface-based searchlights. As exemplary data, the classification accuracy of individual isometric finger presses in the motor cortex and the primary somato-sensory cortex were studied (see Chapter 3 for experimental details).

To compare the classification accuracy of information maps qualitatively, we restricted ourselves to two anatomical ROIs (motor cortex and primary somato-sensory cortex) of nearly equal size. Comparing the average classification performance between the three information maps (Figure 2.4a), it was found that the surface-based searchlight yields always the best performance. This comparison was done by fitting exponential functions ($y = c_1 + c_2 \cdot e^{(x-c_3)}$) over the classification accuracy with increased number of voxels for each of the three methods and each participant. The resultant functions approximated the data well and explained, on average, 98.5% of the variance. Based on these functions we corrected for the number of voxels and compared the classification accuracy of the three methods for the searchlight sizes of 100 to 800 voxels in steps of 100 voxels. This analysis showed that for all participants and all searchlight sizes the classification accuracy of the volume-based searchlight with masking was higher than that of the volume-based searchlight without masking (repeated-measures ANOVA for radii of 4, 6,...,12mm; $F_{(1,6)} = 40$, $p < 0.001$). Also, the

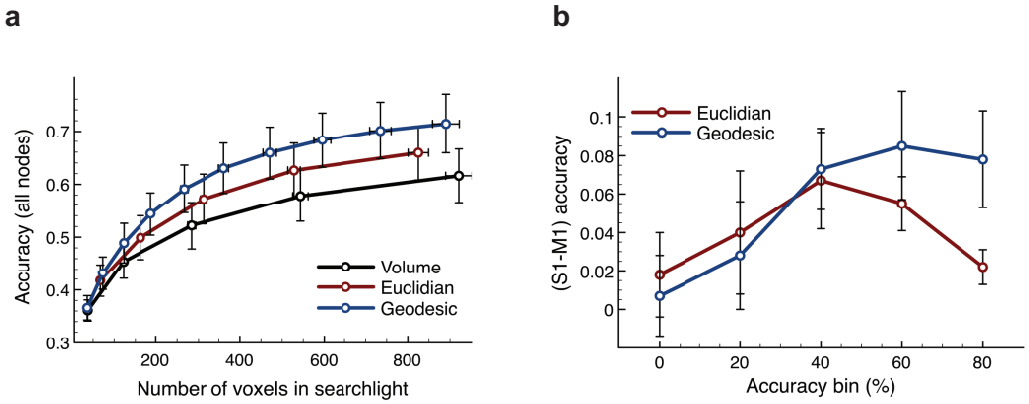

Figure 2.4: *Quantitative comparison of voxel selection methods*
Two anatomically defined regions of interest (motor cortex and primary somato-sensory cortex) were defined to compare the classification accuracy under different voxel selection methods. The voxel selection methods are a traditional volume based searchlight (volume), a volume based search light with grey matter masking (Euclidean) and a surface based searchlight that is based on the geodesic distance along the surface (geodesic). **(a)** shows the averaged classification accuracy across both ROIs when different voxel selection methods are used. The x-axis shows the average number of voxels within a searchlight (for the volume and Euclidian voxel selection radii of r= 4, 6,...,12mm were tested and, for the geodesic method radii of r= 4, 6,...,22mm were used). With the correction for the number of voxels, the best mean classification accuracy across both regions can be achieved with the surface based voxel selection. **(b)** To test for the spatial specificity, the difference in classification accuracy between motor cortex (M1) and primary somato-sensory cortex (S1) was studied for the Euclidian and geodesic voxel selection. The difference in classification accuracy of these two regions is calculated for bins of 20%, 40%, 60%, 80%, 100% top classification accuracy in each region. For the top 20% accuracy bin the difference between S1 and M1 was significantly different from the difference of the Euclidean voxel selection method. Thus the geodesic method increases the spatial specificity of classification accuracy maps. This figure is adapted from Oosterhof et al. (2010)

surface-based searchlight yields better classification performance than the volume-based searchlight with masking ($t_{(6)} \leq 3.08$, all $p < 0.02$). This analysis demonstrated that surface-based search light method is able to improve the performance of the classifier by selecting anatomically adjacent voxel patterns.

In addition to the increased classification performance, it was also expected

to find an improved separation between the primary somato-sensory cortex and the motor cortex when using a surface-based compared to a volume-based searchlight. This is because the surface-based searchlights minimise the crossover of voxels from the opposite site of the sulcus. To test this idea, the volume-based searchlight with grey matter mask was compared with the surface-based searchlight. For both methods, the searchlight radius was set to 10mm. Within the anatomically defined ROIs, vertices were divided into bins of 20%, 40%, 60%, and 80% percentiles of classification accuracy. To analyse the separation between the ROIs, the corresponding bins between the ROIs were subtracted from each other (S1-M1 (Figure 2.4b)). This analysis showed that there was a significant difference between the two searchlight methods for the highest 20% of classification accuracy ($t_{(6)} = 2.06, p = 0.043$). The sensory representation of finger presses was more pronounced than the motor representation, and this difference becomes more apparent at higher accuracy level when surface-based information maps were used.

In summary, these results show that the surface-based information mapping improves the spatial specificity of the information maps. Furthermore this method selects only anatomically adjacent voxels as input patterns to the classifier and thus increases the overall classification accuracy (Oosterhof et al., 2010).In this thesis, I use surface-based information mapping to identify representations of fingers and finger sequences in the neo-cortex.

Interestingly, the difference analysis between S1 and M1 becomes only apparent if nodes with high classification accuracy are selected. This means that the classification accuracy is basically comparable between S1 and M1. A neurophysiological scenario for this result could be that the BOLD activity in both M1 and S1 mainly represents the sensory component of finger movements. This could be explained by the finding that the BOLD signal generally represents the input signals to neurons. Following this idea it would not be

surprising to find that the same amount of information is represented in S1 and M1.

It is an interesting question if the difference between the two areas would increase for other conditions. For example, it could be the case that hand gestures that are most common in daily life are presented clearly in M1 (motor synergies). Hence, the patterns for these hand gestures would differ and high classification accuracy could be seen. Additionally, it could be that case that these gestures produce very similar sensory input. Therefore, the voxel activity patterns in S1 would not differ between conditions and a classifier would not be able to distinguish between conditions. For this experimental design and neurophysiological scenario, M1 and S1 classification accuracies would be discrepant.

2.3 Remarks on the search light methods

The search-light methods that I employed to localise representations in the neo-cortex and cerebellum capture only representations that are mediated through neuronal units clustered locally within the searchlight. Thus, this method would be less sensitive to representations that emerge from the complex interactions between widely-spaced areas. Nevertheless, I believe that this limitation is not too restrictive.

First, there is ample evidence that neurons coding for similar properties of stimuli and actions are organised in locally definable regions. For example, adjacent neurons in the hand area of M1 may show a preference for very different digit movements, but all neurons in this area will exhibit encoding of different aspects of digit movements, rather than, for instance, leg movements. Although this regional clustering of neurons forming a "population code" may be less pronounced when looking at higher-level representations, such as the

content of working memory, for the basic sensory and motor representations studied in this thesis it is likely a reasonable assumption.

Secondly, even for sensory-motor representations, it is probable that the processing arises from interaction of multiple distant areas, such as the hand representation in neocortex and the cerebellum. In general, the exchange of information between different brain areas will lead to a local representation of the information in both areas. For example, if a network of cerebellar and cortical inputs encode for individual finger movements collectively, both areas must show a representation of finger movements. In other words, the nodes of the network represent the information locally. Thus, a local searchlight approach would be appropriate for the identification of the informative nodes of networks.

However, the local search-light method cannot provide any insight into how informative areas interact with each other as parts of a network. To answer these questions, new information-based connectivity analysis methods are needed.

2.4 Behavioural confounds

To identify neuronal representations in the brain I study the information between voxel patterns and their experimental conditions. Using pattern classification, this information can be approximated and is expressed as cross-validated classification accuracy (Section 2.1). Brain areas that show above-chance accuracy are thought to represent the experimental conditions. However, there exist several possibilities of how the BOLD signal of experimental conditions can differ and therefore lead to above chance classification accuracies. Hence, good classification does not necessarily reflect the underlying neuronal representation of interest. In view of this problem,

it is important to define what types of pattern differences are interpreted as neuronal representations.

Suppose, the aim of an experiment is to identify brain areas, which represent individual finger movements. Such brain areas are characterised by systematic differences between activity patterns of movements of fingers. It is also possible that the overall BOLD activity within a brain region scales with the force level of finger movements, yet the underlying pattern of voxel activity remains unchanged. If individual finger presses were performed with different force levels (e.g. little finger presses with low force and index finger presses with high force), any classifier would be able to perform above chance level in this region. The information that a classifier would use to discriminate between finger patterns is just the difference in the scaling. Clearly, it should not be concluded that this region represents and encodes finger movements. Instead it encodes the force level. Currently, it would be difficult to distinguish brain areas that encode finger movement from those that show above chance classification accuracy only due to a force-dependent multiplicative scaling. One strategy would be to add a regressor for the force in the general linear model that is used to estimate the activity of single voxels. However usually it is unknown by which factor a pattern might be scaled. For example, it might not be a difference in force but a difference in movement time or another parameter. To find brain areas that truly represent motor tasks, I developed a method to differentiate between class patterns that differ by a single unknown factor (1-dimensional representation) from class patterns that differ by multiple factors.

The method is based on the idea that it is possible to train a classifier only on a subset of the input data dimensions. Imagine the 1-dimensional representation from above, in this region the activity of voxels scales with the level of force, while the pattern of activation remains unchanged. In other

words, the patterns scale multiplicatively with the force level (Figure 2.5a). In this scenario, the only informative dimension that a classifier can use to distinguish between activity patterns is force. Importantly, if the classifier were to use more dimensions, its accuracy would decrease, because there would be no further information only noise in the additional dimensions. Therefore, the classifier is only fitting noise, which reduces the ability of the classifier to generalise and predict unknown pattern activities correctly. This problem is known as *over fitting*. This phenomenon was used to determine the optimal number of factors to classify certain pattern of activities. In order to do that, the dimensions that a classifier can use for the classification has been manipulated. In Section 2.1.1 I derived the LDA that I am generally using for classification. An equivalent linear classifier (Fisher linear discriminant analysis) can be expressed in the following way:

Maximize the between class variance (S_B) and minimise the within class variance (S_W)

$$S_B = \sum_{i=1}^{c} N_{c_i}(\mu_{c_i} - \mu)(\mu_{c_i} - \mu)^T$$

$$S_W = \sum_{i=1}^{c} \sum_{j}^{N_{c_i}} N_{c_i}(x_j - \mu_{c_i})(x_j - \mu_{c_i})^T$$

where

$$\mu_{c_i} = \frac{1}{N_{c_i}} \sum^{N_{c_i}} x_j \ , \ \mu = \frac{1}{N} \sum^{c} N_{c_i}\mu_{c_i}$$

and

$N_{c_i}$is the number of training samples; $N = \sum^{c} N_{c_i}$

To maximise S_B and minimise S_W the discrimination function uses the eigenvectors of

$$S_W^{-1} S_B \tag{2.10}$$

to project test patterns in a new space and differentiate between the classes of test patterns in this new space.

Assume there are four different classes in the data set. This means that a representation has maximally 3-dimensions. To illustrate this point, imagine four classes in an activity space of two voxels (Figure 2.5a, b). If the classes lie along a line in this space the class patterns do not change but simply scale multiplicatively and form a 1-dimensional representation of the four classes (Figure 2.5a). On the other hand, it is also possible that the four classes are not arranged along a line (Figure 2.5b). Thus, the class patterns would differ truly from each other and represent the experimental conditions.

Using equation 2.10 it becomes possible to manipulate the classifier and allow it to use only the first, first and second or first, second and third eigenvectors of $(S_w^{-1} S_b)$ for the discrimination of unknown voxel activity patterns. With these three different classifiers, it is possible to quantify the optimal dimensionality of the representation. If the activity patterns differ from each other because they are scaled versions of the same common activity pattern, then the classifier should perform best if trained on a single dimension only. Similarly, a representation that is based on multiple dimensions will only be best discriminated with classifiers that are also using multiple dimensions.

How can this idea be used to distinguish multi-dimensional representations from 1-dimensional representations in practice? Take a region that yields a classification accuracy α using the Bayesian-LDA classifier. In the case of four different experimental conditions, a maximum of three dimensions

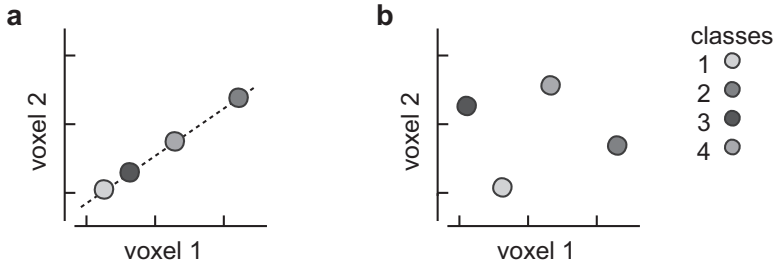

Figure 2.5: *Different types of patterns changes can lead to above chance classification accuracy.*
(a) The four class patterns are arranged in a 2-dimensional representation in an activity space of two voxels. **(b)** However, it is also possible that the class patterns are arranged on a line and the patterns are scaled multiplicative by a single factor, 1-dimensional representation.

are necessary to represent them. Thus, a classifier that uses the first three eigenvectors will yield a classification accuracy that is identical to the Baysian-LDA accuracy. However, classifiers using less eigenvectors should show decreased classification performance if activity patterns of classes differ truly, but should show increased classification performance if the representation is based on less dimensions (for example one dimension). To test this principle, I generated data that have the same noise level but a 1-, 2-, or 3-dimensional representation. Figure 2.6a shows the classification accuracy for the different classifiers on the simulated data. The accuracy for a classifier using only the first eigenvector is highest for the 1-dimensional representation. In contrast, the classifier that takes into account the first three eigenvectors for the discrimination shows the best classification performance for a 3-dimensional representation.

To be able to decide to which representational dimension the real data belongs to, one must compare the real classification performance to the simulated data. I therefore generated simulated data with different noise levels. If a region reveals a classification accuracy α with the LDA, I selected the 1-, 2- and 3- dimensional simulated data that provide a classification

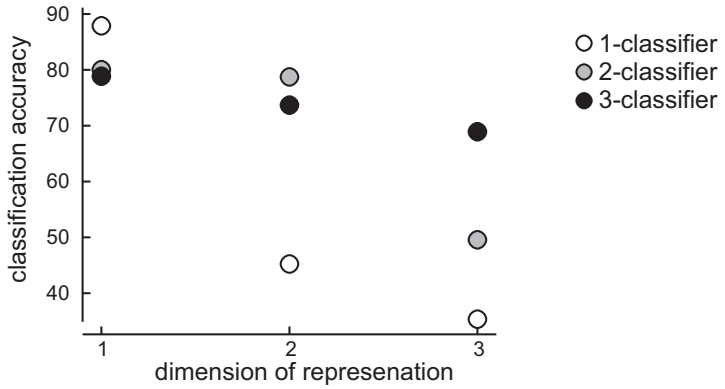

Figure 2.6: *Classification accuracy for manipulated classifiers and patterns with different representational dimensions.*
A classifier that is using more dimensions then necessary overfits the data and cannot generalise to unknown activity patterns. The classifier that is using 1-dimension performs best for data that has a 1-dimensional representational structure. Similarly, the other classifiers (2 and 3) show the best performance for the corresponding representational dimension.

accuracy of α. Plotting the classification performance of the remaining classifiers for these simulated data makes it easier to identify to which type of simulated data the real data is most similar. This method was validated with two fMRI experiments. In the first experiment, one single factor was experimentally manipulated. I gave participants four visual stimuli of different brightness and let them simultaneously produce hand presses with all five fingers of the right hand. The forces of these hand presses were correlated to the brightness of the stimuli. As hypothesised, it was found that activity patterns in the visual cortex scaled to different levels of brightness and those in the motor cortex scaled for force levels, and they were best fit to a 1-2 dimensional representation. The patterns therefore showed a multiplicative scaling with the experimental manipulated factor (Figure 2.7a). In the second experiment (see Chapter 4) participants produced four finger sequences, which differed only in the sequential order of finger presses. In all areas with above chance classification accuracy, there were no voxel patterns that scaled

with a single factor (Figure 2.7b). Hence, I was able to distinguish between true representations and above chance classification accuracy that is due to multiplicative scaling.

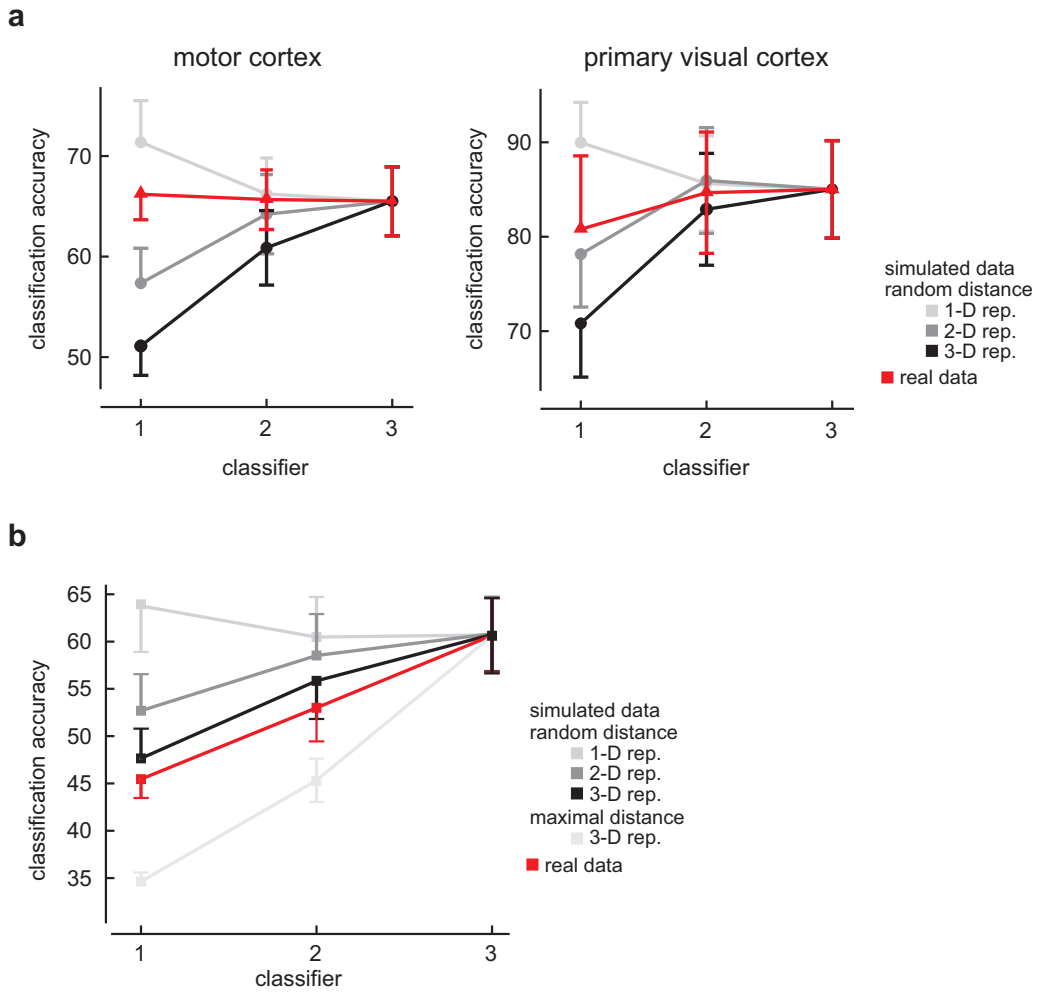

Figure 2.7: *Experimental data validates that it is possible to measure the dimension of a representation.*
Classification accuracy of a linear classifier that can use 1-3 dimensional (x-axis) of the experimental data (red). For comparison, simulated data of a 1, 2 and 3 dimension is shown in grey. **(a)** Experiment with a 1-dimensional manipulation: Participants performed finger presses of different force levels and perceived visual stimuli of different brightness levels. The representations (red) in the motor cortex (left) and primary visual cortex (right) show the hypothesised 1-2 dimensional representations. **(b)** Experiment with a 3-dimensional manipulation: Participants performed different finger sequences (Chapter 4). The voxel activity patterns in the dorsal premotor cortex (red) show a representation that is closest to the 3-dimensional representation of the simulated data.

2.5 Decomposition

A closer understanding of the nature of the neural representation can also be gained using a relatively novel method of multivariate analysis, called representational similarity analysis (Kriegeskorte et al., 2008a). The core idea of this method is to determine dissimilarities between activity patterns of different experimental conditions. The relationships between patterns is then expressed in a dissimilarity matrix $S \in \mathbb{R}^{Q \times Q}$. This matrix can be understood as a fingerprint of the information or representation of a brain region. Consider that a brain area that categorises visual objects such as faces and animals. This brain area would show similar voxel activity patterns if faces are presented. Likewise if animals were presented, this area would show patterns of activation that are nearly equal. Thus, activity patterns of faces would be highly correlated and correlations between voxel activity patterns of animals would be high as well. However the correlations between face patterns and animal patterns would be low. Each entry in the dissimilarity matrix $S_{i,j}(i = 1, \ldots, Q,\ i \in \mathbb{N};\ j = 1, \ldots, Q,\ j \in \mathbb{N})$ is usually estimated by $S_{i,j} = 1 - corr(y_i, y_j)$. This indicates how dissimilar the activity patterns between conditions ($y \in \mathbb{R}^{1 \times P}$) of different experimental condition $1, \ldots, Q$ (for example visual stimuli) in this local region are. With these dissimilarity matrices, one can study representational structures that are based on different measurements such as computational models, electrophysiological recordings or functional imaging with each other. This is possible because the second order representations in the form of dissimilarity matrices and not the raw data are compared. Thus the similarity matrix can be a powerful tool to connect computational models, behavioural data and brain activities with each other (Kriegeskorte et al., 2008b).

However, it is obvious that this approach does not allow contrast of

dissimilarity matrices with each other quantitatively. Even if the same input source is used, such as fMRI voxel activity patterns, it is statistically invalid to compare the absolute values of the dissimilarity matrices of different brain areas with each other. The underlying problem is that distance measures like sample correlations do not measure similarities directly and are highly influenced by other factors. One factor could be unspecific scanner noise. Such noise would reduce correlations between activity patterns. In contrast, factors that can increase the correlation between patterns are unspecific but common to activity patterns. Such common patterns would lead to increased correlations between activity patterns. Usually these problems are avoided by comparing ranks of correlations, for example the spearman rank correlation, instead of absolute values.

For understanding the structure of representations in detail it is however of great interest to be able to compare the absolute and not only the relative values of correlations across different brain areas. In this section, I will describe a novel method that makes it possible to estimate the true correlation between voxel activity patterns. The resultant correlations can be compared quantitatively across brain areas, which allow us to answer interesting questions about the computational nature of representations.

The core idea of the new method is to define a generative model that divides the observed patterns in *pattern components* of noise, conditions and other factors. Importantly these pattern components are not treated as vectors of unknown constants but as random variables. Each random variable is fully described by a probability distribution that has a mean and variance across the voxels and a covariance to other pattern components. Based on the sample covariance of the observed data, it is possible to calculate the unbiased variances and covariance of pattern components directly. Using these estimates, the true correlations between pattern components can be

determinated. This method was developed in cooperation with Diedrichsen et al. (2011) and has been successfully applied to the functional imaging data in Chapter 3 and 5.

Before I demonstrate the new technique, I will define the variables and assumptions of the generative model and explain the basic problem of a traditional correlation analysis in more detail.

The observed input patterns are arranged into a matrix $Y \in \mathbb{R}^{N \times P}$, where P is the number of voxels and N the number of *independent* trials which had been observed. A single row $y^r \in \mathbb{R}^{1 \times P}$ in this matrix shows the spatial activity patterns over P voxels of a single trial, for example the voxel activity pattern during index finger movements. On the other hand, a column vector $y^c \in \mathbb{R}^{N \times 1}$ indicates how a single voxel p ($p = 1, \ldots, P$, $p \in \mathbb{N}$) varies its activity across different trials such as thumb, index, middle and little finger movements. To simplify later notations y^r and y^c are defined as column vectors ($y^r \in \mathbb{R}^{P \times 1}$ and $y^c \in \mathbb{R}^{N \times 1}$). Furthermore each trial is associated with an experimental variable $z_n \in \mathbb{R}^{Q \times 1}$ and combined into a design matrix $Z = [z_1, \ldots, z_N]^T \in \mathbb{R}^{N \times Q}$. Now the following generative model can be defined:

$$Y^{N \times P} = Z^{N \times Q} * U^{Q \times P} + E^{N \times P} \tag{2.11}$$

with $U \in \mathbb{R}^{Q \times P}$ as the pattern components matrix for the Q experimental effects, whereas each row u_q^r, $q = 1, \ldots, Q \in \mathbb{N}$ is a single pattern component for a specific experimental effect. The noise $E \in \mathbb{R}^{N \times P}$ of voxels, is assumed to be independent and identical over trials $\epsilon_p^c \sim N(0, I\sigma_\epsilon^2)$.

It becomes clear that there are $Q \times N$ unknown variables but only N measurements in this model. Consequently, it is impossible to solve this

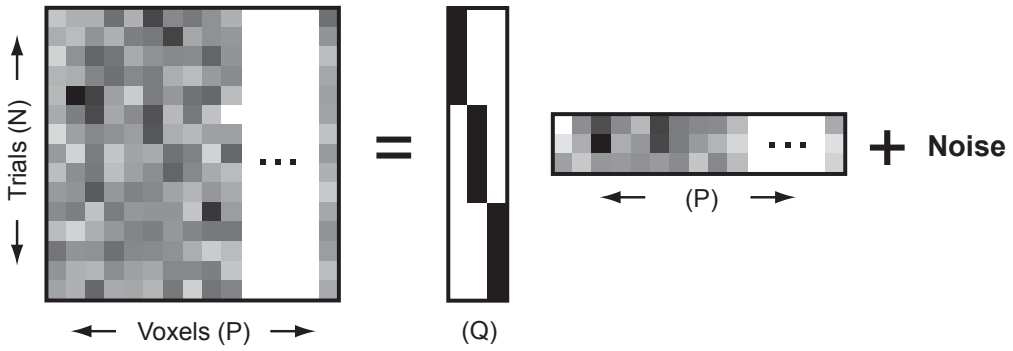

Figure 2.8: *Illustration of the generative model for a one-factorial design with three conditions (reproduced from Diedrichsen et al. (2011))*

equation directly for the pattern components. However, we are not interested in a direct calculation of the pattern components but aim to estimate the variance and covariance directly, which are associated with the pattern components. The idea is to treat the components as random variables across voxels. A random variable is described by a probability distribution and across the P voxels each column $u_p^c \in \mathbb{R}^{Q\times 1}$ in U is defined to be normally distributed with mean $a \in \mathbb{R}^{Q\times 1}$ and covariance $G \in \mathbb{R}^{Q\times Q}$:

$$u_p^c \sim \mathcal{N}(a, G)$$

For mathematical convenience, u_p^c should have a normal distribution with zero mean. This normalisation is possible because each pattern component has its own mean and the estimates of a are independent of G. The mean vector

a can be calculated with:

$$a = \frac{\sum_p y_p^c}{P}$$

Given a we simply subtract a from each column y^c in Y. Finally, without a loss of generality it can be assumed that y_p^c have normal distributions with zero mean and a covariance matrix:

$$var(y_c^p) \quad = \quad var(Zu_c^p + \epsilon_c^p) \quad = \quad Zvar(u_c^p)Z^T + var(\epsilon_c^p) \quad = \quad ZGZ^T + I\sigma_\epsilon^2$$

The model that I just described is a random effects model. This model was used to reformulate the problem of estimating unknown pattern components into the problem of estimating the unknown variance-covariance matrix G of the components. In case of an unconstrained G, such random effect models can be solved with an Expectation-Maximisation (Laird et al., 1987) algorithm. However, in order to enforce assumptions onto the pattern components it needs to be possible to constrain G. Note, that a covariance matrix is by definition a positive definite matrix. Therefore, all constrains have to insure that G is a positive definite matrix. This problem can be solved by replacing G with AA^T and putting all constraints onto A instead of G. The details of the full expectation maximisation algorithm will not be explained here, but interested readers are advised to read the Appendix in (Diedrichsen et al., 2011) for technical details of the algorithm.

To demonstrate the method I use a simple example and explain afterwards the random effects model that was used for the functional imaging data in Chapters 3 (and 5). Consider the following hypothetical data set of a one-factorial experiment with three different conditions. The aim is to

study how similar a region represents two of these conditions. If a brain area represents the two conditions in a similar way it is expected to find a high correlation between the voxel activity patterns of these conditions. Additionally it is of interest to investigate how the representational structure differs in other brain areas. To answer these questions a random effects model with one pattern component for each experimental condition was set up, a variance covariance G of the following form:

$$G = var\begin{bmatrix} u_1 \\ u_2 \\ u_3 \end{bmatrix} = \begin{bmatrix} var(u_1) & cov(u_1, u_2) & cov(u_1, u_3) \\ cov(u_2, u_1) & var(u_2) & cov(u_2, u_3) \\ cov(u_3, u_1) & cov(u_3, u_2) & var(u_3) \end{bmatrix} = \begin{bmatrix} \sigma_1^2 & \gamma_{1,2} & \gamma_{1,3} \\ \gamma_{2,1} & \sigma_2^2 & \gamma_{2,3} \\ \gamma_{3,1} & \gamma_{3,2} & \sigma_3^2 \end{bmatrix}$$

and a design matrix Z (see also Figure 2.8):

$$\begin{bmatrix} 1 & 0 & 0 \\ \vdots & \vdots & \vdots \\ 1 & 0 & 0 \\ 0 & 1 & 0 \\ \vdots & \vdots & \vdots \\ 0 & 1 & 0 \\ 0 & 0 & 1 \\ \vdots & \vdots & \vdots \\ 0 & 0 & 1 \end{bmatrix}$$

Assuming that G is known, the true correlation between two patterns could be calculated directly and it would be possible to study how similar these conditions are represented in a brain region. To calculate such correlations the

standard equation can be used:

$$corr(u_i, u_j) = \frac{cov(u_i, u_j)}{var(u_i)var(u_j)}$$

If G is unknown the true correlation cannot be calculated directly. In such a case it is common practice to estimate the sample correlation based on the mean patterns $\overline{y}_i^r$ of the observed conditions. However, these mean patterns are influenced by noise that will shift the sample correlations towards zero. Given the model, this shift can be described analytically and the correlation between two mean patterns i, j is:

$$E(corr(\overline{y}_i^r, \overline{y}_j^r)) = \frac{cov(\overline{y}_i^r, \overline{y}_j^r)}{var(\overline{y}_i^r)var(\overline{y}_j^r) + \sigma_\epsilon^2/n}$$

To demonstrate the effect of noise, five activity patterns (100 voxels) for each condition were generated. These patterns had the following true variance-covariance structure:

$$G = \begin{bmatrix} 1 & 0 & -0.2 \\ 0 & 1 & 0.8 \\ -0.2 & 0.8 & 1 \end{bmatrix}$$

The levels of noise was varied between $\sigma_\epsilon^2 = 0.5, \ldots, 10$. In this simulation (Figure 2.9), the relative order of the correlation is preserved for all noise levels. However, the absolute sizes of the sample correlations are highly influenced by the level of noise. It is therefore statistically invalid to compare sample correlations quantitatively with each other. In contrast the new pattern component model is able to determine the true correlation between the patterns. Even with high noise levels, the model is able to estimate the variance-covariance matrix of the hidden patterns components directly. It

is therefore possible to calculate the true correlation between the activity patterns of conditions (Figure 2.9). Hence, correlations can be compared between different brain areas even if they are influenced by additional factors, such as noise.

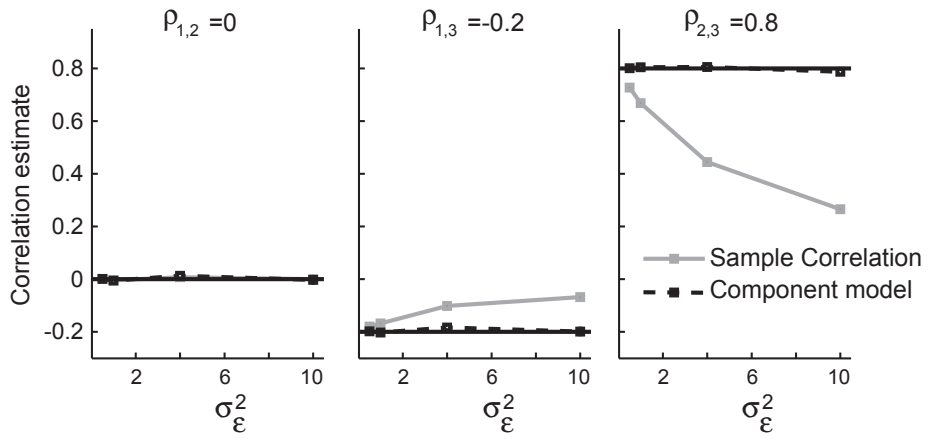

Figure 2.9: *The component model is able to account for different noise levels and estimates the true underlying correlation between activity patterns of stimuli.*
The correlation between stimuli 1 and 2, 1 and 2 and stimulus 2 and 3 are shown. Sample correlations are influenced by the noise level and are unable to estimate the true correlation between the patterns. However the component model can estimate for all noise levels the true correlation. This figure was adapted from Diedrichsen et al. (2011).

In Chapter 3 the pattern component model is used to compare sensory and motor activity patterns of finger representations. I used this dataset to study how much the representations of finger movements and the representations of sensory stimulations have in common. In other words, do similar activity patterns occur during finger movements and during a stimulation of the same finger? Furthermore, do these finger representations interact differently with each other in the cerebellum and the cortex? The study included eight different experimental conditions, which were performed in each of the seven imaging

runs. In the motor conditions individual fingers were moved. In the sensory condition individual fingertips were stimulated. I used four fingers in total. As a first step I studied the sample correlation between the observed motor and sensory activity patterns of fingers. These correlations can be divided into correlations between the same finger and correlations between different fingers (Figure 2.10). This analysis showed that the correlations between cortical activity patterns of sensory and motor conditions were higher when activity patterns of the same fingers were correlated with each other and lower when correlations were based on activity patterns of different fingers. In the cerebellum no difference between the sample correlation of same and different fingers could be found.

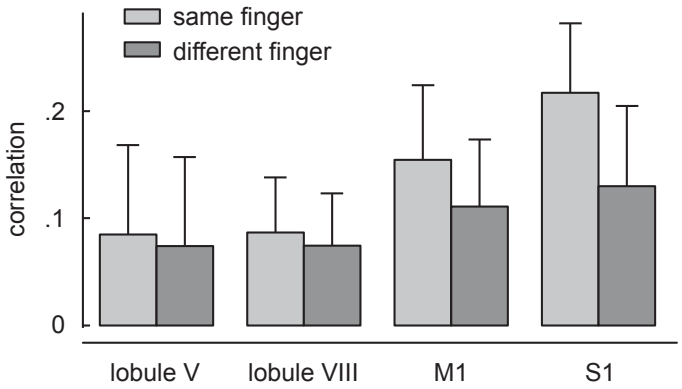

Figure 2.10: *Traditional similarity analysis based on sample correlations* Sample correlations between voxel activity patterns of the sensory and motor condition. Finger patterns of the same fingers correlate higher with each other compared to correlation between different fingers in cortical but not in cerebellar regions.

The comparison of the difference between same and different finger correlations controls for the possibility that sensory and motor pattern have some common activity patterns. However, I discussed before that it is

statistically invalid to compare correlations between regions. Because the level of scanner noise in the cerebellum is expected to be higher, it could be argued that the correlations in the cerebellum are low and differ less from each other because the real correlations are buried under noise. Therefore, the random effects model is used to calculate the true variance-covariance matrix and correlations. I modelled the following experimental effects into the variance-covariance matrix G: 1) All sensory trials share a pattern component $u_{\alpha[1]}$ and all motor trials share a pattern component $u_{\alpha[2]}$. The true correlation between these patterns is modelled with a covariance γ_α. 2) Each finger movement or finger stimulation has its own pattern component $(u_{\beta[1,1]}, \ldots, u_{\beta[1,4]})$ for the stimulation of fingers and $(u_{\beta[2,1]}, \ldots, u_{\beta[2,4]})$ for the movement of fingers. Because the variance of the pattern components can be different for the two conditions, I modelled the variance of the sensory pattern components with $\sigma^2_{\beta[1]}$, whereas the variance of the motor condition is modelled with $\sigma^2_{\beta[2]}$. 3) The same fingers across the conditions share a common covariance γ_β.

$$G = var \begin{bmatrix} u_{\alpha[1]} \\ u_{\alpha[2]} \\ u_{\beta[1,1]} \\ \ldots \\ u_{\beta[1,4]} \\ u_{\beta[2,1]} \\ \ldots \\ u_{\beta[2,4]} \end{bmatrix} = \begin{bmatrix} \sigma^2_{\alpha[1]} & \gamma_\alpha & 0 & \ldots & 0 & 0 & \ldots & 0 \\ \gamma_\alpha & \sigma^2_{\alpha[2]} & 0 & \ldots & 0 & 0 & \ldots & 0 \\ 0 & 0 & \sigma^2_{\beta[1]} & & 0 & \gamma_\beta & & 0 \\ \vdots & \vdots & & \ddots & & & \ddots & \\ 0 & 0 & 0 & & \sigma^2_{\beta[1]} & 0 & & \gamma_\beta \\ 0 & 0 & \gamma_\beta & & 0 & \sigma^2_{\beta[2]} & & 0 \\ \vdots & \vdots & & \ddots & & & \ddots & \\ 0 & 0 & 0 & & \gamma_\beta & 0 & & \sigma^2_{\beta[2]} \end{bmatrix}$$

Additionally, a run effects was added. This became necessary because the sensory and the motor condition were blocked during runs and participants

performed one condition in the first half of a run and the other condition in the second half of a run. Such a design however leads to correlations between the estimation errors of the regression coefficients in runs and conditions. The effect becomes visible when the sample correlations between patterns within a run are calculated and compared to the sample correlations between different runs. The correlations within a run were correlated higher compared to correlations across runs. To control for this effect I included a patterns component for each run i ($i = 1, \ldots, 7 \in \mathbb{N}$) and condition ($u^2_{\delta[1,i]}, u^2_{\delta[2,i]}$) and calculated the variances ($\delta^2_{[1]}, \delta^2_{[2]}$) as well as their covariance γ_δ.

With this model, it was possible to calculate the true correlations between sensory and motor patterns of fingers and finally to compare these correlations quantitatively between the cerebellum and the neocortex (see Chapter 3 for more details).

2.6 Spatial smoothness

Researchers have been able to decode from small clusters that are below the current resolution of fMRI (Swisher et al., 2010). This becomes possible through unequal distribution and spatial grouping of clusters with identical tuning properties. Here I introduce a method to quantitatively measure the size of clusters that are even below the spatial resolution of fMRI.

Imagine a region that shows activity patterns that differ systematically between experimental conditions. Such pattern changes will lead to above chance accuracy in discrimination between conditions. The aim is to estimate the size of the underlying clusters (patches) that made the decoding possible. To measure the size of patches the spatial smoothness of the underlying representation is estimated. This is achieved by first calculating the similarity between each pair of voxels within a region. For example, if two voxels

have similar tuning properties and show high BOLD activity for index finger movements and low activity when all the other fingers move, the activity patterns of this voxel pair will correlate highly with each other. This correlation is estimated between each pair of voxels within a region (Figure 2.11a). The covariance between voxel n and voxel m for c different conditions is given through:

$$cov(n, m) = \frac{1}{c}\Sigma_{i=1}^{c}(n_i - \bar{n})(m_i - \bar{m})$$

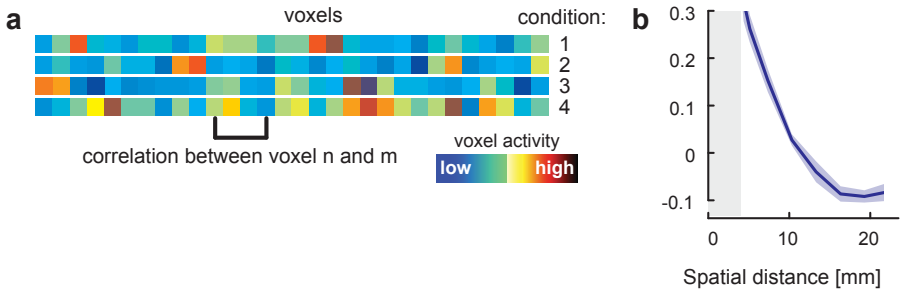

Figure 2.11: *Spatial correlation analysis to measure the size of clusters* **(a)** Voxel activity patterns of four experimental conditions. To estimate the spatial correlation kernel, activity patterns of single voxels are correlated with each other. **(b)** An exemplary auto correlation kernel.

The results are covariance estimates across all voxel pairs. These estimates are then binned according to their distances to each other (Figure 2.11b). To obtain a spatial auto-correlation function, these covariances are also normalised by the variance. In a region that has big clusters of voxels with similar tuning properties, high correlations between non adjacent voxel pairs will exist. As a result, the spatial correlation kernel will be wide and directly reflect the size of the patches. Such a representation can be found in the somato-sensory cortex for individual fingers. The smoothness of the underlying pattern can now be quantitatively expressed using the *full-width-half-maximum* (FWHM) of the spatial convolution kernel. This is achieved by first generating spatially

independent data, which are then smoothed to a certain FWHM. The spatial correlation kernel of the simulated data that fits the spatial correlation of the data best is defined as the FWHM of the data.

In summary, the FWHM is a quantitative measure to express the size of underlying clusters.

2.7 Topology

An alternative, and more traditional approach to identify brain areas that represent certain variables, is to search for topological arrangements. The underlying hypothesis is that a brain region that represents for example finger movements should reveal a distinct cluster of activation when individual fingers are moved. If these finger clusters differ in their spatial location and if the finger clusters show a spatial arrangement that is similar to the arrangement of fingers on a hand, we would say that this area represents individual fingers and has a *topological* arrangement. Most importantly, we would expect to find an equivalent topological arrangement in every participant. This means the development of these neuronal representations must be universal across different individuals and is therefore likely to be caused by the interaction between genetic rules and learning.

Finding topological representations can be difficult and a statistical validation of topological arrangements has yet not been defined. Some researchers report maps for individual participants to visually demonstrate topologies in brain area (e.g. Schluppeck et al., 2006). However, topologies are often studied on group level (e.g. Grodd et al., 2001). In such an approach, individual maps, for example activation maps of individual fingers are smoothed and group T-maps for each condition are estimated. To visualise topology an arbitrary threshold is applied on T-maps and clusters of peak

group T-values of individual finger representations are visually inspected. Using this method, (Grodd et al., 2001) demonstrated a topological ordering of fingers in the cerebellum.

Another methodological problem with this approach is that it is possible to reveal a topology with random data. To further illustrate this, imagine a patch of cortex that is equally active whenever any of the five fingers are moved. However the activity shows no topological information and is random without any true connection to the finger movements. It is clear that this patch would not encode or represent finger movements. Using traditional analysis, the data is smoothed and group T-maps are estimated for each finger movement. With this procedure the peak T-value of fingers will be at different locations. Furthermore, the peak T-values could show a spatial arrangement by chance that is similar to the arrangement of a topology. This means that it is possible to discover topological arrangements although the underlying data is random. Therefore, it is problematic to report topologies that are defined on group maps and individual levels. In general, both traditional methods, viewing topologies on the group level but also demonstrating topology in single subjects, are missing statistical validation.

During my doctoral theses, I became interested in the topological arrangement of individual fingers in the cerebellum (Chapter 3). The representation is characterised by distinct voxel activity patterns for each finger. Pattern differences do not have to originate from a systematic ordering of activation clusters for each finger, but can be composed out of small local variations in the voxel activity. Hence, topological arrangements are special cases of representations that are identified through MVPA. The obvious question to ask is if the finger representations in the cerebellum are based on a topological arrangement. In the following section, I will describe methods that I applied to improve the identification of topology and show how these

findings can be validated with statistics.

The first problem is to define candidate regions that might show a topological order of the experimental stimuli. In the previous example, I demonstrated that it is possible to find a topology in an uninformative area. To locate informative regions that represent the experimental stimuli by distinct activity patterns, a classification approach combined with a searchlight can be used. A classifier signals that the patterns of activation are systematically different between experimental conditions. Regions that represent experimental condition through a topology will have distinct activity patterns for fingers and will therefore also show high classification accuracy. Classification is therefore a useful tool to identify candidate areas for topological arrangements.

In the course of my study, I found two representations in the cerebellum that represented individual finger movements (see Chapter 3). The representations in the cerebellum are generally small. Additionally the cerebellar cortex is highly folded and a single voxel ($2.3mm^3$) will stretch over millions of neurons. Thus, a topology in the cerebellum might be small as well. Given the current fMRI resolution it will be difficult to study a topology of fingers in individual map with clusters of finger activity or peak activations. A more robust measure is the centre of gravity (CoG) of individual fingers because it takes into account all voxels in a region of interest.

$$CoG_x = \frac{\sum_i^N \beta_i \cdot x_i}{1/N \cdot \sum_i^N \beta_i}$$

$$CoG_y = \frac{\sum_i^N \beta_i \cdot y_i}{1/N \cdot \sum_i^N \beta_i}$$

$$CoG_z = \frac{\sum_i^N \beta_i \cdot z_i}{1/N \cdot \sum_i^N \beta_i}$$

whereas, $[x_i, y_i, z_i]$ are the coordinates of voxel $i \in \{1, ..., N\}$ and β_i the voxel activity.

Because CoGs can be highly influenced by scaling factors such as the amount of voxel activity it will be difficult to compare the CoG between fingers. The reliability of CoGs can be improved by normalising the voxel activity of finger maps. I used a softmax function to normalise voxel activity:

$$w_{(i,j)} = \frac{e^{k\beta_{i.j}}}{\sum_{m=1}^{conditions} e^{k\beta_{i,m}}}$$

The idea is to replace the activity β of each finger j and each voxel i by a weight $w_{i,j}$ that is set in relation to the other fingers activities. In the extreme case, ($k \gg 0$) the softmax function would assign a 1 to the finger for which the voxel was most highly activated, and a 0 to all other fingers. In the analysis of cerebellar finger representations k was set to 0.8. This resulted in a softer assignment and accounted for the overlapping finger representations in the cerebellum. The coordinates of the CoGs are estimated separately for each participant and finger. To test statistically if a region has a topological arrangement of fingers it needs to be tested if the CoGs are different and if the spatial arrangement is similar for each participant. A test statistic that provides such an answer is a *multivariate analysis of variance (MANOVA)*. Using *Wilks lambda* it can be tested if CoGs of fingers are arranged systematically across participants. In contrast to the traditional method, where maps were inspected purely visually, I have now a test statistic to validate these findings.

In sum, it is difficult to locate areas in which a topological arrangement of experimental conditions can be expected. However, even after locating such areas, one needs to test for a topological arrangement. Because topological

representations are a special type of representations, classification accuracy maps provide a powerful tool to define target locations. Additionally using a MANOVA it is possible to validate topological findings statistically.

Chapter 3

Integration of sensory and motor representations of single fingers in the human cerebellum[1]

[1]This chapter has been published as: T Wiestler, D J McGonigle and J Diedrichsen. Integration of sensory and motor representations of single fingers in the human cerebellum. *J Neurophysiol*, 105(6):3042-3053, 2011.

Abstract

The cerebellum is thought to play a key role in the integration of sensory and motor events. Little is known, however, how sensory and motor maps in the cerebellum superimpose. Here, I investigate the relationship between these two maps for the representation of single fingers. Participants made isometric key presses with individual fingers or received vibratory tactile stimulation to the fingertips while undergoing high-resolution functional magnetic resonance imaging (fMRI). Using multivariate analysis, I demonstrate that the ipsilateral lobule V and VIII show patterns of activity that encode within the same region – both which finger was pressed and which finger was stimulated. The individual finger-specific activation patches are smaller than 3mm and only show a weak somatotopic organisation. To study the superposition of sensory and motor maps, the finger-specific patterns were correlated across the two conditions. In the neocortex, sensory stimulation of one digit elicited activation of the same patches as force production by the same digit. In the cerebellum, these activation patches were organised in an uncorrelated manner. This suggests that, in the cerebellum, a movement of a particular finger is paired with a range of possible sensory outcomes. In sum, these results indicate a small and fractured representation of single digits in the cerebellum, and suggest a fundamental difference in how the cerebellum and the neocortex integrate sensory and motor events.

3.1 Introduction

The cerebellum is thought to play an important role in sensory-motor integration (Bastian, 2006; Wolpert et al., 1998). The sensory and motor representations of individual fingers in the human cerebellum have been studied in detail with fMRI. Studies have shown that both the anterior and posterior motor regions of the human cerebellum are activated during hand movements (Grodd et al., 2001; Rijntjes et al., 1999). The same regions are also activated – albeit to a much lesser degree - during noxious stimulation (Casey et al., 1996), passive finger movements (Mima et al., 1999; Thickbroom et al., 2003), and vibro-tactile stimulation (Fox et al., 1985; Tempel and Perlmutter, 1992). However, none of these investigations have been able to answer the question whether the cerebellum contains a representation of individual finger movements comparable to those in primary sensory and motor cortex (Indovina and Sanes, 2001; Kaas et al., 1979; Merzenich et al., 1987; Woolsey et al., 1979). If the human cerebellum indeed contains such a map, one should be able to detect different activity patterns for different fingers, and determine how sensory and motor maps superimpose.

Due to the limits on spatial resolution of fMRI, the detection of small and potentially unordered representations constitutes a challenge. In the primary somato-sensory cortex, digit representations are arranged in an orderly sequence of patches with diameters of 4-5mm, and can thus be detected by comparing the activation maps for each finger (Sanchez-Panchuelo et al., 2010). In the cerebellar cortex, however, such finger representations may be smaller and less well organised. For example, based on data from the rat whisker system, some authors have argued that the cerebellar sensory representations are small and fractured (Bower and Woolston 1983). Conversely, others have argued for a more systematic organisation. For instance, stimulation

of the forepaw of cats activates an ordered sequence of parasaggital cerebellar microzones – that is, groups of Purkinje cells with the same climbing fibre input (Apps and Garwicz, 2005). These microzones also receive matched mossy fibre input (Pereira et al., 2009). There is, however, general agreement that such representations are smaller than those found in the cerebral cortex.

While our knowledge of the origin of the cerebellar BOLD signal is still limited, recent evidence indicates that mossy fibre and parallel fibre signalling is the main determinant of activity-induced BOLD changes (Attwell and Iadecola, 2002; Diedrichsen et al., 2010; Zhang et al., 2003). Therefore, BOLD signal from the cerebellar cortex most likely reflects the spatial patterns of sensory and motor input to the granule cell system.

Given the small spatial scale of digit representations, how can they be best detected using fMRI? Although the cerebellum may lack an orderly map of individual digits, groups of microzones that respond preferentially to a particular finger are likely to be clustered together in space. Such clusters are referred to as *digit patches*. It is important to note three possible characteristics of these digit patches: first, there may be multiple patches for the same digit within a region; second, these multiple single finger patches may overlap with patches for other digits; and third, these patches may be arranged without any somatotopic gradient. Because the spatial arrangement of such digit patches is likely to differ across individuals, they cannot be detected employing traditional univariate analysis. Such analysis would require the existence of areas in which there are systematic activation differences between fingers across participants (e.g., a region where, relative to other fingers, thumb movement always leads to more activation).

In contrast, local multivariate pattern analysis (Kriegeskorte et al., 2006) can be used to identify regions in which participants show significantly different finger-related patterns, even if these do not superimpose in a finger-by-finger

fashion in a group analysis. Furthermore, multivariate analysis can also identify regions in which these finger-specific patterns consist of local signal increases and decreases, without changing the activation level of the region overall (Figure 3.1a). In this way, this method relates closely to the criterion employed in neurophysiology, in which a region is considered to be involved in a task if its neurons modulate (i.e., either increase or decrease) their firing rates in relation to an experimental variable, even if the average activity in the region does not change and if the spatial distribution of these modulations differs across individual brains. Multivariate analysis has been successfully employed in the visual system to study neural representations that are small and do not systematically align across individuals (Cox and Savoy, 2003; Haxby et al., 2001; Haynes and Rees, 2005b; Kamitani and Tong, 2006; Kriegeskorte et al., 2008b; Swisher et al., 2010); however, this is the first application of this technique in the cerebellum. Using multivariate analysis, I was able to reveal overlapping sensory and motor representations of single digits in two ipsilateral regions of the cerebellum, in lobule V and lobule VIII. Subsequently, I studied the characteristics of these digit representations in detail and investigated three main issues. First, I compared the results of the multivariate analysis to traditional mass-univariate approaches, which show a part-dissociation between finger-specific modulation of activation patterns and the overall size of the activation. Secondly, I investigated how sensory and motor maps superimpose. Thirdly, I examined the size of the digit patches in the cerebellum and tested for possible somatotopic gradients. In all of these analyses, the characteristics of the cerebellar digit representations were compared to those found in the primary somato-sensory cortex and motor cortex. The results of this study suggest a fundamental difference in the representation of digits in the human neocortex and the cerebellum, with important implications on how these regions relate sensory and motor information.

3.2 Methods

3.2.1 Participants

Seven right-handed, neurologically healthy volunteers, including 5 males and 2 females, participated in the study (age range 20-22). The ethics committee of the School of Psychology, Bangor University, approved all experimental procedures. The cortical data of these participants have been used as example data in a method paper describing the surface-based searchlight technique (Section 2.2.2 and Oosterhof et al. 2010), and both cortical and cerebellar data were used in a technical note on the decomposition method (Section 2.5 and Diedrichsen et al. 2011).

3.2.2 Apparatus

To stimulate individual fingertips and to record individual finger forces, an fMRI-compatible device with five piano-style keys was developed. Each key had a small groove into which the fingertip could be placed. Within the groove was a hole through which a small pin (1mm radius) could be vibrated with finely controlled frequency and amplitude using a piezo motor. The forces applied to the keys were recorded via quantum tunnelling composite pills (Maplin Electronics Ltd., Rotherham, South Yorkshire, ref. N18BU). The stimulation box was operated from outside the scanning room, with a filter panel preventing leakage of RF noise into the MRI environment. The visual instructions and feedback were projected from outside the scanner room onto a back-projection screen, which was viewed by the participants through a mirror.

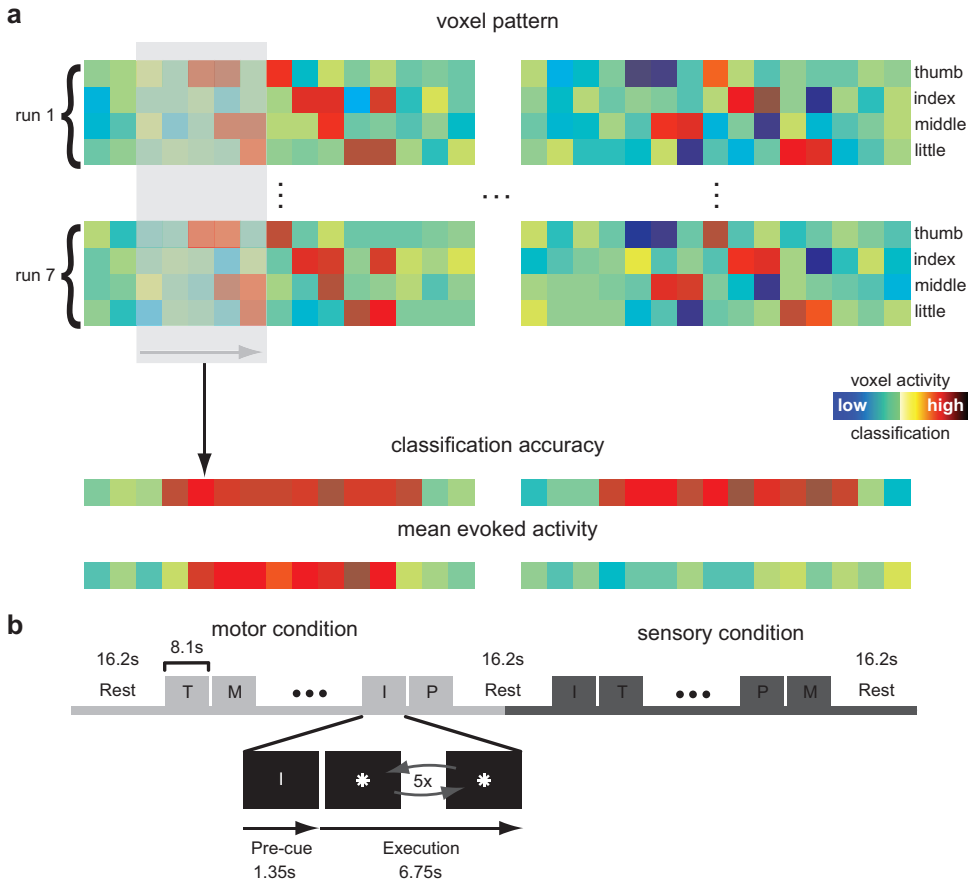

Figure 3.1: *Experimental methods*
(a) Detecting finger representations using multivariate analysis. Each row indicates the activation pattern induced by finger presses or sensory stimulation in two hypothetical neural regions. In each region, there is a finger-specific BOLD pattern that is replicable across multiple imaging runs. The search-light (grey box) method picks continuous groups of voxels and detects the presence of a local informative voxel pattern, which is expressed as classification accuracy. The region on the left has only finger-specific BOLD increases and therefore shows increased activity when comparing all fingers against rest. The region on the right shows both signal increases and decreases, which cancel each other out, such that there is no overall evoked activity. Multivariate analysis can detect the finger-specific modulation of neural activity in both cases. **(b)** In the motor condition, participants isometrically pressed keys five times with the finger indicated by an instruction cue (T thumb, I index finger, M middle finger and for P little finger), which were replaced by an asterisk during execution, to minimise visual cortex activation. In the sensory condition, a vibratory stimulus of 100Hz was applied five times to the selected fingertip. In each functional MRI run, both conditions were performed in a counterbalanced order, which were separated by short rest phases.

3.2.3 Scan acquisition

The imaging data were acquired on a Phillips Achieva 3T scanner (Philips, Best Netherlands). For the functional scans, an echo planar imaging sequence (EPI) with a voxel size of 1.8x1.8x2mm was used. Data acquisition for the cerebellum and the cerebral cortex took place in two separate sessions. Each region was covered with 38 axial slices (no gaps; TR=2.7s), using sensitivity encoding with a factor of 2 (Pruessmann et al., 1999). Runs started with 6 dummy scans and consisted of 128 data images. The T1 weighted structural images were acquired with a volumetric MPRAGE sequence using a voxel size of 1x1x1mm.

3.2.4 Task design

We used an event-related design (Figure 3.1b) with stimulation and motor conditions. In designing the tasks, an attempt was made to minimise movement in the stimulation condition and the contribution of sensory information in the motor condition. Accordingly, in the motor condition, the participants were asked to produce repeated isometric presses with one finger (Figure 3.1b) against a key equipped with a force sensor. Therefore, the main residual sensory information in the motor condition was the stimulation of Golgi tendon organs and Merkel receptors. In the stimulation condition, a 100Hz vibrotactile stimulus was delivered to the glabrous skin of a single fingertip, thereby activating mostly Meissner and Pacinian receptors (Johnson, 2001), and minimising the risk of overt movement.

3.2.5 Procedure

Before the scan acquisition, all participants underwent a training session of 4 runs in which they were familiarised with the task. Subsequently, they

participated in two counterbalanced scanning sessions (one session for the cortex and one for the cerebellum), which were separated by at least 12 hours. Each scanning session comprised 7 runs, each of which consisted of 16 force trials and 16 stimulation trials, separated by a pause of 16.2s (Figure 3.1b). The sequence of conditions was counterbalanced across runs and participants. A single trial lasted 8.1s, and within each condition, every finger was repeated 4 times in randomised order. To obtain sufficient repetitions for each finger, only digits 1,2,3, and 5 were used and the ring finger was excluded from the experiment. Each trial started with a red letter on the screen to indicate the digit to be pressed or stimulated. During the motor condition, participants generated 5 isometric key presses with the indicated finger. Presses were paced by the appearance of a white asterisk on the screen every 1.35s and required a force >1N to be registered. The asterisk turned green if participants pressed the correct finger and red otherwise. In the stimulation condition, a vibratory stimulus was applied every 1.35s for 0.94s, five times to a single fingertip. The stimulation frequency was 100Hz, with small pauses of 20ms inserted every 110ms to minimise the possibility of central or peripheral habituation. As in the motor condition, a white asterisk was presented as a visual pacing signal. The onset of the vibratory stimuli was jittered within an interval of -200 to +200ms around the presentation of the asterisk to reduce habituation. The stimulation intensity was individually adjusted so that the subjective stimulation intensity was comparable across fingers.

3.2.6 Imaging data analysis

The functional imaging data were analysed with SPM5 (http://www.fil.ion.ucl.ac.uk/spm/, Friston et al. (1993)) and custom written routines in MATLAB (The MathWorks, Inc., Natick, MA). The

slices were first realigned in time to correct for the ascending order of slice acquisition. The images were then spatially realigned to the first functional image of the session using a six-parameter rigid-body transformation. To remove slowly varying trends, high-pass filtering was applied to the data, with a cut off frequency of 1/128s. The spatially unsmoothed data were fitted using a linear model, with regressors that represented the 4 trials of each finger (separately for motor and stimulation conditions) within each run. These regressors were boxcar functions (length 8.1s), convolved with the standard hemodynamic response function. The resultant beta estimates (regression coefficients), indicated how much each voxel changed its activation for each run, condition, and finger, and were used as data for the multivariate analysis. Finally, the functional images were co-registered to the individual anatomical images (Collignon et al., 1995). To distinguish between functional data from the primary somato-sensory and motor cortices, special care was taken that the alignment was exact at the central sulcus, and hand correction was applied as necessary (see Figure 3.2 for individual alignments).

For the group analysis, three different methods of inter-subject alignment were applied. First, the cortical data were normalised by aligning the individual anatomical images to the Montreal Neurological Institute (MNI) template with a non-linear segmentation and normalisation algorithm (Ashburner and Friston, 2005). Second, the cortical surface of left hemisphere of each subject was reconstructed, inflated to a spherical representation and finally aligned to average surface-based atlas using the program Freesurfer (Dale et al., 1999). This normalisation ensured a good overlap of the fundus of the central sulcus across participants. Third, for the cerebellar data, we isolated the cerebellum from the rest of the brain and aligned the data to a high-resolution cerebellum-only template (SUIT Diedrichsen, 2006).

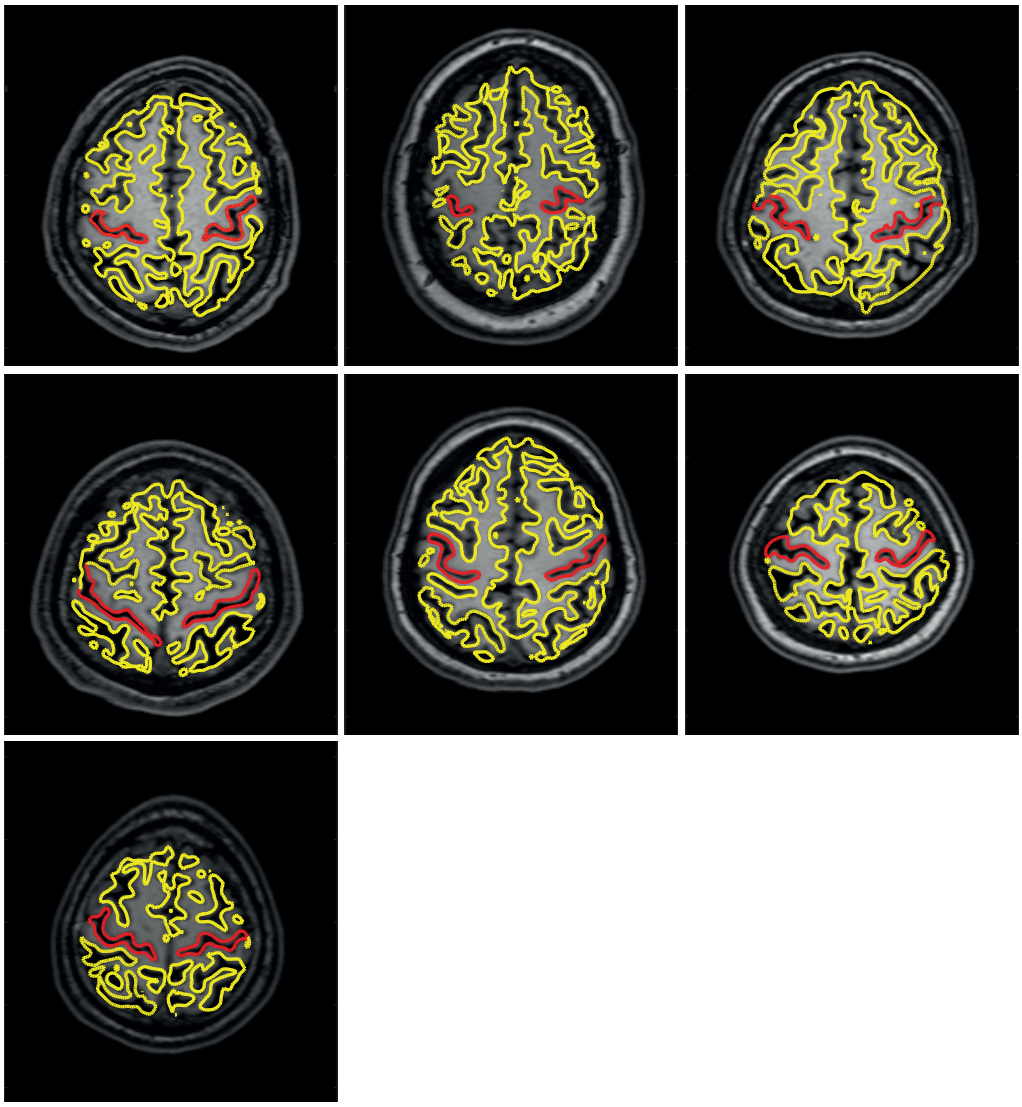

Figure 3.2: *Alignment between anatomical and functional data*
The contour of functional images (yellow) is exactly aligned in participants central sulcus(red). Alignments are shown for an axial slice.

3.2.7 Classification

To detect digit representations in the cerebellum and neocortex, a group of spatially contiguous voxels was selected for each participant individually and separately for the motor and stimulation conditions. It was then tested whether the activity patterns across these voxels differed significantly between digits. This was achieved using a linear classifier (Haxby et al., 2001; Haynes and Rees, 2005a; Misaki et al., 2010).

Inputs to the classifier were the 4×7 pattern vectors x_i, the beta-estimates for a set of N voxels for each finger and run. The classifier was trained with 24 pattern vectors from 6 runs. From this training data, the overall $N \times N$ voxel-covariance matrix Σ and the $N \times 1$ mean vectors of the four classes (fingers) μ_c were estimated. Because Σ was ill-conditioned, it was necessary to regularise the covariance estimate by adding a small constant (1% of the mean of the diagonal elements) to the diagonal. This regularisation made the covariance matrix invertible, while still retaining the advantage that noisy or highly correlated voxels were down-weighted (Pereira et al., 2009).

The discriminant function for each class g_{c_i} is, up to a constant, the log-likelihood that the pattern x belongs to class c_i

$$g_{c_i}(x) = \mu_{c_i}^T \Sigma^{-1} x - \frac{1}{2} \mu_{c_i}^T \Sigma^{-1} \mu_c.$$

As test patterns the four remaining digit patterns of the *left out* run were used. The test pattern x was assigned to the class c with the maximum likelihood:

$$\hat{c} = \arg\max_{c_i}(g_{c_i}(x)).$$

By retraining and cross-validating over all possible test- and training-sets, the average cross-validation accuracy for each set of voxels was determined. All classification accuracies reported here are based on this cross-validation approach, thereby providing a statistically unbiased measure of how much information a voxel neighbourhood contains about which finger moved or was stimulated.

3.2.8 Volume-based searchlight

For the identification of digit representations in the cerebellar cortex, a volume-based searchlight approach (Kriegeskorte et al., 2006) was utilised. The data for the classification came from a 6mm sphere around a chosen centre voxel, which included 145 voxels. All calculations were restricted to cerebellar voxels using an automatic masking algorithm provided by the SUIT toolbox (Diedrichsen, 2006). The classification accuracy was calculated for each group of voxels and assigned to the centre voxel of the sphere. By moving the sphere through the whole volume, an accuracy map was generated. Voxel neighbourhoods (i.e. groups of voxels) that consisted of less than 10 voxels were excluded from the analysis.

3.2.9 Surface-based searchlight

The two main regions for digit representation in the cerebral cortex are the primary somato-sensory and motor cortices. Anatomically these regions are clearly separated by the central sulcus, but they abut each another volumetrically. A volume-based searchlight, as employed for the cerebellum, would therefore combine voxels from both primary somato-sensory and motor cortices into a single classifier. To measure the information content of these regions separately, we implemented a surface-based searchlight method (see section 2.2.2 and Oosterhof et al. 2010). We started with a representation of the pial surface and the grey-matter-white-matter boundary, which were generated by the program Freesurfer (Dale et al., 1999). For each surface node, it was then determined all nodes within a certain radius, with the distance measured along the intermediate surface (Peyre, 2008). The classification was then based on voxels that enclosed the selected nodes, either from the white or pial surface. For each centre node, the radius was adjusted such that each

searchlight contained 145 voxels. The cross-validation accuracy of the classifier was assigned to the centre node. By moving the centre node across the surface, a surface map of classification accuracies was generated.

3.2.10 Regions of interest

To compare the organisation of digit representations across different regions, an anatomically defined region-of-interest approach was used. I focused on four regions that revealed significant digit representations: the left primary somato-sensory (S1) and motor cortices (M1), and right lobules V and VIII of the cerebellum. The cortical regions were defined on a surface representation, guided by anatomical cytoarchitectonic evidence (Geyer et al., 2001). For the motor cortex, the region between the fundus of the central sulcus and the crest of the precentral gyrus, encompassing approximately Brodmann area 4, was selected. For the primary somato-sensory cortex, the region between the fundus of the central sulcus to the crest of the postcentral gyrus, encompassing Brodmann area 3b, and parts of 3a and 1, was selected. Both regions were defined on the surface representation along the whole length of the central sulcus. As for the surface-based searchlight, all voxels that included any node of the region either on the Pial or white-matter surface were selected. Despite this surface-based definition, there was a single layer of voxels in the middle of the central sulcus that was included in both regions. To minimise the overlap, these voxels were excluded from both the primary somato-sensory and motor cortex region-of-interest.

The cerebellar regions were defined based on a probabilistic atlas of the cerebellum (Diedrichsen et al., 2009). Because I was only interested in functional signal from grey matter, only voxels that were assigned a probability of ≥ 0.1 of being grey matter in the probabilistic tissue segmentation

(Ashburner and Friston, 2005) were included. This relatively low threshold ensured that all voxels partially consisting of grey matter were included, while voxels that were clearly situated in white matter were rejected.

3.2.11 Representational similarity pattern component model

To assess the superposition of the sensory and motor maps, correlations between stimulation and motor pattern were calculated (Haynes and Rees, 2005b; Kriegeskorte et al., 2008a; Mur et al., 2009; Norman et al., 2006). I compared the average correlations between the stimulation and motor pattern for the same digit with the correlation for different digits.

When comparing correlations – or differences of correlations – across different regions, it is important to account for other factors that can influence these coefficients: for example, regions with high levels of fMRI noise will generally show lower correlations and lower differences of correlation. Alternatively, strong activation common to all conditions may increase correlations artificially. To account for these factors, a novel method that decomposes patterns into different components was used (see Section 2.5 and Diedrichsen et al. 2011). The 56 measured patterns ($y_{i,j,k}, i^{th}$ condition x j^{th} digits x k^{th} run) were modeled as the sum of a component that was common to all digits within each condition (c_i), a component that was unique to the finger in each condition ($f_{i,j}$), and noise components shared by all trials in a run $r_{i,k}$, as well as an independent noise component $\varepsilon_{i,j,k}$.

$$y_{i,j,k} = c_i + f_{i,j} + r_{i,k} + \varepsilon_{i,j,k}$$

The variance and covariance of these components across voxels was then estimated from the data. The finger components ($f_{i,j}$) captured the patterns

unique to force production or stimulation of each digit. The variance for the stimulation, σ^2_{f1}, and for the motor condition, σ^2_{f2}, and the covariance of patterns across the two conditions for the same digit, $cov(f_{1,j}, f_{2,j}) = \gamma_f$ were estimated. Because the non-specific determinants of the correlations were captured in the pattern component for the condition, noise, and run, the corrected correlation coefficient $\gamma_f / \sigma_{f,1} \cdot \sigma_{f,2}$ served as a direct measure of the similarity of finger patterns, normalised by the strength of the finger patterns in this region.

Using Monte-Carlo simulations, it was ensured that these estimates – in contrast to the sample correlations – were not influenced by changes in noise level, number of informative voxels, or spatial size of digit patches (Diedrichsen et al., 2011). Thus, the new method allowed one to compare across different anatomical regions how similar the pattern evoked by isometric presses with a digit was to the pattern evoked by stimulating the same digit.

3.2.12 Spatial correlations

To compare the size of finger patches quantitatively across regions, we used the estimates of the pattern components (Equation 3.1) to calculate the spatial covariance between each pair of voxels within a region. For example, for the finger component the covariance estimate between voxel n and voxel m is:

$$cov_f(n, m) = \frac{1}{4} \sum_{i=1}^{4} (f^n_{i,j} - \bar{f_{i,j}})((f^m_{i,j} - \bar{f_{i,j}}) \tag{3.1}$$

The covariance across voxel pairs was then averaged, depending on spatial distance. Bins from 0.1-2.5mm (directly neighbouring), 2.5-3.6mm (diagonally neighbouring), up to a total distance of 23.8mm, were used. The covariance was normalised by the variance to obtain a spatial auto-correlation function.

The smoothness of the underlying pattern component was expressed using the full-width-half-maximum (FWHM) of the spatial convolution kernel which – when used to smooth spatially independent data – resulted in the best fitting spatial auto-correlation function (Section 2.6; Diedrichsen et al., 2011). Again, Monte-Carlo studies were conducted so that the width of the spatial kernel could be estimated with relatively high accuracy, independent of the level of noise.

3.2.13 Somatotopy

Within the digit-related area of each anatomically defined region of interest, I searched for a somatotopic organisation. As for the other analyses, the digit-related area was defined by selecting the voxels with the 20% highest classification accuracy in the region, and the biggest spatially contiguous cluster was selected from these. For each condition, a weight was assigned to every voxel i for every finger condition j using a softmax function across all fingers.

$$w_{i,j} = \frac{e_{k\beta_{i,j}}}{\sum_{m=1}^{4} e^{k\beta_{i,m}}}$$

In the extreme case, ($k \gg 0$) the function would assign a 1 to the finger for which the voxel was most highly activated, and a 0 to all other fingers. Considering the likely overlap of different digit patches, k was set to 0.8, resulting in a softer assignment. Similar results were obtained for a range of k from 0.6 to 1. The Centre of Gravity (CoG) for each finger was calculated as the mean coordinate of all voxels weighted by $w_{i,j}$. To be able to compare locations across participants, the individual voxel coordinates were transformed to a standard atlas space SUIT (Diedrichsen, 2006) for the cerebellar regions and MNI152 for the cerebral regions.

3.3 Results

3.3.1 Finger representations in the human cerebellum

Sensory and motor representations in the cerebellar cortex were expected to be relatively small, and possibly unordered. To detect such representations, multivariate analysis was employed to obtain a digit information map. This map showed whether the activity patterns evoked by different digits differed systematically from each other and, therefore, revealed whether the region encoded for (or contained information about) the pressed or stimulated finger.

In the cerebellum, the resulting maps of cross-validation accuracy showed two areas with above-chance accuracy in the ipsilateral, right hemisphere, for both motor and stimulation conditions (Figure 3.3a). These clusters were located in lobule V and lobule VIII and were significant in a random-effects group analysis, corrected for multiple tests (Table 3.1).

Additionally, a region in right Crus I crossed the threshold of statistical significance in the stimulation condition (Table 3.1). However, the same region was not present in the motor condition. Although it is possible that a third region for tactile processes exists, this region was not analysed further here, because the main aim was to investigate the relationship between sensory and motor maps. In sum, these results show the existence of at least two overlapping motor and sensory representations of individual digits in the cerebellar cortex.

3.3.2 Finger representations in the human neocortex

A similar analysis was conducted for the neocortical data. An extended area with high classification accuracy was found along the central sulcus (Figure 3.4a, b). The main part of both sensory and motor representation is located

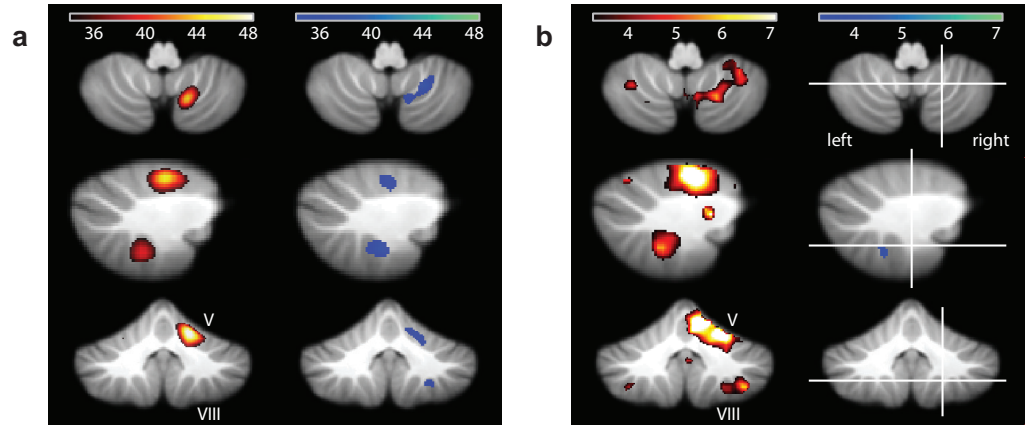

Figure 3.3: *Digit representations in the human cerebellum*
Two digit representations in the human cerebellum revealed by local multivariate pattern analysis. **(a)** Multivariate analysis showed two regions (Lobule V and VIII) that contained information about individual fingers in the motor (red) and stimulation (blue) conditions. The group-average maps demonstrated the cross-validated classification accuracy (threshold 34%, chance 25%). **(b)** Traditional mass-univariate analysis showed strong responses in the motor (red), but not in the stimulation (blue) condition. Group t-map of the evoked BOLD signal for task vs. rest in motor (red) and stimulation conditions (blue), shown at an uncorrected threshold of $t_{(6)} = 3.14$, $p = 0.01$. The results are presented on axial (z= - 49), parasaggital (x= 21) and coronal (y= -52) slices of the SUIT template (Diedrichsen, 2006)

.

in S1, encompassing a substantial portion of the post-central gyrus. A digit representation was also visible in M1, with the best classification accuracies located at the bend of the pre-central gyrus, within the so-called hand knob (Yousry et al., 1997).

Neocortical digit representations were localised with a surface-based searchlight. This technique minimised the mixing of voxels from different sides

Table 3.1: Cerebellar regions showing significant classification accuracy across participants.

					SUIT		
Side	**Area**	**Size (cm^3)**	**$P_{(cluster)}$**	**Peak $t_{(6)}$**	**X**	**Y**	**Z**
Motor condition							
right	Lobules V	0.84	0.001	5.94	16	-54	-24
right	Lobules VIII	0.4	0.036	8.46	10	-70	-40
Stimulation condition							
right	Lobules V	0.53	0.008	6.29	22	-54	-26
right	Lobules VIII	0.38	0.042	7.04	28	-44	-50
right	Crus I	0.41	0.029	10.56	40	-50	-38

Random effects analysis of classification accuracy in motor and stimulation conditions. Clusters are identified at a uncorrected threshold of $p < 0.004$, $t_{(6)} > 3.89$, and corrected for multiple comparisons over the volume of the cerebellum using the cluster-size (Worsley et al., 1996). The coordinates reflect the location of the peak of the cluster in SUIT space (Diedrichsen, 2006).

of the central sulcus within a single classifier (see Section 2.2.2 and Oosterhof et al. 2010). Hence, the informative regions in M1 and S1 could be mapped fairly independently.

3.3.3 Evoked activity vs. information content

To compare the cortical and cerebellar digit representations quantitatively, regions-of-interest were defined for cerebellar lobules V and VIII, M1, and S1 based on anatomical criteria (see methods 3.2.10) for each participant. Within these regions, digit representation was defined for each condition by selecting the 20% of voxels with the highest accuracies in each region. The information content (assessed by average classification accuracy) for these voxels was substantially higher in the neocortical compared to the cerebellar regions (Figure 3.5a). The classification accuracy in S1 was slightly higher for

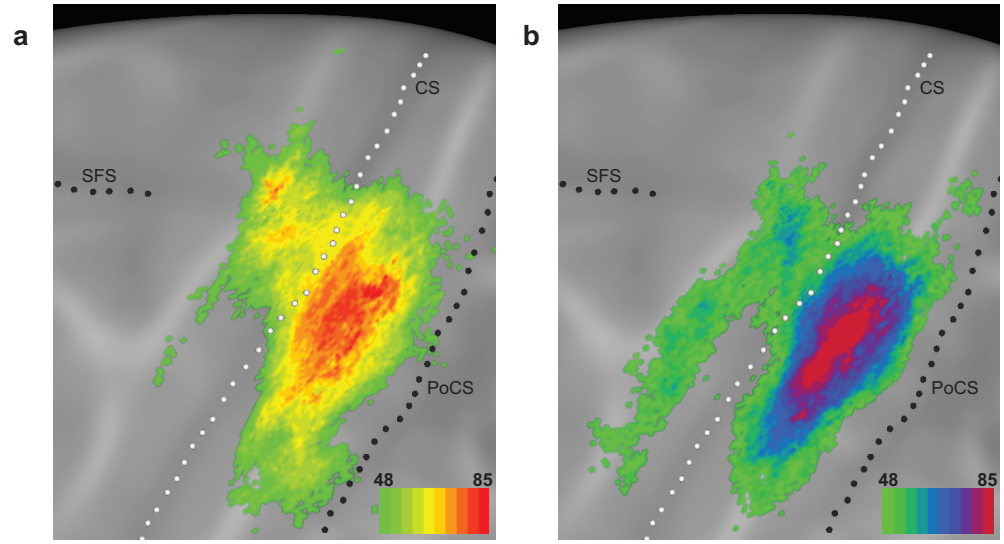

Figure 3.4: *Digit representation in S1 and M1 revealed by local multivariate pattern analysis*
The group average maps show the cross-validated classification accuracy on an inflated cortical surface for **(a)** motor and **(b)** stimulation conditions. Accuracy is shown at a 48% threshold. CS: Central Sulcus, PoCS: Post central Sulcus, SFS: Superior frontal sulcus.

the sensory than for the motor condition. In contrast, the motor condition yielded slightly higher accuracies in lobule V. However, none of the differences between the conditions were significant (for all regions, $t_{(6)} < 1.704$, p> 0.139). Thus, the strength of the systematic modulation of different neural patches, as assessed by the classification accuracy, was roughly matched across motor and stimulation condition.

In contrast, the overall task-related activity (averaged over all digits and compared to rest, Figure 3.3b) differed substantially between conditions. In the motor condition, strong activity increases were found in the right hemispheric lobule V and VIII, bilaterally in hemispheric lobule VI, and in the vermal regions of lobule VI and VII. For sensory stimulation, however, no significant evoked activity was observed in the cerebellum. Even when the threshold was lowered to an uncorrected level of p<0.01, no clusters above the size of $0.13cm^3$ were visible (corresponding to a cluster-size p-value of 0.997, corrected

for multiple comparison across the cerebellum).

To quantify this observation further, the average percent signal change was extracted in the digit representations, which were defined as before (Figure 3.5b). Isometric finger presses led to robust signal changes in all regions (all $t_{(6)} > 3.864$, $p < 0.002$), whereas sensory stimulation did not (all $t_{(6)} < 2.11$, $p > 0.078$). In the informative region of lobule V, on average, sensory stimulation even elicited slight signal decreases compared to rest. This finding is consistent with previous imaging studies, which found no significant, or only small signal increases, during light tactile stimulation (Fox et al., 1985; Tempel and Perlmutter, 1992).

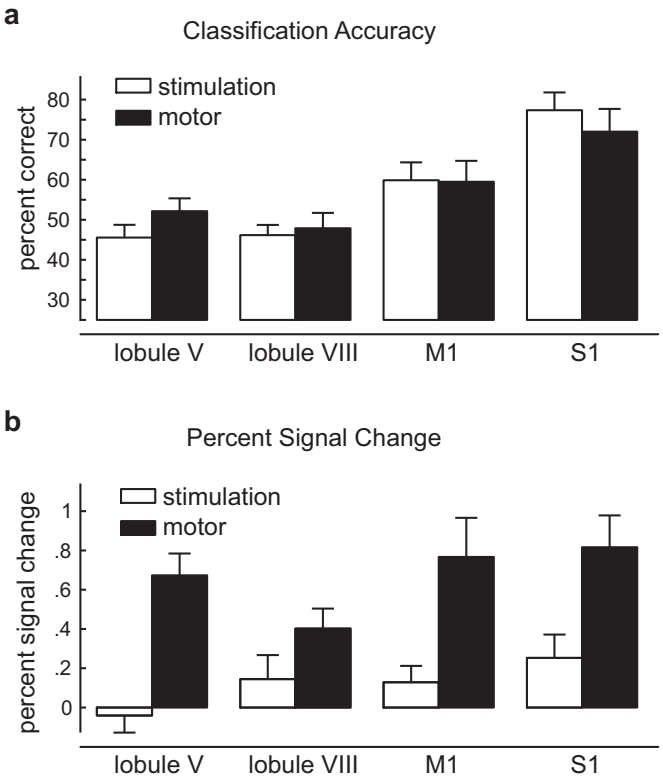

Figure 3.5: *Dissociation of information content and evoked activity*
The digit regions were identified as the voxels with the 20% highest classification accuracies within the anatomically defined regions-of-interests. **(a)** Average classification accuracy for stimulation and motor conditions. **(b)** Average percent signal change (compared to rest) in the same regions. Error-bars indicate between-participant standard error.

These results suggest that the degree to which a region increases its activity overall, and the degree to which it modulates the local activity pattern based on the digit involved, are partly dissociated. In the motor condition, regions with highly informative patterns also showed high overall activity (Figure 3.1a, left). In the stimulation condition, the informative regions did not show large increases in overall BOLD signal during task performance compared to rest. Despite this, the region exhibited strong finger-specific modulation. Thus, it can be concluded that this modulation consisted of both finger-specific increases and decreases, which cancelled each other out when averaging across digits (Figure 3.1a, right).

3.3.4 Integration of sensory and motor information

The group analysis (Figure 3.3 and 3.4) indicated that the areas representing force production and stimulation of single digits overlapped macroscopically in the same areas – both in the neocortex and in the cerebellar cortex. However, how is sensory and motor information integrated in these regions? Specifically, how do activation patterns caused by exerting force and stimulation superimpose? For example, it is possible that the patches of neurons that respond to stimulation of a certain finger also respond to the isometric presses with the same finger. Alternatively, force production and stimulation may activate separate patches that are independently arranged. In such an organisation, a patch that is activated by a ring finger press would not necessarily be paired with a patch that is activated by ring finger stimulation, but may be located adjacent to a patch that is activated by stimulation of the thumb. The use of multivariate analysis allows me to distinguish between these two alternatives.

To assess the similarity between the patterns evoked by force production

and stimulation, the activation patterns of two conditions were correlated across different voxels (Kriegeskorte et al., 2008a). To restrict the analysis to the region that was informative for both motor and stimulation conditions, differences between the fingers were tested for, and the resultant F-values were averaged across motor and stimulation conditions. Subsequently, 20% of the voxels with the highest values were selected. If motor and sensory representations of individual digits were mapped on top of each other, the correlation between stimulation and motor patterns from the same digit should be higher than the correlation between patterns of different digits. If the maps were organised in an independent fashion, no difference in correlation should be present.

These results show a clearly significant difference between same-finger and different-finger correlations (Figure 3.6a) for S1 ($t_{(6)} = 5.18$, $p = .0002$) and M1 ($t_{(6)} = 4.16$, $p = .006$), but no significant difference for lobule V ($t_{(6)} = 1.90$, $p = .11$), and only a small difference for lobule VIII ($t_{(6)} = 2.94$, $p = .026$). While these results may suggest weaker correlations between sensory and motor maps in the cerebellum than in the neocortex, correlations or differences between correlations cannot be simply compared across different regions. This is because factors other than the similarity of sensory and motor representations influence these coefficients. For instance, if the fMRI data were noisier in one region, or if there were fewer informative voxels in that region, correlations, and difference in correlations, would be lower. To account for these effects, the observed patterns were decomposed into different components, each of which had characteristic variance (or power) across voxels (Section 2.5 and Diedrichsen et al. (2011)). After accounting for components of no interest, the correlation between the finger specific components for stimulation and motor conditions could be directly compared.

The decomposition method showed that the estimated variance of the

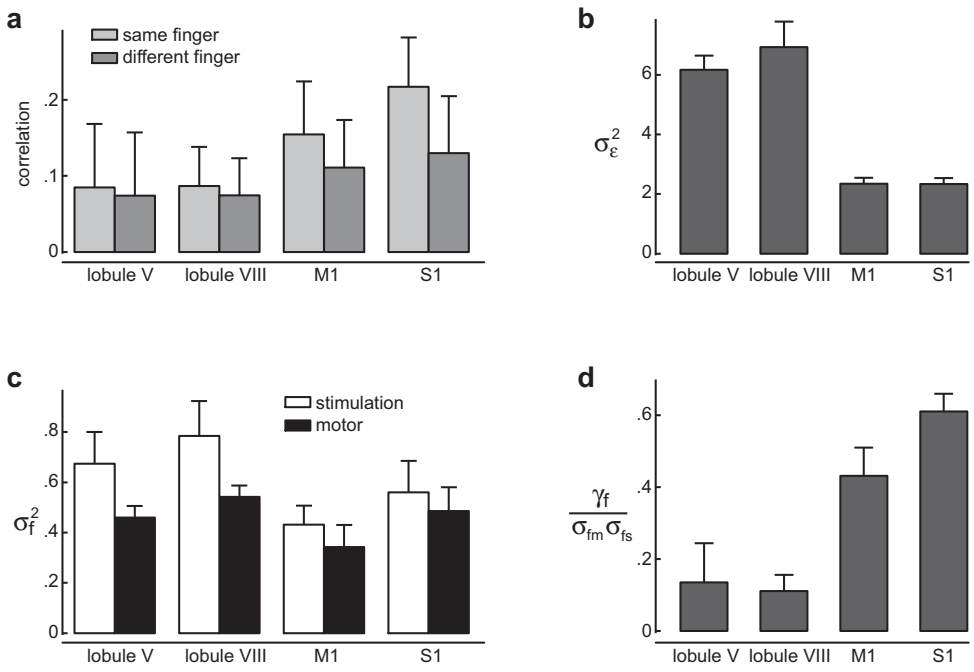

Figure 3.6: *Representational similarity analysis indicates different arrangement of sensory and motor maps in cortex and cerebellum.*
(a) Correlations between average stimulation and motor patterns for the same finger or for different fingers, calculated in digit regions of cerebellar lobule V and VIII, primary somato-sensory (S1), and motor (M1)cortex. **(b)** Result from the variance-decomposition of these correlations. Trial-by-trial noise (σ_ϵ^2) is increased in the cerebellum compared to neocortical regions. **(c)** The variance of the patterns associated with individual fingers (σ_f^2) for stimulation (white) and motor (black) conditions. **(d)** The normalised correlation between motor and stimulation patterns of the same digit is significantly reduced in cerebellar regions.

noise component was 2.5 times higher in the cerebellum than in the neocortex (Figure 3.6b). This effect likely reflects the larger exposure to physiological noise and lower sensitivity of the coil-array for sub-tentorial regions. In contrast, the variances of the patterns encoding specific fingers were roughly equivalent across regions (Figure 3.6c).

Having accounted for these sources of variance, the similarity of motor and stimulation patterns for the same finger could be directly compared across regions (Figure 3.6d). In the neocortex, the corrected correlation coefficient ranged between 0.12 and 0.70. In contrast, the corresponding correlations

for the two cerebellar regions were significantly smaller than in the neocortex ($t_{(6)} = -4.259$, $p = .005$). Thus, this analysis confirms the initial finding with uncorrected correlations was not simply due to increased noise level: in neocortical regions, stimulation and motor conditions must have activated patches of neurons that overlap in a finger-specific fashion. Contrastingly, in the cerebellum, patches that were activated in the motor and stimulation conditions for one particular finger must have neighbouring patches that were activated by the stimulation of a different, unrelated finger. These results indicate a fundamental difference in how sensory and motor events are integrated in cerebellar and neocortical digit areas.

3.3.5 Size of finger patches

How large are these putative finger patches in the human cerebellum? While the size of digit patches in S1 can be visually estimated to be between 4 and 6mm (Nelson and Chen, 2008; Sanchez-Panchuelo et al., 2010), the spatial extent of such patches cannot be assessed easily in the more irregular representations in the cerebellum or M1. One way to quantify the spatial size of digit representations is to calculate the correlation between finger-specific activations for each pair of voxels within an informative region. These correlations can then be plotted as a function of the spatial distance between the voxel pair. If stimulation of each finger activates a larger spatially contiguous groups of voxels, the finger effects should be correlated over longer spatial distances (Figure 3.7a). In contrast, if the patches representing each digit are small (Figure 3.7b), the spatial correlations should fall rapidly to zero as spatial distance increases. One can estimate the smoothness of the underlying maps (in terms of the full-width-at-half-maximum, FWHM) from these spatial correlation functions (Diedrichsen et al., 2011).

The spatial correlations functions for the finger pattern component (Figure 3.7c) revealed that in cortical regions, finger information was correlated over larger spatial distances than in the cerebellum. The FWHM of the spatial kernel in S1 was estimated to be 5mm, and in M1 4.1mm; a small but significant difference, $t_{(6)} = 2.97$, $p < 0.05$. This result was specific to the finger effect and not found in the noise of condition effect component. By contrast, the finger information in cerebellar voxels was essentially uncorrelated (FWHM=2.6mm; significantly different from cortical regions, $t_{(6)} = 7.04$, $p < 0.05$). Positive correlations were found for distances up to 3mm (indicating neighbouring voxels). These correlations, however, can be accounted for by head movements, and the necessary spatial realignment, which induced a statistical dependence between the data of neighbouring voxels (Grootoonk et al., 2000). Thus, it can be concluded that representations of single digits in the cerebellum are smaller than the effective resolution of 3mm.

3.3.6 Somatotopy of finger representations

Thus far, the results indicate that digit patches in the cerebellum are small and arranged such that motor and sensory representations correlate with each other far less than in the neocortex. However, this independent arrangement does not preclude the existence of a systematic somatotopic gradient. Even in M1, where digit movements are represented in a highly overlapping and inter-digitated fashion (Rathelot and Strick, 2006; Schieber, 2002), systematic differences in the centroids of activation for different digits movements have been found (Indovina and Sanes, 2001; Schieber and Hibbard, 1993).

To test whether there is also a somatotopic gradient for single digits in the human cerebellum, for each participant and condition the centre of gravity (CoG) of the activation caused by each of the 4 tested digits was

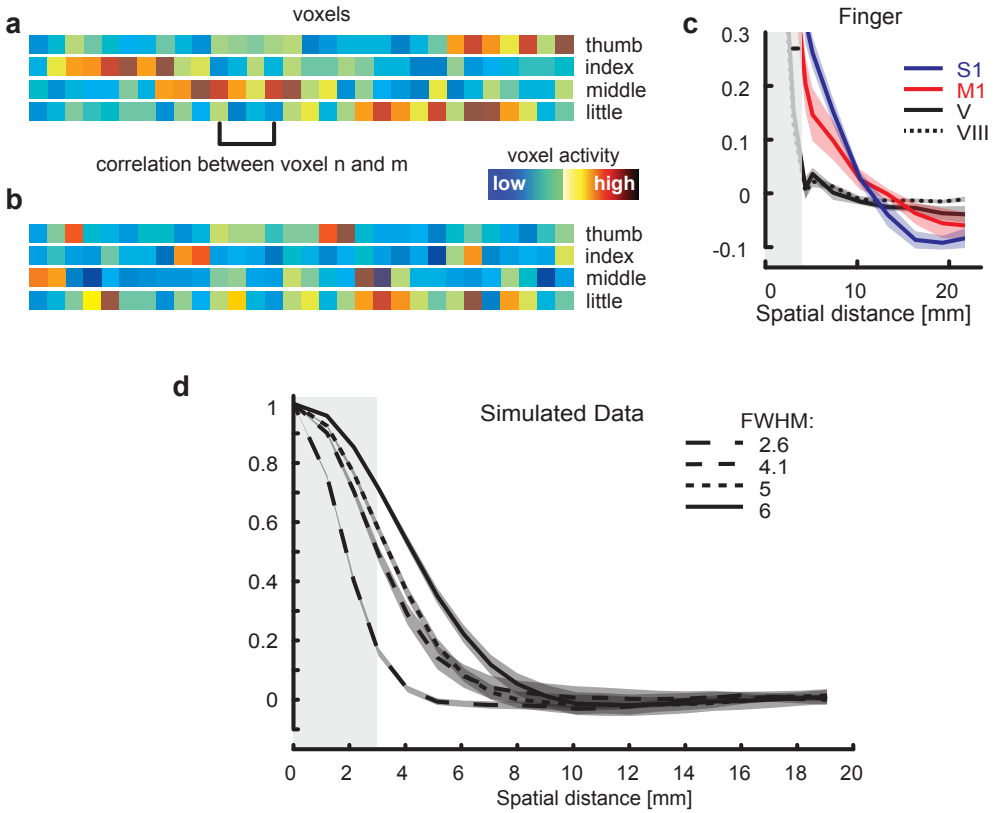

Figure 3.7: *Spatial correlation analysis reveals different sizes of digit patches in the neocortex compared to the cerebellum.*
(a) Hypothetical voxel activity related to individual fingers. If a finger activates a large patch of voxels, the correlation between voxel pairs will be positive up to a distance that relates to the size of the digit patch. **(b)** If fingers activate small and scattered patches, the correlation will be absent for larger spatial distances. **(c)** Correlation of voxel pairs within an informative region as a function of the spatial distance of the pair. Correlations were calculated separately for the estimates for the finger component. No significant differences between motor and stimulation conditions were found; therefore, the presented data are averaged across conditions. Shaded areas indicate between-participant standard error. The vertical grey bands demarcate the distances for neighbouring voxels, for which correlations are induced by motion correction and resampling of the images. **(d)** Autocorrelation kernel of simulated data with a FWHM of 2.6, 4.2, 5 and 6.

calculated. When displaying these CoGs for lobules V in a common atlas space (Figure 3.8a), no clear spatial organisation was observed. The centre of the informative region (as indicated by spatial average location of the digit CoGs for each participant) varied substantially in medio-lateral direction between

individuals (Figure 3.8b). However, when aligning the CoGs for each subject by subtracting out this overall centre, a topography became apparent (Figure 3.8c), with the CoG for D1 being located more medially and for D5 more laterally. To test this observation statistically, a repeated measures MANOVA on the x, y, and z coordinates of the CoGs was used. For the motor condition in lobule V, there was a systematic difference in the location of the finger CoGs (see Table 3.2). This result provides the strongest evidence to date for a somatotopic gradient in the digit representations in the cerebellum. Grodd et al.(2001) reported a similar ordering for lobule V; however, these observations were based on a group map and were not statistically substantiated. No systematic gradient could be found in lobule VIII.

The somatotopic gradient in lobule V was compared to those found in neocortical regions, using the effect-size (η^2) of the MANOVA as a parameter of the strength of the gradient (Table 3.2). The strongest gradient was detected in S1, with D1 being represented most ventrally and D5 represented most dorsally (Nelson and Chen, 2008; Sanchez-Panchuelo et al., 2010). In comparison, the gradient found in lobule V was substantially weaker, and more similar in strength to the one found in M1 (Figure 3.8d), where a lateral to-medial D1-D5 gradient could be detected (see also Indovina and Sanes, 2001). Overall, these results argue for a weak somatotopic organisation of finger representations in the anterior, but not posterior, hand region of the human cerebellum.

3.4 Discussion

These results establish the existence of two overlapping representations for active force production and passive sensory stimulation of single digits in the human cerebellum: in the ipsilateral hemisphere of lobule V and in lobule VIII. In the capuchin monkey (Cebus paella), both of these regions have been shown

Table 3.2: Cerebellar regions showing significant classification accuracy across participants.

	Stimulation condition			**Motor condition**		
Area	$\Lambda(3,3,18)$	p	η^2	$\Lambda(3,3,18)$	p	η^2
Sensory cortex	0.39	**0.059**	0.61	0.13	**<0.001**	0.87
Motor cortex	0.66	0.598	0.34	0.29	**0.011**	0.71
Lobules V	0.42	0.089	0.58	0.22	**0.002**	0.78
Lobules VIII	0.76	0.855	0.24	0.66	0.621	0.34

The first column reports Wilks Λ as a statistical test of whether there is a systematic difference in the spatial x,y,z location of the CoGs for the 4 fingers. P-values are derived from a standard χ^2-approximation (Pearson and Hartley, 1976). Effect size η^2 indicates the percent variance explained (after subtraction of the between-participant factor).

to receive input from – and provide output to – the hand area of primary motor cortex (Kelly and Strick, 2003).

The identification of digit representations that are close to the spatial resolution of fMRI and that do not show a systematic spatial arrangement across individuals was made possible by employing multivariate analysis techniques (see also Kamitani and Tong, 2006; Kay et al., 2008). Rather than searching for areas that increase in overall BOLD signal compared to a control condition, multivariate analysis identifies regions where the pattern of activations or deactivations differs systematically between experimental conditions. This approach is similar to that employed in many neurophysiological analyses: a neural area is considered to be involved in a task if the population of neurons encodes the factor of interest, even if it does not increase activity during the task.

These results highlight the difference between information-based mapping and more traditional analysis techniques. For example, a number of regions

were found that reliably increased activity in the motor condition, but were not detected in the information-based analysis. One such example is the posterior vermis (lobule VI & VIII), which has been recently shown to receive input from parts of the primary motor cortex (Coffman and Strick, 2009) that relate to the proximal, rather than distal, musculature. These results are consistent with this notion, as no representation of individual digits was detected in this region. Another site is lobule VI, which was consistently activated bilaterally during force production (Desmond et al., 1997; Diedrichsen et al., 2005a), but did not show evidence of single-digit representations. This region may respond preferentially to more complex movements (Schlerf et al., 2010) and may be involved in movement preparation and planning (Hulsmann et al., 2003).

For vibratory stimulation, regions were found that did not notably increase the overall BOLD-signal, but modulated the activity pattern systematically with the stimulated digit. Although some modest increases were found in average activity in lobule VIII, these were far below the statistical threshold when correcting for multiple comparisons (Fox et al., 1985; Tempel and Perlmutter, 1992). This finding can only be explained by the fact that vibratory stimulation led to systematic and finger-specific local increases and decreases in activation, which, when averaged over the whole area, cancelled each other out (Fig. 1a, right panel). This is congruent with observations that vibrotactile stimulation can lead both to local increases and decreases of mossy fibre activity (Eccles et al., 1972).

One possible methodological confound in the study is that the activity in the motor condition not only reflected motor processes, but also sensory input. While the keyboard was designed to minimise sensory feedback, it is impossible to eradicate the sensory information that is provided by Golgi-tendon organs, muscle spindle and Merkel discs during an isometric finger press. Given these results, however, it appears that the BOLD signal

in the motor condition reflected mostly motor processes, as the overall BOLD signal was much stronger than in the sensory condition. This difference was also present in other studies, which compared active to passive movement (Mima et al., 1999; Thickbroom et al., 2003). Thus, while sensory information may have contributed to the BOLD signal activation, it is likely that active force production was the main determinant of the BOLD activity in the motor condition. Furthermore, the lack of correlation between motor and sensory patterns in the cerebellum is likely not simply due to the fact that the two conditions activated different sensory channels: in the neocortex, sensory and motor patterns correlated highly. While these results need to be replicated with other forms of sensory stimulation, these results can be taken to reflect an interaction between motor and sensory processes.

Interestingly, the classification accuracy for the motor condition seems to be more extended in S1 compared to M1 (Figure 3.4). This result is surprising at first glance, and raises the question whether M1 actually encodes individual finger movements, as I have assumed in the presented decoding model. Alternatively, M1 could encode muscle programs (movement synergies) that are eventually combined to produce individual finger movements.

Neurons in S1 represent fingers in topological clusters that are, for most individuals, visible by simply colouring voxels according to the finger to which they respond highest. When analysing the underlying tuning function of S1 voxels, it can be seen that voxels are mainly active when a certain finger is involved, and that they have less BOLD signal for all other finger movements. Additionally, voxels with similar tuning are spatially closer together and finger representations are more clustered in S1. Thus, using individual finger movements in an experimental design triggers this representation optimally. It is therefore not surprising that S1 shows robust classification accuracy in this study.

In contrast, when M1 voxels are coloured by the most active finger, no finger clusters are visible. This result suggests that the tuning functions of M1 and S1 differ fundamentally. In M1, the tuning function of fingers is of higher complexity and voxels do not respond exclusively to only one finger movement. This is consistent with results from neurophysiological recordings from this area, which show that individual neurons always respond to multiple fingers (Schieber, 2002). Importantly, both the S1 and the M1 tuning functions can result in highly distinguishable voxel activity patterns of fingers and, therefore, lead to high classification accuracy. The results of the current study show that the strength of the classification accuracy is not different between S1 and M1. Rather, the cortical area that allows differentiation between fingers is larger in S1. The bigger finger clusters, which have been found in S1 but not M1 can, in part, explain the extended representation of classification accuracy in S1.

To demonstrate a quantitative difference between the encoded information in M1 and S1, a similarity matrix of finger patterns of the two areas could be compared with each other. If similar tuning properties or similar information were present, the similarity matrix of the two regions would reveal identical correlation patterns between finger pairs. In contrast, if a different type of information were encoded in these areas, the similarity matrix of finger pairs would be different. A possible result of this analysis could be that voxel activity patterns in S1 show very low correlations with each other, whereas voxel activity patterns in M1 correlate, depending on the movement synergies that they share.

A further way to test this idea would be to design specific experimental conditions, which may show higher classification accuracy in M1. (Ingram et al., 2008) studied the natural statistics of hand movements. From this data, they extracted the movement combinations that form the building blocks of every-day movements ((see also Gentner and Classen, 2006). Using these

movement primitives as experimental conditions may, therefore, lead to a high classification accuracy in M1, but not S1.

In addition to the identification of sensory and motor digit representations, the multivariate approach allowed the investigation of the features of these representations in detail. These results suggest a fundamental difference between digit representations in human neocortex and cerebellum, with several important characteristics (summarised in Figure 3.9).

First, analysis of the spatial correlation of finger effects shows that the size of digit patches in S1 is around 5mm and slightly smaller in M1 (Figure 3.7). These figures are in accordance with results from monkey neurophysiology (Kaas et al., 1979; Sur et al., 1982) and human fMRI studies (Nelson and Chen, 2008; Sanchez-Panchuelo et al., 2010). In the cerebellum, it was found that the patterns encoding finger information were uncorrelated across voxels. This argues that these representations exist at a spatial scale below the effective spatial resolution of our fMRI data (taking into account motion realignment, 3mm). This result is consistent with neurophysiological studies which suggest that sensory representations in the cerebellum are small and possibly fractured (Apps and Garwicz, 2005; Bower and Woolston, 1983). Although it cannot be excluded that the differences in representations in the cerebellum compared to the neocortex were partly caused by the more complex folding structure of the cerebellum, this idea would have predicted that the spatial correlations would be higher in the direction of the folia (roughly horizontal in lobule V) than across this direction. No such spatial dependence was found, however.

Second, a somatotopic gradient was shown in lobule V of the cerebellum, where the digit representations were arranged in a medial to lateral order. This gradient was only significant in the motor condition, and was not present in lobule VIII. These findings are in accord with an earlier fMRI study that used a traditional group analysis (Grodd et al., 2001). At first inspection,

the presence of a somatotopic gradient may seem at odds with the small and fractured representation highlighted in our other analyses. The presence of a gradient, however, does not imply that individual digits are represented in separate patches of neurons with a strict somatotopic ordering. A gradient of similar strength was found in M1, where digit movement led to activity in strongly overlapping population of neurons (Schieber, 2002; Schieber and Hibbard, 1993). Thus, a weak somatotopic gradient can indeed occur within a region without a strict ordering of clearly delineated digit patches.

Third, these results show that the representations involved during passive sensory stimulation and during active force production are differently arranged in the cerebellum and the neocortex, although they overlap in both areas on a macroscopic scale. In the neocortex, it was demonstrated that the pattern elicited by pressing a particular finger was similar qualitatively to the pattern elicited by sensory stimulation of the same finger. This indicates that patches that are activated by sensory stimulation are also active during isometric contraction of the same finger (Figure 3.9a). In contrast, this correlation was significantly smaller in the cerebellum.

Given the results of a different arrangement of sensory and motor representations in the neocortex and cerebellum, what underlying neurobiological architectures might give rise to these findings? One possibility is that sensory and motor processes activate separate sets of neuronal maps. However, given that the cerebellum is often considered to be a site where sensory and motor information are integrated (Gao et al., 1996; Wolpert et al., 1998), such architecture would be surprising. Furthermore, in the group analysis, the informative regions for motor and stimulation condition overlapped substantially, and no significant difference in mean location was found. One can suggest that these results are congruent with the following arrangement (Figure 3.9b): cerebellar digit patches that modulate their

responses during active motor output and during passive stimulation may be closely inter-digitated. However, patches that are activated by action of a particular digit directly neighbour or even overlap with patches that are activated by sensory stimulation of a different digit. Thus, sensory and motor patches referring to the same finger would not overlap with much higher probability than sensory and motor patches of unrelated fingers. Such an organisation would account for the finding of macroscopic spatial overlap but low correlation between patterns.

What could the computational function of such an inter-digitated arrangement be? In the neocortex, the movement of each digit is closely paired with the most likely sensory consequence of that action - sensory stimulation of the same finger. Contrastingly, in the cerebellum, movement of a digit may lead to activity in neurons that are also activated by a variety of different sensory consequences, ranging from stimulation of other fingers to even sensory input from the arm or face. Such an arrangement may enable the cerebellum to quickly generate new associations between movements and relatively arbitrary, remote sensory consequences. This is a key computational requirement for learning new motor tasks, in which actions and outcomes can take on novel relationships. Consistent with this functional hypothesis, cerebellar patients are severely and specifically impaired on such tasks (Diedrichsen et al., 2005b; Smith and Shadmehr, 2005). In sum, the way motor and sensory events are represented may support the quick learning of action-outcome associations (i.e., forward models), which has been hypothesised to be the main computational function of the cerebellum (Wolpert et al., 1998).

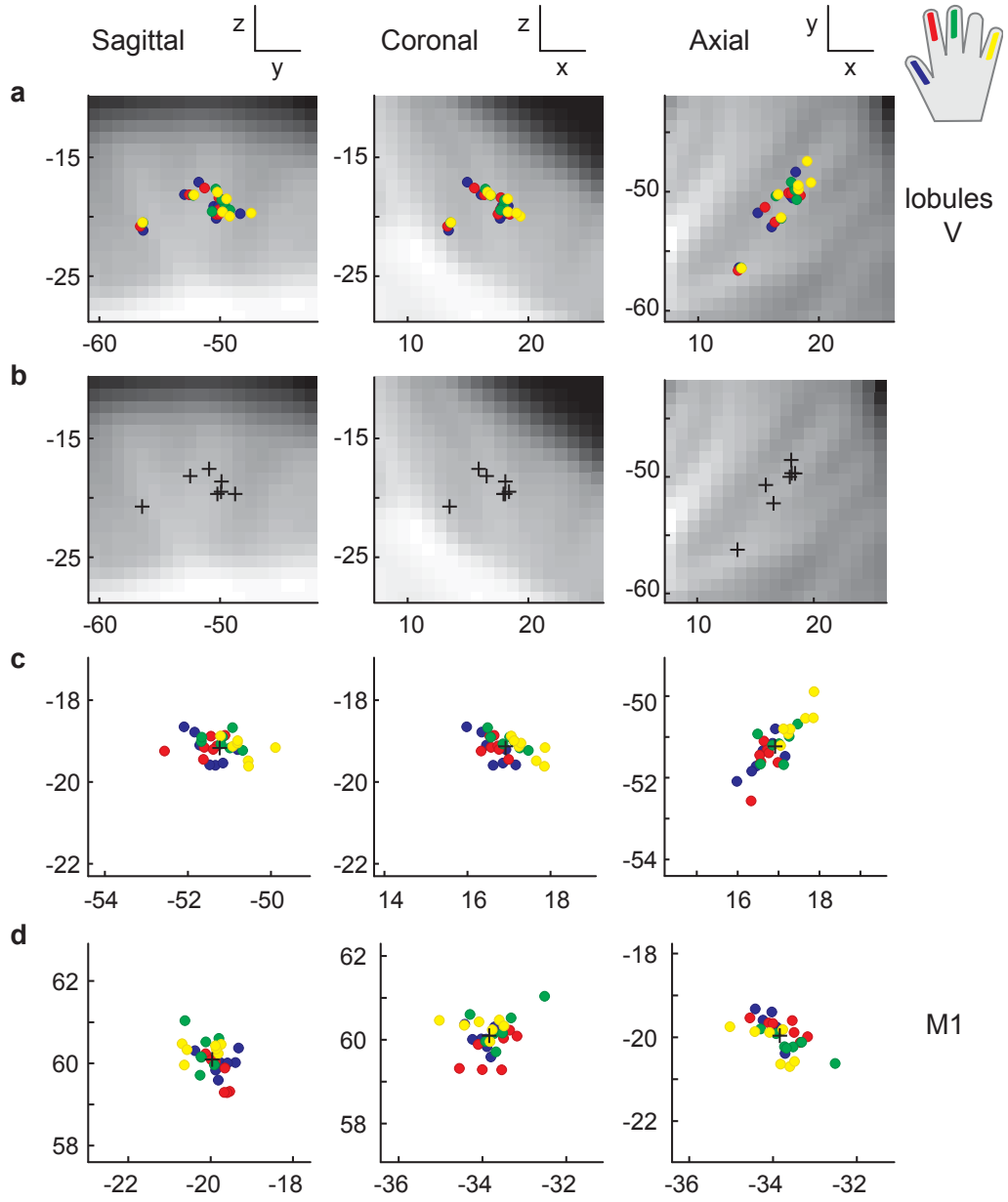

Figure 3.8: *Somatotopic gradient in the finger representation in lobule V and M1 for the motor condition*
(a) Coloured circles reflect the centre of gravity (CoG) of activation elicited by force production with a single digit (D1 blue, D2 red, D3 green and D5 yellow), presented for all participants in an average group space (SUIT). This analysis did not reveal any systematic somatotopy. **(b)** The mean location of the four CoGs indicated the centre of the informative digit region for each participant. These centres varied substantially across subjects in medio-lateral direction along the folia. **(c)** After aligning the CoGs to the centre of the informative region, an orderly digit representation with D1 more medial and D5 more lateral became apparent. **(d)** Aligned CoGs for fingers in the motor condition in M1. A systematic somatotopic gradient was visible, with D1 represented in the most lateral region and D5 in the most medial region.

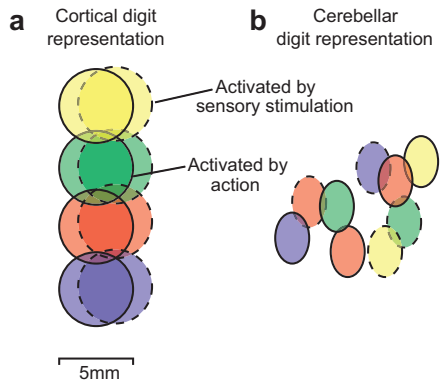

Figure 3.9: *Hypothetical structure of cortical and cerebellar digit representations based on the results of the multivariate analysis.*
(a) In the neocortex, representations for the thumb (blue), index (red), middle (green) and little finger (yellow) are arranged in 5mm (S1) or 4mm (M1) large patches. The ring finger was not tested in the experiment. Patches activated by an action (solid outline) or passive vibratory stimulation (dashed outline) overlap spatially. The orderly somatotopic organisation of S1 is shown, while the somatotopy in M1 is much less pronounced. **(b)** In the cerebellum, patches are smaller than 3mm. Sensory and motor patches for the same finger do not overlap systematically, but are inter-digitated in an unrelated fashion.

Chapter 4

Motor skill learning makes cortical representations more distinguishable

Abstract

Motor-skill learning is accompanied by a complex pattern of increases and decreases in brain activity. Increases may indicate increased neural recruitment, while decreases may imply that a region became unimportant or, alternatively, developed a more efficient neural representation of the same behaviour. Such overlapping mechanisms make the interpretation of overall activity changes during learning difficult. In this chapter, three key aspects of motor learning of skills are elucidated: first, it is shown that motor skills are associated with the existence of specialised neuronal units, and that these are detectable using multivariate analysis of functional magnetic resonance imaging data, in the absence of overall brain activity changes; second, it is demonstrated that the baseline skill level of participants correlates with the ability to decode these sequences from the activity in cortical motor areas; third, it is shown that motor training leads to specific increases in decoding accuracy for the learned sequences in supplementary motor area. Thus, these results provide a novel theoretical concept for assessing the development of skilled representations in the human brain.

4.1 Introduction

The human brain has an unparalleled ability to learn novel and complex motor skills. Numerous functional magnetic resonance imaging (fMRI), stimulation, and neural recording studies have indicated that sequence learning is supported by a complex system of brain areas, including the motor cortex, the supplementary motor area, lateral premotor and parietal cortex, and associated parallel circuits through the basal ganglia and the cerebellum (Dayan and Cohen, 2011; Penhune and Steele, 2012). However, the respective contributions of these areas in various stages of the learning process remain unclear.

The majority of fMRI studies of motor sequence learning are based on the assumption that a region that develops a skill representation with learning should increase neural recruitment for the behaviour, and should therefore show increases in overall BOLD signal (Karni et al., 1995). Such increases are sometimes, but not always, observed in motor cortices (Floyer-Lea and Matthews, 2005; Grafton et al., 1995; Hazeltine et al., 1997; Karni et al., 1998; Penhune and Doyon, 2002, 2005), premotor areas (Penhune and Doyon, 2002), and in the basal ganglia (Hazeltine et al., 1997; Lehericy et al., 2005). In contrast, many fMRI studies find overall signal decreases, most often in the cerebellum (Penhune and Doyon, 2005), parietal and premotor regions (Poldrack et al., 2005) but also in the primary motor cortex (Jenkins et al., 1994; Toni et al., 1998; Ungerleider et al., 2002). Such decreases may suggest that this region becomes unimportant for the production and retention of sequences as learning progresses (Sakai et al., 1999). These conclusions are based on the premise that the size of the overall BOLD activity correlates with the strength of the sequence representation. However, there is an alternative explanation for these signal decreases. A region that

acquires a representation of a sequence may be less activated during production because the learned motor behaviour becomes encoded more efficiently than an unlearned behaviour. This may explain why activity in the motor cortex often decreases after prolonged learning (Ma et al., 2010; Poldrack et al., 2005; Xiong et al., 2009). Considering the discrepancies in the extant literature of brain function associated with motor learning, another scenario is more likely: repeated practice of a motor skill induces simultaneous signal increases (due to increased recruitment) and signal decreases (due to more efficient encoding). This would, in fact, make learning-related regions invisible to traditional fMRI studies and could account for the inconsistencies in the literature. Along these lines, a recent study suggested that learning elicits small increases within an overall reduction of the BOLD signal (Steele and Penhune, 2010).

In this chapter, a new concept to study motor learning with fMRI is proposed. The key idea is that areas involved in controlled movements exhibit specific neuronal activity for these movements. In other words, it is possible to predict movements based on the neuronal activity patterns. Hence, these areas can be said to *represent* movements. Assume someone learns to make two different sequences of 5 finger movements. Now, imagine a cortical region that, before learning, encodes each of the 5 movements in a separate neuronal population (Figure 4.1a). Because each sequence involves each finger, the activity pattern integrated over time is the same no matter which sequence is performed. With learning, the region starts to develop specialised neuronal populations that code for the sequential transitions between two or more finger presses. Controlling multiple finger movements through a single neuronal population would improve the speed of sequence production. Such specialised neurons have been found, for example, in the supplementary motor area (Tanji and Shima, 1994) and the motor cortex (Matsuzaka et al., 2007). After learning, therefore, the two sequences rely on partly separate neuronal

populations (Figure 4.1b). After prolonged training, the area may develop units that code for sequences of more than two finger presses, further reducing the overlap between the neuronal populations (Figure 4.1c). Therefore, it is hypothesised that learning leads to an increasing distance between the neural activity patterns associated with each of the trained sequences.

This hypothesis can be tested by using functional magnetic resonance imaging and multi-voxel pattern analysis (MVPA). MVPA can detect minute modulations of the voxel-by-voxel activity patterns over a small area of cortex, even if the patterns are highly overlapping and rely on neuronal differences of small spatial scale (Swisher et al., 2010). Note that this hypothesis makes no prediction about whether the overall BOLD signal should increase or decrease with learning.

Participants were trained for 4 days to produce 4 different movement sequences. Every sequence consisted of 5 isometric finger presses in a different order. After training, participants underwent two fMRI scans, either performing the 4 trained, or 4 untrained sequences, which were matched for baseline difficulty. Using MVPA, the following three hypotheses were tested. First, it was hypothesised that different sequences would lead to differential patterns of activity in regions involved in their production. Second, it was hypothesised that participants with high skill levels posses more specialised units that code for unique combination of finger movements (Figure 4.1b, c). Lastly, it was predicted that in the multidimensional space of voxel activity patterns, the distance between activity patterns for trained sequences would be larger than for untrained sequences; thus, indicating a neural specialisation for the trained behaviours.

4.2 Methods

4.2.1 Participants

Six female and five male neurologically healthy, right-handed volunteers (average age 23, SD=2.2) participated in this study. The UCL Ethics Committee approved all study procedures.

4.2.2 Apparatus

An fMRI-compatible response box was generated to measure the motor output. The box was equipped with 5 piano-like keys, with grooves in which participants placed their fingertips. Below each groove was a force sensor (FSG-15N1A, Sensing & Control Honeywell Inc.), that continuously measured the isometric forces during sequence production. The force measurements were transmitted to a control computer outside the scanning room through a set of shielded cables, which were passed through a filter panel to prevent RF-signal leakage into the MR-environment.

To equate the conditions between training and scanning, participants performed the task in a supine position on a (mock-) scanner bed, with the keyboard firmly placed on their lap at a 45° angle to the horizontal. Participants received visual instructions and feedback though a back-projection screen, which was viewed by a mirror. A rectangular box and a central asterisk served for visual fixation were presented throughout training and scanning.

4.2.3 General procedure

At the beginning of each trial, the sequence was announced by five numbers presented in the central box for 2.7s (Figure 4.1d). Each number referred to a digit (1 for thumb - 5 for little finger), and the sequence had to be executed from

left to right. During the announcement phase, participants were instructed to memorise the sequence. During the execution phase, five white asterisks were presented in the box, given the starting signal to produce the finger sequence as quickly as possible. A key press was recognised when the force of that finger exceeded a threshold of 2.5N, while the other fingers were below 2.2N. If the correct finger was pressed, the corresponding asterisk turned green, whereas an incorrect press lead the relevant asterisk to turn red. To match the finger presses across sequences, it was also required that each peak force to was below 8.9N. If a press exceeded this threshold, the appropriate asterisk turned yellow. Participants were instructed to complete the full sequence despite error feedback.

After sequence execution, the colour change of the central fixation cross signalled the overall success of the trial: green indicated that the sequence was produced correctly (1 point), red meant that there were one or more errors (-1 point), yellow designated that the force threshold was exceeded (0 point), and blue corresponded to a slow sequence trial, i.e. when it was produced 20% slower compared to the average movement time MT in the previous block (0 points). To motivate participants during the training, three green stars were presented if the sequence was produced 20% faster than the average MT (3 points). After the end of this short feedback phase (800ms), all asterisks turned white again to signal the execution of the next sequence. A trial consisted of either 5 (training) or 3 (scan) repetitions of the same sequence before the next sequence was announced.

Based on a pilot experiment with N=5 independent participants, 12 different finger sequences were selected. These sequences were approximately matched for difficulty and movement speed. Each sequence contained all 5 fingers once and differed only in the sequential order of the presses. None of the sequence contained an ascending or descending sub-sequence of more

than 3 presses. For each of the participants, these 12 sequences were randomly divided into a set of four sequences to be trained, a set to be used as untrained control sequences for the pre- and post-tests, and a set to be used as the untrained control sequences for the scan.

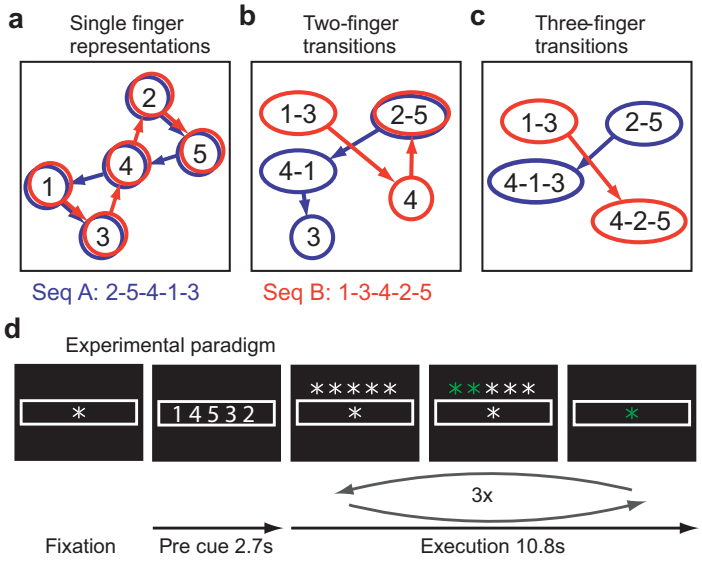

Figure 4.1: *It was hypothesised that activity patterns associated with different sequences would become more distinguishable with learning.*
(a) If a region consists of units that are preferentially activated for single-finger presses, both sequence A (blue) and sequence B (red) activate the same units in a different temporal order. **(b)** As a region develops units that preferentially encode specific finger transitions, sequence A and B will activate partly separate, partly overlapping components of the network. **(c)** When the network becomes highly specialised for transitions of multiple fingers, the two sequences activate independent components of the network. **(d)** In the experimental paradigm, a sequence was cued, and then executed three times from memory.

4.2.4 Behavioural testing and training

The experiment started with a short familiarisation phase of 8 trials, in which participants performed two simple finger sequences (4-2-5-3-1 and 2-5-4-1-3) with their left and right hands. This was followed by a pre-test consisting of 8 of the 12 sequences which were performed by both left hand and right hand

separately. Pre-test performance was used to ascertain a participants baseline skill (in other words, to measure how well participants performed sequences that would later be trained and sequences that would remain untrained). Identical to left hand execution of sequences, for the right hand, participants were again instructed to press the thumb for the number 1 and the little finger for 5, etc. In this way, the "trained" sequences for the right hand were mirror-symmetric to the trained sequences on the left hand. The pre-test consisted of 4 runs per hand, each of which contained 4 of the 8 sequences, and 5 trials per sequence. Every sequence trial set was repeated twice per hand, yielding 10 executions total. Reversing the stimuli order of the first half of the pre-test in the second half counterbalanced the order of conditions.

After each run, feedback with error rate, average MT and points was presented. Participants were instructed to try to decrease their MT if they had an error-rate of less than 20% and to focus on the accuracy of the sequence execution if the error rate exceeded 20%. Due to this clear instruction regarding the speed-accuracy trade-off (Reis et al., 2009), error-rates were stable across the experiment.

Subsequent to the pre-test, participants were trained to perform the sequences in the training set with their non-dominant, left hand. On each of the four separate training sessions, they performed 24 runs (96 trials, and 480 sequence executions). The sessions were usually separated by 24 hours, with a few exceptions in which there was a 48 hour gap between sessions.

4.2.5 Scanning procedure

After 4 days of sequence training, participants underwent two sessions of fMRI scanning. During one session, participants performed the four trained sequences, and during the other session, they executed the four novel sequences

that were not included in the pre- or post-tests. The order of these two sessions (trained and untrained sequence production) was counterbalanced between participants. Each imaging session was comprised of 8 runs, and each run consisted of 16 randomly ordered trials (four per sequence). Each trial included an announcement phase of 2.7s and 3 sequence executions. Because the paradigm was synchronised to the image acquisition, participants had maximal 2.8s to complete each sequence repetition. In contrast to the training sessions, there was no separate feedback for hard presses, and no extra points for exceptionally fast sequences. Additionally, 4 rest phases of 13.5s length were randomly interspersed into each run. During a rest phase, participants did not move and fixated upon the asterisks in the middle of the screen.

4.2.6 Scan acquisition

The imaging data were acquired on a 3T Siemens Trio MRI scanner using a 32 channel head coil. For each participant, an anatomical scan was conducted using a 3D MPRAGE sequence (1mm isotropic, 240 x 256 x 176 mm FOV). The functional data were acquired using a 2D echo-planar image sequence (TR= 2.72s). Each functional scanning session consisted of 8 runs, each containing 110 volumes. The first 3 images of each sequence were excluded from the analysis. A single volume consisted of 32 slices with 2.15mm thickness and was acquired in an axial orientation and an interleaved manner (0.15mm gap, 2.3x2.3mm^2 resolution). With this arrangement, it was possible to cover the dorsal part of both cerebral hemispheres, but most of the temporal lobe and the cerebellum were lost. To correct for distortions arising from field inhomogeneities, a B0 field-map was acquired in the same slice prescription as the functional data (Hutton et al., 2002).

4.2.7 Imaging data analysis

The imaging data were analysed using SPM8 (Wellcome Trust Centre for Neuroimaging, London, UK; http://www.fil.ion.ucl.ac.uk/spm/), and custom written MATLAB routines (The MathWorks, Inc., Natick, MA). Preprocessing consisted of correction for field inhomogeneities (Hutton et al., 2002), motion realignment, and co-registration between functional and individual anatomical data. Additionally, slowly varying trends were removed using a high-pass filter with a cut off frequency of 1/128s.

To measure the BOLD signal changes for each voxel during sequence performance, the unsmoothed data were modelled with a general linear model. For each sequence and run, a single regressor was defined. These regressors were boxcar-function (length 13.5s) and convolved with the standard SPM-hemodynamic response function. The regression-coefficients were then estimated using a robust linear estimation method (Diedrichsen and Shadmehr, 2005), which corrected for movement artefacts by down weighting noisy images. The regression coefficients indicated how much the activity of each voxel changed when a specific sequence was performed. These activity estimates were used as input to both traditional univariate analysis and multivoxel pattern analysis.

4.2.8 Classification

To determine whether a specific area of cortex showed reliably different patterns of activity for the four tested sequences, 160 voxels within a spherical patch of cortex were selected (see surface-based searchlight below) and these were subsequently submitted to a linear discriminant analysis (LDA). The input data (x_i), therefore, consisted of 4 (sequences) $\times$ 8 (runs) activation estimates for the N=160 neighbouring voxels. Using the data from 7 runs, the

mean activation vector for each sequence, and the average within-class N×N covariance matrix Σ was calculated. To prevent Σ from being ill-conditioned, the matrix was regularised by adding 1% of the diagonal mean to all diagonal elements. The discrimination functions g_{c_i} (Gaussian-LDA) described up to a constant the log-likelihood that a pattern vector x belongs to class c_i

$$g_{c_i}(x) = \mu_{c_i}^T \Sigma^{-1} x - \frac{1}{2} \mu_{c_i}^T \Sigma^{-1} \mu_{c_i}. \tag{4.1}$$

The activation vectors from the remaining 8^{th} runs were then classified by assigning them to the class with the highest likelihood (maximum $g_{c_i}(x)$). By retraining and cross-validating the classifier with all possible training and test sets (8 in total), an average classification accuracy was obtained. If the neural activation patterns did not differ systematically between sequences, this value was 25% (guessing rate), on average. Systematically higher classification rates indicated that the region showed differential activation patterns for the 4 sequences. The size of the classification accuracy can serve as a measure of the strength of the sequence representation in that region.

4.2.9 Surface-based searchlight

To detect a significant representation of sequential information anywhere on the cortex, a surface-based searchlight approach was implemented (see Section 2.2.2; Oosterhof et al., 2010). First, the cortical surfaces were reconstructed for each participant using Freesurfer (Dale et al., 1999) and these surfaces were aligned to the template surface. As a result, each surface had the same number of nodes (and node-numbers referred to corresponding locations on the individual surfaces), while the coordinates for each of these nodes were specific to each participant.

For each surface node, a set of N=160 voxels were selected by growing a circular region around the centre node until the required number of voxels were reached. Voxels that partly touched, or lay between, the pial and grey-white matter surface were selected. This resulted in a searchlight radius of 10.4mm, on average. The calculated classification performance accuracy for this group of voxels was then assigned to the centre node. By sequentially selecting each node of the cortical surface, a classification accuracy map was generated. This map revealed where and how well sequences were represented in the neocortex.

4.2.10 Behavioural confounds

The size of the classification accuracy may also be influenced by certain behavioural confounds. If the four sequences were executed with a significantly different average force, or with different MTs, the classification may produce an above-chance accuracy, even though the activity in the region may simply reflect an increased force or faster movement, rather than truly reflecting the underlying sequential information. As the classification analysis is performed for each participant separately, these differences would not have to be systematic, but could be idiosyncratic to each individual. If such differences exist, classification accuracy would also be larger if the within-sequence variability was smaller. This is a concern, as behavioural variability usually decreases with training.

To determine the size of the between-sequence differences relative to the within-sequence variability, the classification analysis was also performed on the behavioural data. As for the neural activation, an average estimate was obtained for each sequence and run. The average MT and the average force were used as the two variables of interest. Before submitting these values to the classification analysis, they were z-standardised.

4.2.11 Dimensionality of the representation

It was hypothesised that a neural region involved in skill acquisition should develop specialised representations of each of the trained sequences. This predicts that each sequence should be associated with a unique activation pattern. On the other hand, above-chance classification accuracy could also arise because the same activation pattern is differentially scaled in magnitude for each of the four sequences. For instance, this could be the case if the activity in each of the voxels scaled (perhaps by different amounts) with the perceived difficulty of each sequence. To test whether the detected representation was composed of unique activation patterns for each sequence or a scalar modulation of a common pattern, a series of modified LDA classifiers were used. Each of the classifiers projects the voxel activity data first onto the first P eigenvectors of $S_w^{-1}S_b$, where

$$S_b = \sum_{i=1}^{c} N_{c_i}(\mu_{c_i} - \mu)(\mu_{c_i} - \mu)^T$$

$$S_w = \sum_{i=1}^{c} \sum_{j}^{N_{c_i}} N_{c_i}(x_j - \mu_{c_i})(x_j - \mu_{c_i})^T$$

with

$$\mu_{c_i} = \frac{1}{N_{c_i}} \sum^{N_{c_i}} x_j \ , \ \mu = \frac{1}{N} \sum^{c} N_{c_i}\mu_{c_i}$$

and

$$N_{c_i} \text{is the number of training samples; } N = \sum^{c} N_{c_i}.$$

The classification of an unknown pattern is then carried out in this new space. When using the 3 largest eigenvalues, the cross-validated classification

accuracy does not differ from the full classifier, which was used initially, as three dimensions are sufficient to fully separate four patterns.

With less dimensions, classification accuracy should decrease. However, if all activation patterns are simply different modulations of the same overall pattern, then the class means will all reside on a single line in the N-dimensional pattern space. Thus, in this case, removing the second and third eigenvector should improve classification performance, as it prevents overfitting in the cross-validation approach.

To demonstrate this, simulated data were generated. The class means in these data were random mixtures of 1, 2, or 3 different activation patterns. By adjusting the within-class noise, the classification accuracy for a full classification analysis could be equated between the different artificial data sets. The classification accuracy for the lower-dimensional classifiers differed strongly with the true dimensionality of the underlying representation. As predicted, the one-dimensional representation was classified best with a one-dimensional classifier, and the three-dimensional representation was classified most effectively with the three-dimensional classifier (Figure 4.3c).

The real data for 14 selected ROIs were analysed with the full and reduced classifiers. To compare this to the theoretical results, the within-class noise of the artificial data set was adjusted, such that it matched the classification performance of the full classification of each subject. The real classification accuracies were compared using a paired t-test to the individually matched simulations.

4.3 Results

4.3.1 Behavioural correlates of skill learning

Initially, participants executed the sequences of 5 finger presses slowly and deliberately with pauses between individual presses (Figure 4.2a). In four 1-hr sessions on consecutive days, participants practiced 4 specific finger sequences with their left, non-dominant hand. As a result of training, movement times (Figure 4.2c, blue line) were reduced approximately by half. By the end of the training, the individual finger presses overlapped and sequences were produced as one behavioural unit (Figure 4.2b).

During the pre- and post-tests, the left and right hands were probed on the trained sequences and on 4 untrained sequences, which were matched for difficulty. This allowed determination of how much learning generalised to the other hand, and to novel sequences. It was found that MTs for the untrained sequences decreased by 849ms for the left hand ($t_{(10)} = 6.973$, $p < 0.001$) and by 547ms for the right hand ($t_{(10)} = -5.656$, $p < 0.001$) indicating that the acquired motor skills improved the execution of both trained and untrained sequences. One reason for such general improvement may be that participants learned to transition faster between two specific fingers. This ability would have helped in the production of the untrained sequences, which shared 59.6% of the digit transitions with a least one of the four trained sequences.

The data also shows that some of the learning was sequence-specific. After training, the left-hand MTs were 286ms faster for trained than for untrained sequences ($t_{(10)} = 5.84$, $p < 0.001$). On the right hand, the sequence specific advantage was 117ms ($t_{(10)} = 3.01$, $p = 0.013$). Therefore, participants also acquired specific representations of the four trained finger sequences.

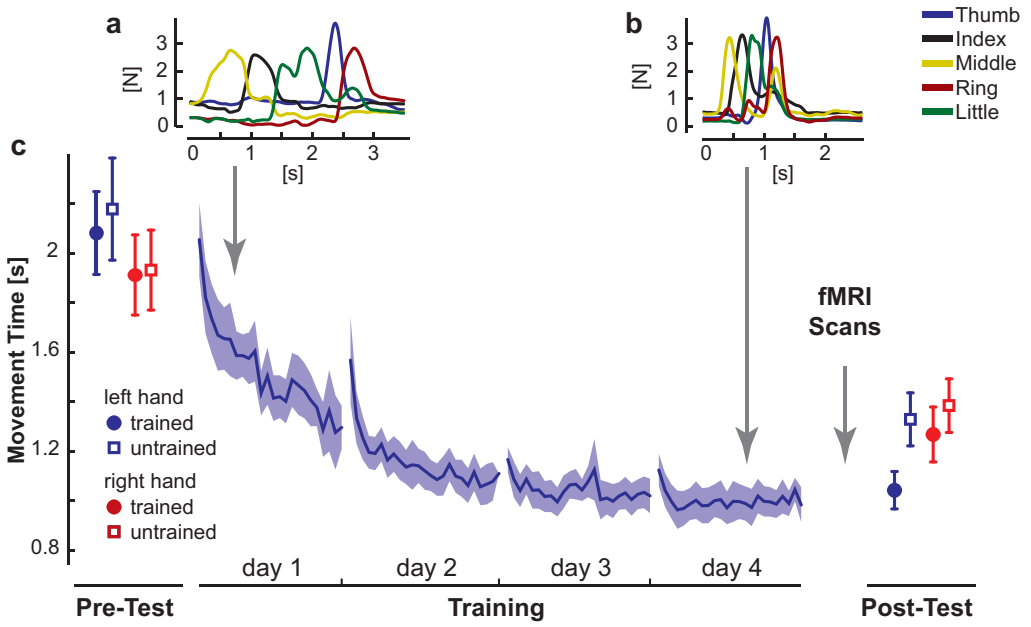

Figure 4.2: *Behavioral consequences of sequence learning.*
(a) Before learning, the finger sequence was executed in a slow, deliberate fashion. The force trace of one exemplary trial (sequence: 3-2-5-1-4) is shown. **(b)** After training, the same sequence is produced much faster, with individual finger forces greatly overlapping. **(c)** Group-average MT for the left hand (blue line) is reduced during training (blue line). In the pre- and post-tests, the left (blue) and right (red) hands were tested on trained (filled circle) and untrained (empty circle) sequences. The results show general learning (reduction in MT for all conditions), and sequence- and limb- specific learning (stronger reduction for the trained sequences on the left hand).

4.3.2 Sequences are represented in spatial activation patterns

Participants were scanned twice between the end of training and the post-test (Figure 4.2c). In one scan, participants produced the 4 trained sequences and in the other session, the 4 untrained sequences. The order of these sessions was counterbalanced between participants.

Following traditional univariate analysis, the regions showing increases in activity during sequence execution were determined (Figure 4.3a). As expected, the BOLD signal was increased in the contralateral primary somato-sensory (S1) and motor cortex (M1). Significant activation was also

found in secondary motor areas, such as the dorsal and ventral premotor cortex (PMd, PMv), the supplementary motor area (SMA / preSMA), and the intra-parietal sulcus (IPS). These areas were not only active in the contralateral right hemisphere, but also in the ipsilateral left hemisphere. This is consistent with previous studies (Verstynen et al., 2005), which have shown that ipsilateral activation is common during complex non-dominant hand movements.

A critical assumption in this approach is that the activity in small patches of neocortex is modulated by the sequential context of the movements. Thus, it was hypothesised that regions involved in the production of the skill represent the sequential information in specific spatial patterns of neuronal activity. Therefore, in such regions, it was expected that different spatial fMRI activation patterns for the four different sequential actions would be found. To detect these sequence representations, a linear classifier was trained to distinguish between the four sequences based on local voxel activity patterns. The classifier was then tested on a single run that was withheld from the training set. Above-chance classification accuracy indicated that the activity pattern differed systematically between sequences, i.e. it implies that the region represented some aspect of the sequential behaviour. The strength of the sequential representation was mapped across the whole cortical surface by selecting for each surface node 160 neighbouring voxels, determining the cross-validation accuracy for this group of voxels, and finally assigning this number to the centre node.

The resultant classification accuracy map (Figure 4.3b) showed a widespread representation of sequential actions. Consistent above-chance accuracy was found in the right sensory and motor areas, bilaterally along the intra-parietal sulcus, and in both dorsal and ventral premotor cortex. Even though the classification accuracies were somewhat lower, significant sequence

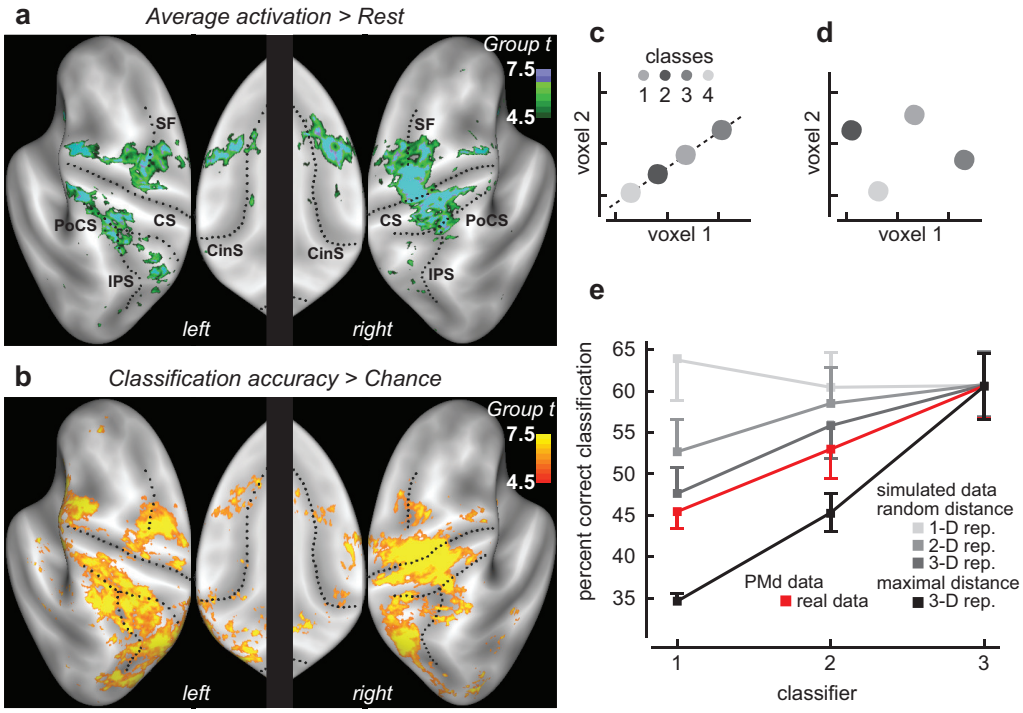

Figure 4.3: *Activation and representation of sequential motor skills.* **(a)** The traditional mass-univariate contrast of movement vs. rest, averaged over trained and untrained sequences, shows large activation changes in both left and right hemispheres. The group map is thresholded at t=4.5, p=0.0004. **(b)** Classification accuracy maps compared to chance indicate which regions of differential patterns of the four sequences show representations of sequential information. The group map is averaged over trained and untrained sequences, and thresholded at t=5.5, p=0.0001. **(c)** Hypothetical distribution of activity patterns in pattern space. The activity for the two voxels scales linearly for different sequences, indicating the encoding of one underlying hidden factor (force, speed, etc.). **(d)** The activity patterns show a 2-dimensional representation and do not scale with a single factor. **(e)** Classification performance of linear classifier relying on 1-3 dimensions of the data (x-axis), as a function of whether the simulated data is distributed in 1, 2, or 3 dimensions (grey lines). Red is the exemplary accuracy for the dorsal premotor cortex. The real data is closest to the 3-dimensional representations. CS: Central Sulcus, PoCS: Post central Sulcus, SF: Superior frontal sulcus CinS: cingulate sulcus IPS: intra-parietal sulcus.

representations were also found in the SMA and preSMA (Table 4.1). In general, the regions that represented sequential actions also showed increased mean signal during the task compared to rest. However, the group t-values for the contrast of classification accuracy > chance (Figure 4.3b) were generally

higher than for the contrast of mean activation during task > rest (Figure 4.3a), suggesting that the multivariate measure detects functional involvement more sensitively than average activation.

Table 4.1: Cortical regions showing significant classification accuracy across participants.

				MNI		
Area	**Size (cm^3)**	**$P_{(cluster)}$**	**Peak $t_{(10)}$**	**X**	**Y**	**Z**
left Hemisphere						
IPS	8.5	>0.001	12.5	-22	-63	53
dPM/M1	1.2	>0.001	9.5	-20	-9	56
M1	0.11	>0.001	8.25	-17	-25	66
SMA	0.08	>0.001	7.6	-12	13	36
right Hemisphere						
M1	3.9	<0.001	15.79	36	-23	56
IPS	1.7	<0.001	12.21	21	-63	52
SMA	0.1	<0.001	9.13	6	-18	61
vPM	0.1	<0.001	6.71	57	-2	36

Random effects analysis of the averaged classification accuracy maps in the neocortex. The average classification accuracy was estimated by averaging the classification performance maps of the trained and untrained sequence performance. Clusters are identified at an uncorrected threshold of $p<0.00015$, $t_{(10)} > 5.4$, and corrected for multiple comparisons over the surface of the neocortex using the cluster-size 6.5mm (Woolsey et al., 1979). The coordinates reflect the location of the peak of the cluster in MNI space.

One important question is whether the regions with above-chance classification accuracy represent sequential information, or whether the differences in activation reflect a simpler behavioural difference between the sequences. While the sequences were carefully selected to be equally difficult, they may have differed systematically in terms of MT or average force. Thus, if the BOLD activity in a region scaled with MT or force, the region would

show above-chance classification accuracy. Indeed, if MT and average force were used to distinguish the four trained or untrained sequences (within each participant) with the classification approach, accuracies of 58% were achieved. To complicate matters further, activity in the region may have scaled not with MT or force, but with another, hidden factor, such as the perceived difficulty of each action.

To rule out this class of explanation, the informative patterns were studied in detail. If these patterns were caused by scaling of a common activation pattern (for example, by difficulty or force), then all activation patterns should lie on a single line in the high-dimensional pattern space (Figure 4.3c). In this case, the classifier should perform best when relying only on the first and strongest dimension that separates the patterns (Figure 4.3e, simulated data, grey line, see methods for details). Using more dimensions should lead to a decrease in accuracy, because the classifier would start over-fitting (see Section 2.4).

In contrast, if the four sequences each recruited a different part of the network, the patterns should be distinct on multiple dimensions (Figure 4.3d). Therefore, the classifier should perform best using 3 dimensions (Figure 4.3e, simulated, dark grey line), as this is the maximum dimensionality necessary to separate 4 actions in pattern space. For the real activation patterns in the ROIs (Figure 4.3e, red line), the 1-dimensional classifier performed significantly worse than the 3-dimensional classifier. Indeed, when comparing the classification accuracies quantitatively to simulated data sets, the data was most consistent with a 3-dimensional representation, but not with a 1- or 2-dimensional representation, (e.g. right dorsal premotor cortex, $t_{(10)} = 2.411$, $p = 0.037$).

These results, therefore, show that the sequence representations did not consist of the modulation of the same activity pattern, but that each sequence

had its own unique spatial pattern of activity. Therefore, each of the four regions activated a different subset of the network.

4.3.3 Skilful participants show more distinguishable activation patterns

The ability to execute novel finger sequences differed substantially across participants. Although musicians were excluded from the study, the average pre-test MTs ranged from 1101 to 2572ms. I hypothesised that a high level of skill before the onset of training should be reflected in a good neural representation of even untrained finger sequences. The idea is that fast production of sequential movements relies on the formation of behavioural units, or chunks (Koch and Hoffmann, 2000), i.e specific two-digit or three-digit transitions.

A person who has neural units that only control single finger presses needs to activate all five units individually while performing a sequence and, therefore, executes sequences slowly. In this individual, all sequences use exactly the same neural substrate, as each finger is involved in each sequence once. Thus, activity patterns will be identical across sequences. In contrast, a person who has dedicated neural units for two- or three-finger transitions will be able to call upon these units and execute the whole sequence faster. In this person, slightly different neural populations should be involved for the different sequences. Indeed, the more specialised or higher-order the representation of these neuronal elements is (i.e. the more fingers are coded together), the more distinct the neural representations are. Accordingly, a negative correlation was found between the levels of skill exhibited by the participants in the pre-test with the classification accuracy for the untrained sequences.

A map-wise contrast (Figure 4.4a) showed a consistent and strong negative

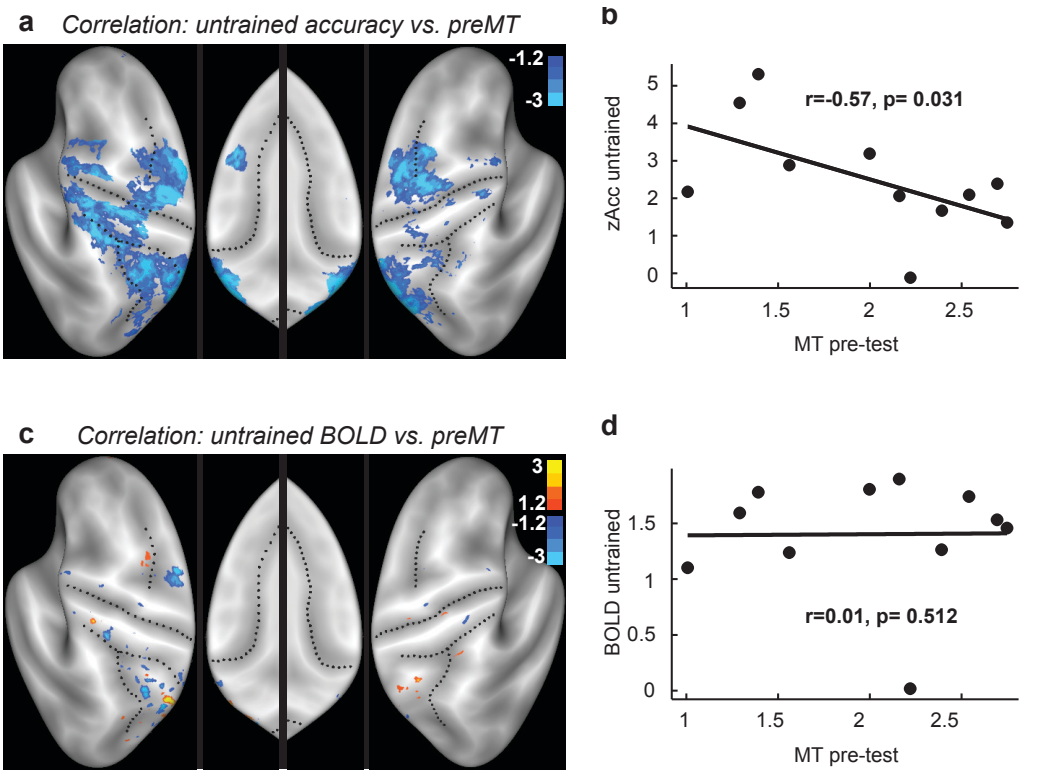

Figure 4.4: *The latent skill of participants correlates with classification accuracy, but not with the overall level of activation.*
(a) The correlation map between classification accuracy maps when participants performed untrained sequences and the average pre-test MT, shown at a low statistical threshold of $t_{(10)} = -1.8$ $p = 0.05$, uncorrected. The negative correlation indicates that participants who were fast at baseline showed highly distinguishable activation patterns. **(b)** Average accuracy over the whole motor circuit (defined as all areas with a group-average classification accuracy of >40%), plotted against the MT on the pre-test. **(c)** The correlation map between overall activation and pre-test MT did not yield any significant areas. **(d)** Average overall activity of the whole motor circuit (defined as in b) did not correlate with pre-test MTs.

correlation between pre-test MTs and classification accuracy for untrained sequences. When correcting for multiple comparisons (Table 4.2), significant clusters were found along the intra-parietal sulcus, in the left dorsal premotor cortex and in left pre-SMA. Even when the classification accuracies were averaged over all regions of the left and right hemispheres, the correlation remained significant, r=-0.577, p=0.031, (Figure 4.4b). Therefore, participants who showed a high level of sequential skill during the pre-test had neuronal

representations that were more distinct between different, un-practiced sequences. That is to say, their motor system was able to represent the sequential information better.

Table 4.2: Cortical regions showing significant correlation between initial MT and untrained representation strength.

				MNI		
Area	**Size (cm^3)**	**$P_{(cluster)}$**	**Peak $t_{(10)}$**	**X**	**Y**	**Z**
left Hemisphere						
dPM	0.15	-4.85	0.006	-22	-19	68
SMA	0.11	-4.92	0.023	-9	4	59
IPS	0.1	-5.96	0.029	-37	-50	58
IPS	0.43	-11.17	<0.001	-7	-71	53
right Hemisphere						
IPS	0.01	0.007	-4.66	7	-59	56

Random effects analysis of the correlation map. The correlation was estimated between the accuracy of the untrained sequence performance maps and the average MTs in the pre-test. Clusters are identified at an uncorrected threshold of $p < 0.007$, $t_{(10)} > -3.04$, and corrected for multiple comparisons over the surface of the neocortex using the cluster-size 12.8mm (Worsley et al. 1996). The coordinates reflect the location of the peak of the cluster in MNI space.

By contrast, the average BOLD signal in these regions did not correlate with performance. A map-wise comparison (Figure 4.4c) did not yield any significant regions. When averaging the BOLD signal across the same areas as before, no significant correlation was detected, r=0.01, p=0.512 (Figure 4.4d). Therefore, skilful participants were characterised by the more distinct representations of untrained sequences, rather than by a particularly high or low average activation.

It is important to note the possibility of two key behavioural confounds.

First, it is possible that the significant correlation observed between behavioural performance and classification accuracy may be due to a performance confound. To test for this idea, the accuracy was correlated with the MTs produced during the scan, rather than those produced during the pre-test. Here, participants were not instructed to go as fast as possible, but to perform the sequences at a comfortable speed that ensured accurate performance. No significant areas of negative correlation were found in this analysis, and the overall correlation was r=0.057, p=0.567. Therefore, the classification accuracy in motor cortical areas correlated with how fast participants could perform the task (i.e. their latent skill), but not with how quickly they actually went during image acquisition. A second possible behavioural confound is that the more skilful participants performed the movements more invariantly, therefore reducing the variability of the neural activation patterns. To test for this possibility, a classifier was used to distinguish between the untrained sequences based on the average MTs and average forces produced during the scan, and the influence of this variable was regressed out. The remaining partial correlation between MT during the pre-test and average neural classification accuracy decreased only minimally to r=-0.558, p=0.047. In sum, participants with a natural capability to produce fast finger sequences also showed neural representations that distinguished more accurately between different sequences. In contrast, participants with high and low skill levels did not differ in terms of their average BOLD signal. It was, therefore, concluded that the distinctiveness of neural activation patterns can serve as a functional indicator of motor skill.

4.3.4 Activation patterns become more distinct with learning

Finally, it was predicted that the specialisation of skill representations, as measured by the accuracy of the multivariate classifier, increases with training. Rather than acquiring the fMRI data before and after training, the BOLD activity was measured while participants performed either four trained or four novel sequences after the training had been completed. The advantage of this design is that the participants are able to produce both the trained and untrained sequences with relatively high skill, such that it is possible to closely match the performance of the two during the scan (see Table 4.3). The strong general learning, however, will also attenuate differences between the two conditions, because even the untrained sequences will partly utilise the acquired skill representation. Any differences between the conditions, must, therefore, be due to a highly specialised sequential representation, likely one that codes for transitions of three and more finger presses (Figure 4.1c).

The area that encoded trained sequences appeared to be bigger than the area that encoded untrained sequences (Figure 4.5a, b). Indeed, it was found that the cortical surface area with an above chance-level accuracy was significantly higher for trained than for untrained sequences ($t_{(10)} = 2.2$, $p = 0.025$). Furthermore, in a direct contrast, it was found that the left pre-SMA showed higher classification accuracies for trained than for untrained sequences. This difference was significant after correcting for multiple comparisons over the cortical surface (uncorrected threshold p=0.007, $t_{(10)} > 8.40$; p corrected=0.045; cluster size= 0.1cm^2). In this area, accuracy increased from 34% to 45% (Figure 4.5d). In the homologous area in the right hemisphere, a similar difference was found, although this cluster was not significant when correcting for multiple comparisons. These results indicate

Table 4.3: Basic performance variables during for the fMRI sessions for the trained and untrained sequences. A paired t-test for difference between sessions is reported.

	Trained	**Untrained**	**T**	**P**
MT (ms)	1307.96 (292.12)	1438.72 (271.08)	-3.51	0.006
Force (N)	4.29 (0.57)	3.99 (0.42)	1.85	0.094
Error Rate (%)	11.0 (6.92)	12.84 (4.32)	-0.69	0.506
ACC (%)	56.25 (18.49)	59.38 (7.91)	-0.57	0.583

MT is the total movement time in ms. The Force is the maximal force produced for each finger, averaged across the fingers. Error rate (%) indicates the percentage of trials where a wrong finger was pressed. Accuracy is the classification obtained when distinguishing the 4 trained or untrained sequences based on the MT and force.

that the pre-SMA acquires a highly specialised representation of the trained sequences, likely encoding transitions of multiple finger presses. Because very few transitions of more than 2-finger presses were shared between the training and test sets, this representation could not be used for the untrained sequences, resulting in the difference in performance accuracy in this region.

These differences in classification accuracy cannot be explained by the lower behavioural variability for the trained sequences: the classification accuracy based on behavioural variables alone was not significantly different between trained and untrained sequence, with the untrained sequences being even slightly more distinguishable from each other (Table 4.3). Furthermore, the difference in classification accuracy in pre-SMA did not correlate with difference in MTs between the trained and untrained sequences, r=0.085,

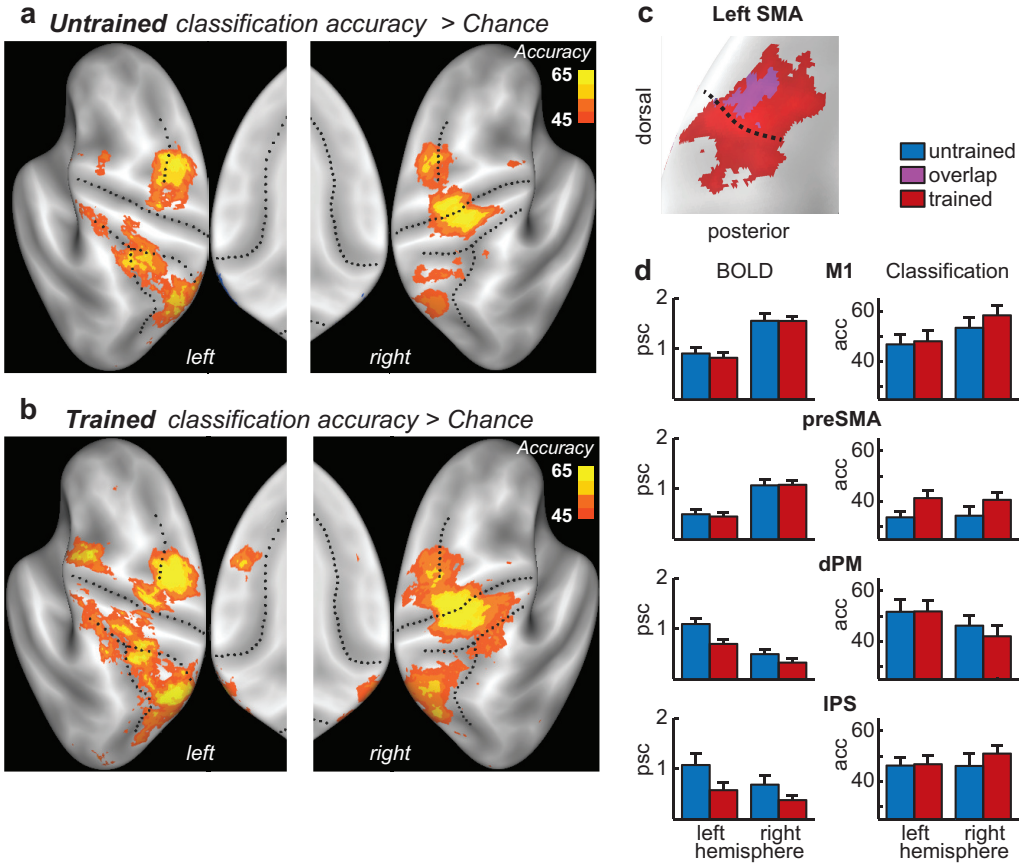

Figure 4.5: *Sequence learning enhances the sequential information in voxel activity patterns.*
Group average maps of the cross-validated classification accuracy shown on an inflated cortical surface for **(a)** untrained and **(b)** trained sequences, at a threshold of 45%. **(c)** The left pre-SMA (shown at 40% threshold) shows a substantial increase of accuracy for trained (red) compared to untrained (blue) sequences. The black dotted line indicates the approximate boundary between SMA and pre-SMA (height of the AC in anterior-posterior direction). **(d)** Left panel: Percent signal change (psc, left panels) and average classification accuracy (% correct, right panel) in left and right primary motor cortex (M1), pre-supplementary motor areas (preSMA), dorsolateral premotor cortex, and intra-parietal sulcus (IPS) for trained (red) and untrained (blue) sequences.

p=0.383. Interestingly, no differences in overall BOLD signal in the pre-SMA (Figure 4.5d) could be found. This indicates that a region can become increasingly specialised for certain behaviour, without changing its overall activity. When searching over the whole cortical surface, significant signal decreases were found in left PMd, and in the IPS. These areas however did

not show increases in classification accuracy as found in the pre-SMA (Figure 4.5d). Thus, these results indicate that the overall activation in a region and the distinctiveness of the neural activation patterns can change independently through learning.

4.4 Discussion

Traditional fMRI and PET studies of motor learning (Dayan and Cohen, 2011) are limited by the ambiguity inherent in overall activity changes induced by learning: Increased activity is often interpreted as increased involvement in control (Karni et al., 1995, 1998). Conversely, decreased activity may imply that the region is less involved in the production of the movement (Sakai et al., 1999) and that the representation moves elsewhere (Penhune and Doyon, 2002). Alternatively, the region may have developed a more efficient representation of the motor skill and is hence able to support the same function with less activity (Ma et al., 2010; Poldrack et al., 2005; Xiong et al., 2009). It is also possible that both processes occur at the same time, rendering learning-related areas invisible to traditional fMRI studies.

In this study, a new concept has been proposed to study learning-related changes with fMRI that circumvents this problem. This method relies on the assumption that different motor skills – here, sequences of 5 finger presses – are subserved by slightly different neuronal populations. Preferential tuning of neurons to movement sequences has been reported in M1 (Matsuzaka et al., 2007) and the pre-SMA (Tanji and Shima, 1994). After practice, neurons in these areas were preferentially active whenever a specific pair of movements was performed. Some cells even discharged specifically at the beginning of longer sequences, but not when the same movements were ordered differently. Regions that contain either type of these neurons will, therefore, activate

slightly different neuronal population for two different sequences of the same set of movements.

To discover such regions with fMRI relies on the fact that these activation patterns exhibit variations on a relatively coarse spatial scale. Although MVPA at standard fMRI resolution is able to decode information from spatial orientation columns in primary visual cortex, where activity patterns vary on a spatial scale of 0.3-0.5mm (Kamitani and Tong, 2005; Swisher et al., 2010), it was not clear a priori that this would generalise to sequential coding. However, a highly replicable set of areas with activity patterns was found that distinguished reliably between sequences. Importantly, these differences did not simply consist of the overall modulation of a single activity pattern (as would be expected if a region simply encoded the overall speed, force, or perceived difficulty of the movement), but rather that each sequence was associated with its own unique activity pattern.

Sequence-specific activation patterns were found in a number of motor areas. While the most obvious difference between the sequences was the order of the finger movements, the current design does not allow the determination of whether some areas may have been sensitive to other distinguishing factors. For example, the PMd (Catalan et al., 1998; Harrington et al., 2000) may have encoded the spatial sequence of key presses, whereas other areas may have represented the temporal information of the sequential motor behaviour. New MVPA experiments that vary multiple factors simultaneously will allow us to test for such representational differences.

The main hypothesis was that high levels of motor skill are associated with neural representations, in which different sequences are associated with highly distinguishable activity patterns. First, it was shown that the distance between activity patterns (as measured by the classification accuracy) for untrained sequences correlated highly with the baseline performance of the

participants. Secondly, it was found that the classification accuracy in the left pre-SMA was significantly higher for trained than for untrained sequences. It is important to note that much of the training generalised to the untrained sequences. Therefore, the contrast between trained and untrained sequences after training highlights only the highly sequence-specific representation in medial motor areas, but not the development of more generic representations that may have occurred in other cortical areas.

The SMA finding is consistent with both human and non-human primate studies, which indicate that the SMA and pre-SMA are critical for skilful production of highly trained sequential motor behaviours. Disruption of the mesial frontal cortex (including SMA and pre-SMA) has been found to be associated with increased production of errors while performing complex, but not simple, sequential finger movements (Gerloff et al., 1997). A second study showed slowing of sequence performance after pre-SMA stimulation specifically at points when a new chunk had to be retrieved (Kennerley et al., 2004). In the non-human primate, muscimol injections into SMA and pre-SMA led to errors in the memory-guided performance of sequences of arm movements (Shima and Tanji, 1998). In the current experiment, a functional correlate of this sequence-specific representation has been found. Interestingly, the representation was predominantly left hemispheric, consistent with the relatively strong inter-manual transfer.

A novel criterion for inferring plastic changes in motor representations from fMRI data was introduced. This technique has important advantages over traditional approaches, which base inferences on changes in overall regional activity. There is good evidence that multiple processes occur simultaneously when a region undergoes plasticity: training may lead to an increased recruitment of neuronal populations, which would increase overall activity. At the same time, the neural representation may become sparser and more

efficient. After training, highly specialised units may be recruited for the computation, hence decreasing the activity for the majority of the neurons in the region (Poldrack, 2000). The overlap of these processes likely explains the relatively inconsistent results in which sequence-related regions show increase in BOLD activity (Floyer-Lea and Matthews, 2005; Grafton et al., 1995; Hazeltine et al., 1997; Karni et al., 1995, 1998), decrease in activity (Poldrack et al., 2005; Wu et al., 2004), or show nonlinear changes over the course of learning (Ma et al., 2010; Xiong et al., 2009).

Notably, in the current study, decreases in activity were only found when comparing trained and untrained sequences, with no changes in the SMA / preSMA. However, clear evidence was provided that the structure of the representation of sequential movements can change, despite the lack of overall activation change, indicating that the region has developed more specialised units for the trained behaviours. Accessing this representational change via classification methods provides a much more robust measure of the development of expertise compared to traditional, univariate methods.

This classification method also circumvents the interpretational problem that task-related activity in fMRI studies is always compared to rest. Using both PET and fMRI, a recent study has shown that resting-state perfusion changes as a consequence of long-term training (Xiong et al., 2009). The proposed novel classification method is independent of such changes, as it only relies on the comparison of activity patterns during different skilful movements against each other.

After prolonged training, the process that makes neural representations more efficient clearly outpaces any additional neural recruitment that may occur early in learning: highly-trained musicians show, compared to novices, reduced overall neuronal activity when producing sequential movements (Hund-Georgiadis and von Cramon, 1999; Meister et al., 2005). These

reductions occur in regions that also exhibit increases in grey and white matter volume (Bengtsson et al., 2005; Gaser and Schlaug, 2003a,b; Imfeld et al., 2009), indicating increased, rather than decreased, importance in the production of the skilled behaviour. It has been hypothesised that these regions will also show more unique neural activation patterns associated with a set of these highly trained behaviours.

In sum, this study supports the idea that the development of sequential motor skills is connected with an increased differentiation of neural activation patterns for different sequences. It was found that naturally skilled individuals showed more differentiated representations of sequences in a range of pre-motor and motor areas, and that the training a specific set of sequences was accompanied with a increase in representation in the supplementary motor area. These differences in representational strength were independent of differences in the overall BOLD signal. Therefore, this study provides a new way of studying plasticity and reorganisation in the human motor system.

Chapter 5

Effector specific and effector independent representations of motor skill

Abstract

In the previous chapter, I have studied skilled and unskilled finger sequence representation. Behaviourally, it was found that skill acquired when generating sequences trained with the left hand can generalise and improve the performance of untrained finger sequences. In this chapter, I discuss work in which I investigated sequence representations of the left and right hands to locate representations that allow for the transfer of skill between the hands. It was hypothesised that, in order to transfer motor skill between effectors, the same information must be represented in a local region for both the trained hand and the untrained hand. To identify informative regions, multi voxel pattern analysis was applied.

Participants were trained to produce 4 different finger sequences with their non-dominant left hand. The sequence set consisted of 2 sequences and their corresponding mirror sequences. During the functional MRI scan, participants performed the sequence set with their trained, left hand, as well as their untrained, right hand. With this paradigm, it was possible to revisit the results in the representational changes of trained vs. untrained skill performance. Identical to Chapter 4, the amount of cortical area, which allows to decode between the sequences of the untrained right hand is smaller compared to the areas that showed sequential information when the left hand performs the same sequences. Additionally, the experimental design made it possible to distinguish between representation of intrinsic and extrinsic information across hands. The results show that, despite extrinsic cueing, the representations encode the sequential information mainly in intrinsic reference frames. Along the intra-parietal sulcus, there is a posterior to anterior shift from intrinsic and extrinsic to mainly intrinsic representation. These results demonstrate that transfer of information can be studied and distinguished using the concept of

representation.

5.1 Introduction

New motor tasks require a lot of effort if they are performed for the first time. However, these tasks become easier with practice and can be carried out effortlessly eventually. One important type of motor learning is *sequence learning*. For instance, a series of individual movements are carried out by different effectors, like 5 fingers of the hand playing the piano. To understand the neuronal processes that underlie motor sequence learning, brain imaging and neurophysiological techniques have been used to identify brain areas that are involved in the learning process (e.g. see Clegg et al., 1998; Hikosaka et al., 2002; Shea et al., 2011, for reviews).

An important characteristic of the motor system is the ability to *transfer* motor skills. Conceptually, transfer describes the competence to apply knowledge that was acquired under a certain situation to a different situation. Using sequence learning, previous studies have investigated which aspects of learned sequences transfer between the hands. In contrast to the present work, most of these studies employ the serial reaction time task (SRTT). In these experiments, participants perceive a visual stimulus and have to press a corresponding button. There are usually two conditions: a random order of button presses and a sequence of button presses. The reaction time (RT) of button presses decreases, and participants press buttons more quickly when the same sequence of button presses is performed repeatedly. Importantly, the sequence is learned implicitly and participants are not explicitly aware of the sequence of button presses. Additionally, it has been found that the RT also decreases when the untrained, contralateral hand is tested. However, motor skills rarely transfer completely, suggesting that independent systems encode a sequence. Based on motor sequence transfer experiments in monkeys (Hikosaka et al., 1995) and humans (Hikosaka et al., 1996; Sakai et al., 1998; Bapi et al.,

2000), Hikosaka et al. (2002) proposed two independent neuronal circuitries for the processing of motor sequences. One represents the sequences in *extrinsic coordinates* and involves the prefrontal and parietal cortices, anterior basal ganglia and parietal lobe, whereas the motor cortex, putamen, anterior lobe of the cerebellum and the dentate nucleus circuits represent motor sequences in *intrinsic coordinates*. Furthermore, it has been suggested that these two circuits are involved at different time points during the learning process. Bapi et al. (2000) investigated this by testing the intrinsic (different visual stimuli but same finger responses) and extrinsic (different finger responses but same visual stimuli) transfer in the early and later stages of sequence learning. In the early stage of learning, RTs of the intrinsic and extrinsic tests were found to be equal, indicating that both systems are important for the sequence representation. However, after learning, RTs in the intrinsic test are shorter compared to the extrinsic test. This shows that sequences are coded increasingly in intrinsic coordinates as learning progresses. However, these effects could not be replicated for more complex arm movements (Kovacs et al., 2009b), and the transfer in extrinsic spatial coordinates was more pronounced during all stages of learning. This raises the question whether the coordinate systems for sequence representations depend on the complexity of the task. In a recent study, Kovacs et al. (2009a) ttested this idea with more complex and simpler arm movements. They found that for simple sequences the performance in the intrinsic test and the originally practiced condition (retrieval test) were similar, whereas for more complex sequences, participants showed similar performance for the extrinsic test and the originally practiced movements (retrieval test). That means that for simple movements the intrinsic information transfers, whereas for more complex movements the extrinsic information transfers. Collectively, the described previous studies demonstrate behaviourally that both extrinsic and intrinsic representations

can transfer, but some dynamic of a movement remain specific for effectors and are not transferable.

Skill transfer is, therefore, a well-defined and measurable behavioural phenomenon. However, the types of neuronal modifications that underlie this process and where in the brain such transfer takes place are not fully understood. The first difficulty is to conceptualise transfer on the neurological level. In previous studies, transfer was considered to be a separate process that occurs at the time when transfer becomes visible in the behaviour. It has been suggested that this separate process is reflected by increased overall activity in areas that are involved in this process (Grafton et al., 2002; Perez et al., 2007a). In contrast, transfer can also be conceptualised as the *direct usage of information* that is already available. Hence, brain areas that underlie the observed intermanual transfer of information must represent the identical information for both the skilled and the unskilled effector. Under this model, no isolated process for the transfer of information exists. Hence, in a brain area that has a representation for both unskilled and skilled hands, similar information might be used to produce the motor behaviours, thereby making transfer possible. Areas with common information for the hands are *effector independent representations*. In contrast, movements of effectors could also be represented through different but informative voxel activity patterns of sequences for each hand and would therefore show *effector specific representations*.

If there is an effector independent representation of finger sequences (i.e. a representation that can be used to produce these sequences both with left and right hands), the question arises which *reference frame* this information is stored in. Traditionally, researchers discuss two types of reference frames in which movement variables are encoded (Soechting and Flanders, 1992), intrinsic and extrinsic (Kawato et al., 1988; Atkeson, 1989; Andersen et al.,

1993). An intrinsic (or motor) coordinate frame represents the information in body centred coordinates, such as the order of finger presses in a sequence. This means that mirror symmetric muscles are active when the sequences are performed with the other hand. Contrastingly, an extrinsic(for example visual) coordinate frame represents the external target of a movement, such as the order of key presses in a sequence. Hence, the extrinsic frame is independent of the configuration of the body. Theoretically, both coordinate frames are essential to perform a successful movement. Behaviourally, it has been found that intrinsic but also extrinsic information can transfer to an untrained hand when using a serial reaction time task (e.g. Romei et al., 2009; Grafton et al., 2002).

The use of multi-voxel pattern analysis and similarity analysis allows us to determine which brain areas have a common representation of sequences for the left and the right hands, and whether this representation is coded in an intrinsic or extrinsic reference frame. In the fMRI experiment to be described, participants performed 4 finger sequences with the left and 4 with the right hand. From all 16 possible pairings between a right hand and a left hand sequence, 4 pairs were the same in intrinsic coordinates, 4 pairs were the same in extrinsic coordinates and 8 pairs were unrelated (see Figure 5.2b). For a region that represents an effector independent representation of sequences in extrinsic coordinates, it is hypothesised that the voxel activity patterns of the 4 extrinsic sequence pairs will correlate highly with each other. In contrast, for a region that represents the sequences in intrinsic coordinates, it was hypothesised that the voxel patterns of intrinsic sequence pairs would have high correlations (see Figure 5.2a).

This experiment had four key aims. First, it aimed to re-test the central hypothesis of Chapter 4 –namely, that training (or development of skill) leads to cortical representations that are more distinguishable. This was examined

in Chapter 4 by comparing representations of trained and untrained *sequences*. Here, I compare the trained and untrained *hands*. It was predicted that the classification accuracy for the left hand would be higher than that of the right hands. A second aim was to identify the regions which show sequence representations for the left and right hands. As argued before, these regions are areas where transfer of information might occur. Thirdly, a central aim was to investigate whether, within these regions, there is a common representation, and if the shared information is in extrinsic or intrinsic reference frame. Finally, a fourth aim was to investigate whether there is an asymmetry of the ipsilateral representation between the left and right hemispheres. Existing evidence suggests that the *left hemisphere* might be particularly important for motor learning, as it active when performing complex tasks with the left or the right hands (Kawashima et al., 1993; Kim et al., 1993; Singh et al., 1998; Cramer et al., 1999; Nirkko et al., 2001; Kobayashi et al., 2003; Li et al., 1996; Verstynen et al., 2005). This makes motor areas of the left hemisphere potentially interesting for the generalisation between hands. Here, I investigated whether this asymmetry is present not only in the overall activation, but also in the distribution of the representation.

5.2 Methods

5.2.1 Participants

Twelve participants were recruited for this study (3 female and 8 male). All of them were neurologically healthy, right-handed and had not received any significant musical training. The UCL Ethic Committee approved all study procedures.

5.2.2 Apparatus

For the behavioural training and experimental testing during the fMRI scan, a *ten-finger response box* was used. This MR-compatible box has been described in detail before (Section 4.2.2). The box had a piano-like key for each finger. To assist the finger placement, each key was equipped with a groove that allowed participants to securely place their fingers on the panels. A pressure-sensitive sensor (FSG-15N1A, Sensing & Control Honeywell Inc.) was affixed beneath each key, which continuously measured the force changes of individual finger presses while a behavioural task was performed. The force changes were measured and processed with an update rate of 5ms in a control computer. During MRI scans, this computer was placed in the scanner control room. To prevent the linkage of RF signals into the MRI environment, filter panels were installed and all cables inside the magnetic field were shielded.

5.2.3 General procedure

The procedure of this experiment is similar to the sequence learning experiment in Chapter 4. The key alterations in procedure to the current experiment included announcing sequences in extrinsic coordinates and announcing hand (Figure 5.1). As was emphasised in Chapter 4, it is important to have matching conditions between training and scanning. For that reason, the behavioural task was performed on a mock scanner bed. The keyboard was placed on the lap of the participant and tilted upwards to establish an ergonomic position for the finger placement. During the task, participants were visually instructed through a back-projection screen.

Each trial started with a 2.7s long announcement phase, which informed the participant about which sequence to perform and which hand to perform the sequence with. The latter information was provided through flanker signals

on the left and right of the central box. If the square on the right was coloured green and the left square was red, the sequence was performed with the right hand. Conversely, if the left square was coloured green and the right was red, the sequence was performed with the left hand (Figure 5.1a). Sequences were symbolised by five numbers in the central box (Figure 5.1a). Each number referred to a specific key (1 for leftmost - 5 for rightmost key, left panel Figure 5.1a). In this way, the sequences were indicated in extrinsic coordinates, in contrast to the experiment in Chapter 4. During the announcement phase, participants memorised the sequence but did not produce any movements.

As a go signal for sequence performance, the digit string turned from light blue to white in the testing phase, and was replaced by the white asterisks during training and scanning. The asterisks or digits changed colour according to the finger response. Identical to the previous experiment (Section 4.2.3), a key press was recognised when a press exceeded a threshold of 2.5N, while the other fingers had to be below 2.2N. For correct key presses, the corresponding asterisk/number turned green. If, however, the participant made an error, the asterisk/number turned red. In order to match the force level across different sequences, individual finger presses were not allowed to surpass a force level of 8.9N. In case a key press was beyond this threshold, the asterisks turned yellow. Even if participants made errors during the execution of a sequence, they were instructed to complete the full sequence as quickly as possible.

The visual feedback after the completion of a sequence is identical to the feedback that was used in the previous experiment (Section 4.2.3).

5.2.4 Sequence selection

In total, three sequence sets were defined. Each set included four different sequences (Table 5.1). These four sequences can be grouped into two pairs,

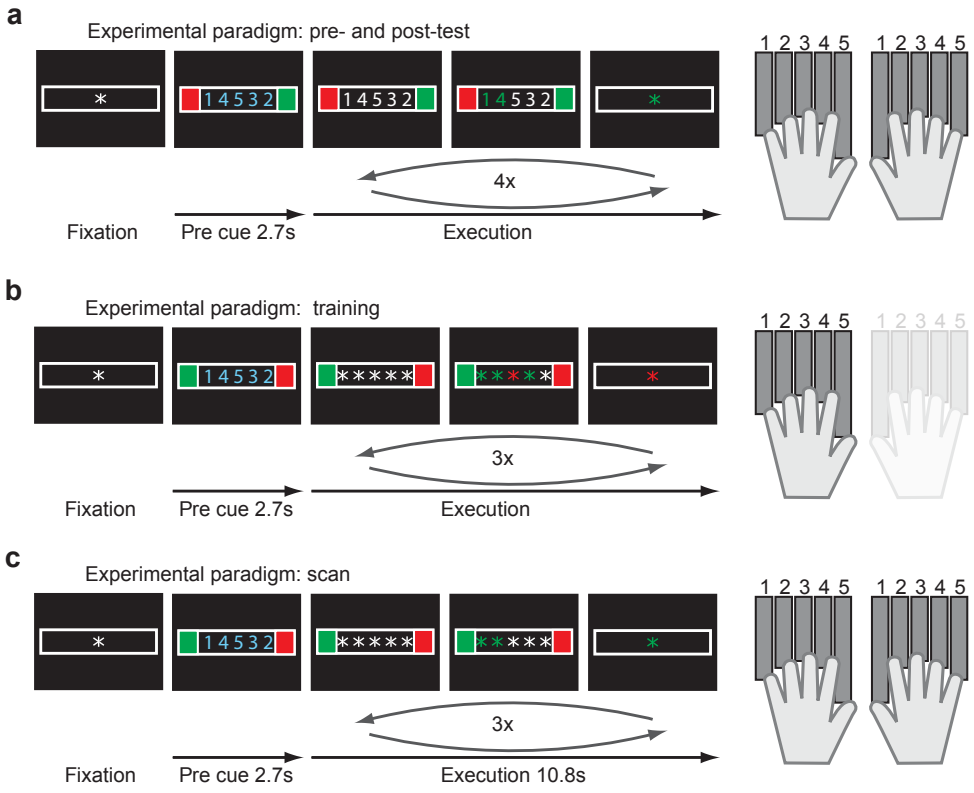

Figure 5.1: *Experimental paradigm*
(a) During the pre- and post-tests, the performance of participants was tested on three sequence sets (12 sequences total). The green flanker signal on the left or right side provided the information with which hand a sequence had to be produced. Each sequence was repeated four times in a row before a new sequence was announced. The numbers corresponding to sequences were visible during the performance of sequences. **(b)** During the training phase, participants performed a set of four sequences with their non-dominant left hand. After the announcement of the sequence, asterisks replaced the sequence, and the sequence had to be performed from memory. **(c)** During the scan, participants performed the trained sequences with both the left and right hands. Because the task needed to be synchronised with the MRI scanner, the time for the sequence production was restricted to 2.8s.

which were mirror sequences of each other. That means sequence A is the mirror sequence of sequence A′ and vice versa. If a sequence is produced by different hands, the same sequences are in *extrinsic* space to each other, whereas the corresponding mirrored sequence is in *intrinsic* space (Figure 5.2a). Additionally, the four sequences within a set did not share any finger transitions with each other (Table 5.2). This was essential because the amount

of shared sequential information had to be minimal and equal across sequences in order to compare, for example, voxel patterns of sequences from the left and right hand with each other in an unbiased manner.

Table 5.1: Sequence sets

Set	Label	Sequence
Set 1	A	4 1 3 5 2
	A'	2 5 3 1 4
	B	1 5 4 2 3
	B'	5 1 2 4 3
Set 2	C	4 5 1 3 2
	C'	2 1 5 3 4
	D	3 1 4 2 5
	D'	3 5 2 4 1
Set 3	E	5 2 1 3 4
	E'	1 4 5 3 2
	F	2 3 5 4 1
	F'	4 3 1 2 5
Instruction sequences		
	i_1	1 2 3 4 5
	i_2	5 4 3 2 1
	i_3	5 3 4 2 1
	i_4	1 3 2 4 5

5.2.5 Behavioural testing and training

To introduce the labelling of the keys, four simple sequences (see explain sequence in Table 5.2) were produced with the left and the right hands in the first 16 trials of the experiment.

After this initial familiarisation with the finger keyboard, participants had to perform a pre-test. With this test, it was measured how well participants

Table 5.2: Number of shared transition between sequences

	A	**A'**	**B**	**B'**	**C**	**C'**	**D**	**D'**	**E**	**E'**	**F**	**F'**	i_1	i_2	i_3	i_4
A	**4**	**0**	**0**	**0**	1	0	0	3	2	0	2	0	0	0	0	1
A'	**0**	**4**	**0**	**0**	0	1	3	0	0	2	0	2	0	0	1	0
B	**0**	**0**	**4**	**0**	0	1	1	0	0	0	2	0	1	1	1	0
B'	**0**	**0**	**0**	**4**	1	0	0	1	0	0	0	2	1	1	0	1
C	1	0	0	1	**4**	**0**	**0**	**0**	1	2	0	0	1	1	0	3
C'	0	1	1	0	**0**	**4**	**0**	**0**	2	1	0	0	1	1	3	0
D	0	3	1	0	**0**	**0**	**4**	**0**	0	1	0	2	0	0	1	0
D'	3	0	0	1	**0**	**0**	**0**	**4**	1	0	2	0	0	0	0	1
E	2	0	0	0	1	2	0	1	**4**	**0**	**0**	**0**	1	1	2	1
E'	0	2	0	0	2	1	1	0	**0**	**4**	**0**	**0**	1	1	1	2
F	2	0	2	0	0	0	0	2	**0**	**0**	**4**	**0**	1	1	0	0
F'	0	2	0	2	0	0	2	0	**0**	**0**	**0**	**4**	1	1	0	0
i_1	0	0	1	1	1	1	0	0	1	1	1	1	4	0	1	1
i_2	0	0	1	1	1	1	0	0	1	1	1	1	0	4	1	1
i_3	0	1	1	0	0	3	1	0	2	1	0	0	1	1	4	0
i_4	1	0	0	1	3	0	0	1	1	2	0	0	1	1	0	4

were able to perform finger sequences before any training. In total, the twelve sequences of all 3 finger sequence sets were tested on the left and right hands. This pre-test included 8 runs, which contained 6 trials each. Therefore, each sequence was produced twice per hand at different time points (8 executions in total). To counterbalance the order of the sequence production, and to account for general learning effects within the test-phase, the initial presentation of the sequences was reversed in the second half of the pre-test.

At the end of each run, participants received feedback about error rate, average movement time and points awarded, which was the same feedback scheme used in the previous experiment (Chapter 4). Participants were encouraged to produce the sequences as fast as possible, while keeping the error rate below 20%. In case more errors occurred, participants were instructed to

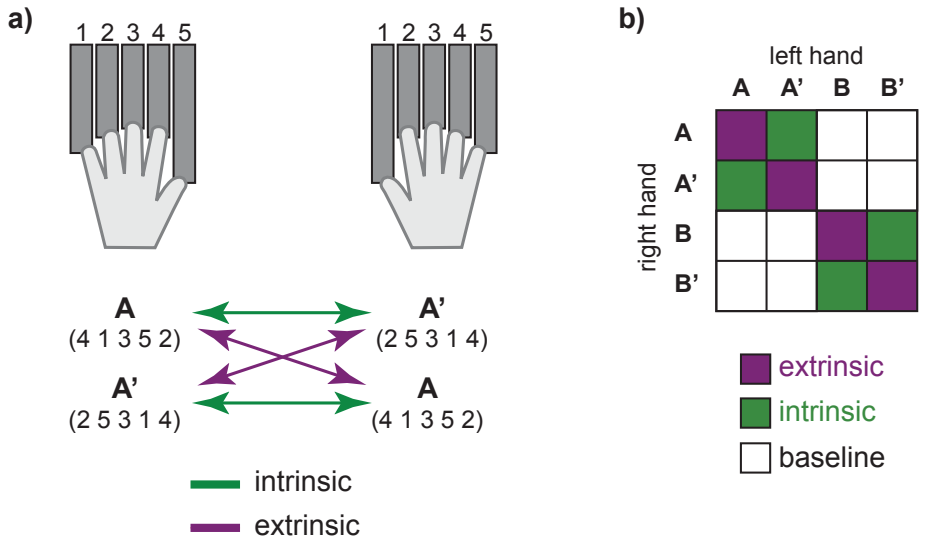

Figure 5.2: *Relationship between a sequences*
(a) To produce a sequence A (4 1 3 5 2) correctly with the left hand, a participant needs to press the finger in the order *index-little-middle-thumb-ring finger*. When sequences are produced by different hands, sequence A and its mirror sequence A′ will have the following relationship to each other: A-A′ or A′-A are in intrinsic space, which means in finger space, whereas A-A or A′-A′ are in extrinsic space, which means the space of the keyboard. **(b)** Correlation matrix between activity patterns of sequences across hands.

focus on the accuracy, and, if necessary, to slow down their finger movements. With this experimental instruction, stable error rates could be insured across the experiment; hence, it was not necessary to determine the speed-accuracy trade-off, as has been performed in previous studies (Reis et al., 2009).

Over the course of four days, participants were trained to produce four sequences of a particular set with their non-dominant left hand. A single training session lasted for one hour and included 16 runs. Each trial of a sequence consisted of 3 sequence executions in a row. In total, 128 trials and 384 sequence executions were performed each day.

After the training phase, the initial pre-test was repeated on day 6. Again, all 12 sequences were tested. Importantly, the order for the sequence presentation in this post-test was identical to the one in the pre-test.

5.2.6 Scanning procedure

On day 7, participants performed the trained sequences with their left and right hands while they underwent a functional MRI scan. The imaging session of a participant consisted of 8 runs, whereas each run included 28 randomly ordered trials (three trials per sequence). A trial started with an announcement phase, which lasted 1 TR (2.7s). Afterwards, the announced sequence had to be performed with the correct hand and needed to be completed within a time window of 2.8s. In contrast to Chapter 4, a sequence was repeated three times before another sequence was announced. In order to match the performance between the trained left and the untrained right hands, participants were instructed to perform all sequences with a comfortable movement time of 1.3s.

To restrict the feedback to the essential information, no hard presses or feedback for exceptionally fast sequence performance were given. To measure the baseline activity of the BOLD signal, 8 rest phases of 13.5s length were randomly included in each run. During these phases, participants stopped all movements and only fixated upon the asterisks in the middle of the screen.

5.2.7 Scan acquisition

Functional and anatomical images were acquired using a 3T Siemens Trio MRI system and a 32 channel head coil. The anatomical images were acquired with a novel scanner sequence, which resulted in 4 quantitative anatomical images (longitudinal relaxation rate, effective transverse relaxation rate, proton density and magnetisation transfer, Draganski et al. (2011)). A 2D echo-planar image sequence (TR= 2.72s) was used to acquire the functional images. The functional images of the 8 runs contained 160 volumes. The 32 slices (2.3mm thick) were conducted with an interleaved sequence (15% gap, 2.3×2.3×2.7mm resolution) and oriented in a way, such that the

cerebellum, the motor cortex and the parietal cortex were covered. To correct for distortions caused by field inhomogeneities, a B0 field-map was acquired (Hutton et al., 2002).

5.2.8 Imaging data analysis

As in Chapter 4 the imaging data were processed with custom written Matlab routines and the SPM 8 software package (Wellcome Trust Centre for Neuroimaging, London, UK; http://www.fil.ion.ucl.ac.uk/spm/). For the current imaging data, the preprocessing procedures were identical to the steps that were applied for the preprocessing of the sequence learning experiment (Section 4.2.7). The images were slice time corrected, corrected for field inhomogeneities (Hutton et al., 2002), motion realigned, and co-registrated. A general linear model was employed to model, within each voxel, the BOLD signal changes when sequences were performed. In this general linear model, one regressor was defined for each sequence, hand and run. This resulted in a total of 64 regressors for the sequences. Each regressor was initialised as a boxcar function (length 13.5s), before it was convolved with the standard spm-hemodynamic response function. Using a robust linear estimation method (Diedrichsen and Shadmehr, 2005), the noisy images were down weighted and the corrected regression coefficients were estimated. The value of these regression coefficients reflected how much a voxel changed its activity when a certain sequence was performed. These unsmoothed activity estimates for each voxel were later used for the traditional univariate analysis and the multivoxel pattern analysis.

5.2.9 Classification performance maps

In Chapter 4, Section 2.1, a classification approach was employed to identify brain areas that represent the sequential information when trained and untrained sequences were performed. Here, the identical approach is used to identify sequence representations of the left and right hands. To map the sequence representations in the whole cortex, a surface based search light was used (Section 2.2.2, Oosterhof et al. (2010)). Identical to the previous chapter (Section 4.2.9), this resulted in a classification accuracy map for sequences that were performed with the left hand and a second classification accuracy map for sequences that were performed with the untrained right hand.

5.2.10 Correlation between the informative components of activity patterns.

The aim of this study was to understand what type of information a brain area encodes for. Of particular interest are areas that show sequence representation for both left and right hand sequences. In these overlapping areas, the common sequence information could be encoded in intrinsic space, in extrinsic space or the information could be overlapping, but nonetheless represented independently for the two hands.

The relationship between sequences within the sequence sets was designed to allow the investigation of both intrinsic and extrinsic encoding (Figure 5.2a). This was achieved by estimating a correlation matrix between the activity patterns of sequences across the two hands (Figure 5.2b). Baseline correlations (Figure 5.2b, white) were calculated between sequences that did not share an intrinsic or extrinsic representation with each other. If a region encodes the sequences in keyboard space (extrinsic representation), the diagonal elements of the correlation matrix (Figure 5.2b, lilac) would

show a significantly higher correlation compared to the baseline correlation between sequences. Conversely, if a region encodes the finger space (intrinsic representation), the four diagonal elements (see Figure 5.2b, green) would show an increased correlation compared to baseline. Another possibility is that the region does not share information between effectors. In such a case, no significant increase in any correlation would be expected (Figure 5.2).

Ideally, correlations can be compared across regions. However to make this comparison possible, it was necessary to control factors that influenced the correlations. Such factors could be different levels of noise in regions or different amounts of common patterns in regions. To account for these factors, the activity patterns of sequences were decomposed (Section 2.5 and Diedrichsen et al. 2011) and the informative correlation was estimated.

The input data to the decomposition model consisted of the 64 voxel activity patterns of sequences ($y_{i,j,k}$, whereas i is the index for the hand, j is the index for the sequences and k is the index for the run). This input pattern was modelled as the sum of different components. One component was a common pattern (c_i) that was shared by all sequences within a condition. Additionally, there was a pattern component that was unique to the sequence in each condition ($s_{i,j}$). A third component reflected the patterns shared by all trials in a run $r_{i,k}$. Finally, there was an independent noise component $\varepsilon_{i,j,k}$.

$$y_{i,j,k} = c_i + s_{i,j} + r_{i,k} + \varepsilon_{i,j,k}$$

Based on this model, the variance and covariance of the components were estimated across voxels from the data. Note that the structure of variances and covariances was constrained by the model. To capture the baseline correlation, the covariance between conditions was introduced ($cov(c_1, c_2)$). This summarises the covariance that is shared by all left and right hand

sequences. Furthermore, the variance for the left hand and right hand sequences captures the variance of each effector. Additionally, the sequences were allowed to covary for intrinsic and extrinsic patterns. Because these variances and the intrinsic and extrinsic covariance were estimated directly for the informative patterns of sequences (and, therefore, corrected for the baseline correlation and noise), it is valid to compare these correlations quantitatively across areas.

5.3 Results

5.3.1 Behavioural correlates of skill learning

In the pre-test and post-test, it was probed how well participants performed the 12 sequences of the 3 sequence sets (Figure 5.3). The pre-test showed no significant difference between the sequences that were trained and the sequences that remained untrained (left hand: $t_{(10)} = 1.235$, $p = 0.245$; right hand: $t_{(10)} = 1.609$, $p = 0.139$). However, the right handed participants were able to perform the sequences initially 110ms faster with the right hand ($t_{(10)} = 2.515$, $p = 0.031$).

When participants were tested after the learning phase, they performed trained sequences 131ms faster with the left hand compared to the right hand ($t_{(10)} = 2.894$, $p = 0.016$). In contrast, no difference between hands for untrained sequences ($t_{(10)} = -0.414$, $p = 0.688$) could be found. That implies that there was a sequence specific learning effect when participants performed trained sequences with the hand that was used during training.

Additionally, with regard to the training-specific improvement, a substantial amount of the learning generalised to the untrained right hand and to the untrained sequences. After learning, participants were able to perform the untrained sequences 760ms faster with the left hand ($t_{(10)} = 5.685$,

$p < 0.001$). Hence, becoming skilled improves not only the performance of trained sequences but also leads to decreased movement times when untrained sequences are executed. Moreover, this improvement also transfers to the right hand, which was not used during the learning phase, and untrained sequences are performed 644ms faster in the post test ($t_{(10)} = 4.498$, $p = 0.001$).

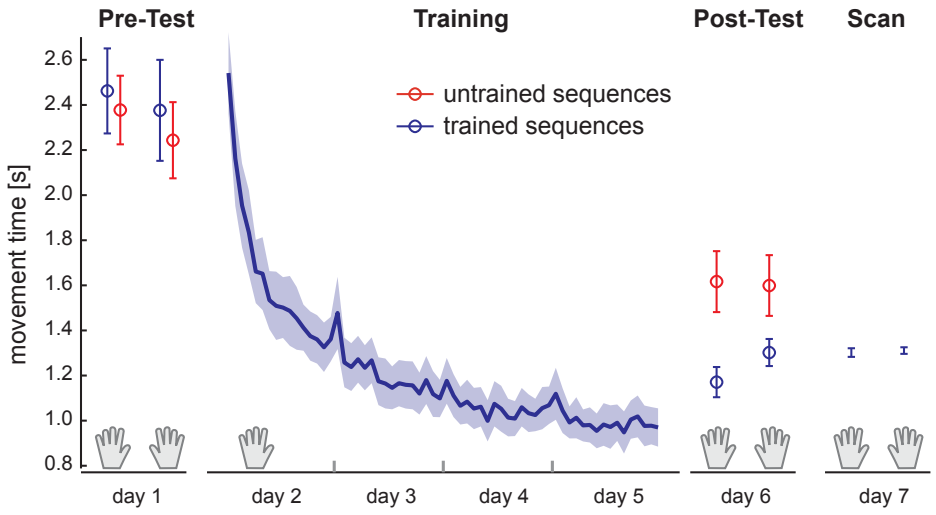

Figure 5.3: *Behavioural changes with sequence learning*
Group average movement time for the left hand and right hands, shown for trained (blue) and untrained (red) sequences. The movement time reduces while participants learned to perform the sequences of a training set. In the pre- and post-tests, the left and right hands were tested on trained and untrained sequences. The results showed general reduction of the movement time for all conditions after the learning phase and a sequence and limb specific learning reduction of the movement time for the trained sequences of the left hand. Hence, skill transferred from the left hand to the right hand. Note that mirror sequences were also used for the training. It is therefore impossible to distinguish between extrinsic and intrinsic transfer behaviourally.

5.3.2 Representations of left and right hand sequence performance

After successful behavioural training, the participants underwent a functional MRI scan. During this scan, subjects performed the learned sequence set with

the trained left hand, but also with the non-trained right hand. To match the performance between hands, the participants were instructed to execute the sequences with a comfortable speed of 1300ms for both hands. The behavioural data showed that there was no difference between the average movement times of the hands (average left movement time=1356ms, average right movement time=1365ms; $t_{(10)} = -0.516$, $p = 0.617$).

To identify effector dependent and effector independent representations, sequences were mapped separately for each hand. Similar to Chapter 4, a linear classifier was employed to detect representations (Figure 5.4).

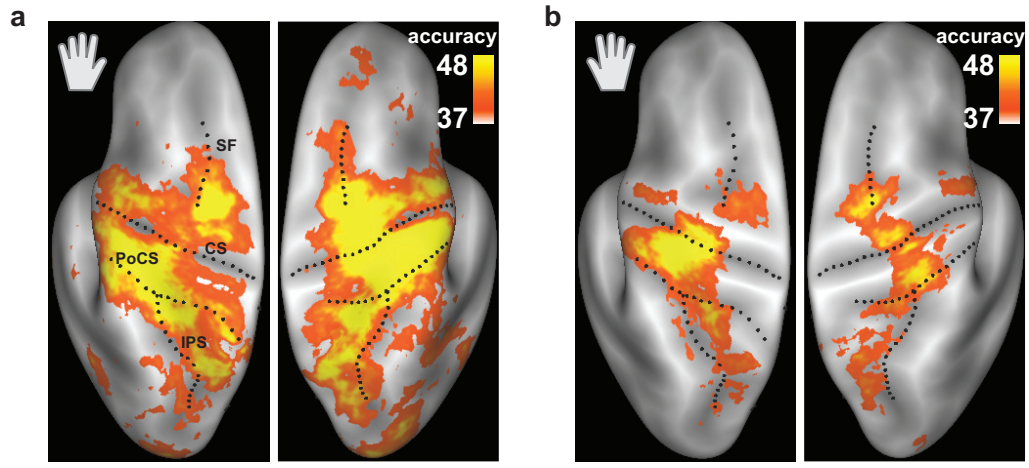

Figure 5.4: *Left and right hand sequence representation overlap highly.* Group average maps of the cross-validated classification accuracy shown on an inflated cortical surface for **(a)** left hand performance **(b)** right hand performance.

In Chapter 4 the representations of trained and untrained finger sequence performance of the left hand have been compared with each other. It was found that the areas that represent sequences were enlarged. In the current experiment, participants performed a set of four sequences with their left and right hands while undergoing an fMRI scan. Because sequences were trained with the left hand, the right hand performance can also be interpreted as executing "untrained" finger sequences. Following the main hypothesis, it

Table 5.3: Cortical regions showing significant difference between representation of effectors across participants.

				MNI		
Area	**Size (mm^3)**	**P$_{(cluster)}$**	**Peak t$_{(10)}$**	**X**	**Y**	**Z**
left Hemisphere right hand > left hand						
IPS	90	0.002	7.33	-56	-34	40
right Hemisphere left hand > right hand						
S1/M1	179	0.000	6.73	45	-19	42
S1/M1	59	0.014	5.27	38	-27	53

Clusters are identified at an uncorrected threshold of p<0.001, t(10)> 4.14, and corrected for multiple comparisons over the surface of the neocortex using the cluster-size 11mm (Woolsey et al., 1979). The coordinates reflect the location of the peak of the cluster in MNI space.

was predicted that the representations of left hand performance would be higher than for the right hand performance. When comparing the classification performance maps between the left and the right hand visually, it can be seen that the size of the cortical areas that represent "trained" sequences is bigger compared to the areas that represent "untrained" sequences (Figure 5.7). To test this, the number of vertices that had classification accuracy above 37% (equal to z-value=1.6) were counted for each participant. On average, 50% (SD= 30%) more vertices were above this threshold ($t_{(10)} = 2.747$ $p = 0.010$) when the sequences were performed with the trained left hand compared to the right hand.

It was also hypothesised that the voxel patterns would become more distinct and, therefore, the strength of the trained left hand would be higher compared to the representational strength of the untrained right hand. When testing for differences between left and right hand sequence representations, only

the intra-parietal sulcus was significantly higher in the left hemisphere for right hand sequence performance compared to left hand sequence performance (Table 5.3). In the right hemisphere, only the primary somato-sensory cortex showed a stronger representation for left compared to right hand sequence performance. This suggests, that through sequence training, a focal representation of the trained left hand develops in right S1 and M1. One explanation for this finding is that, through motor learning, specialised units evolve within a small area in the brain. If a skilled behaviour is executed after learning, only specialised units are recruited. This would lead to a higher accuracy map in this area, because the specialised representation leads to distinct voxel patterns for sequences. My data supports this idea and motor programs of a skilled finger sequences may evolve through such reorganisation in the neuronal network (Table 5.3). I found that when sequences are performed with the left hand the representation is stronger in right hemisphere compared to the right hand classification accuracy in the in the right hemisphere. Furthermore, the representation in the left hemisphere did not differ in the strength of the classification performance accuracy when sequences were performed with the left or right hand. This could be explained through the fact that the right hand was not used for training and, therefore, no specialised units for the sequences were formed in the left motor cortex.

Usually it is assumed that representations, which encode a skill, are locally restricted and become more focal through learning. However, the current results, together with our observations in Chapter 4, argue that skill leads to a more extended and distributed representation of the trained skill. It would be interesting to investigate if this effect reverses and the representation becomes more focal in contralateral M1 through prolonged and intensive sequence training. Under this scenario, a sequence could become an independent motor synergy that does not acquire additional cortical areas to produce a finger

sequence.

5.3.3 Extrinsic and Intrinsic representation of fingers

The behavioural data showed that skill acquired for the left hand generalises to the right hand. One way to transfer information from the left to the right hand is to have a representation that can be used by both. This would demand an area in which the representation of skill overlaps for the left and right hand. When visually comparing the classification accuracy map of the right hand (Figure 5.4b) to the map of the left hand (Figure 5.4a), every area which shows a representation of the sequences when the right hand is used shows also a representation of the sequences when the left hand is performing the sequences. The imaging results demonstrate that several areas (intra-parietal sulcus, motor, primary somato-sensory, ventral and dorsal pre motor cortex) in the neocortex represent both left and right hand finger sequences.

For these areas, I tested whether the common representation were in an intrinsic or extrinsic reference frame. The extrinsic exchange of information would mean that the sequential information of the key presses is represented for the left hand and the right hand. Conversely, intrinsic information would represent the sequential information of finger presses. Because sequences were cued in extrinsic coordinates any finding of intrinsic representation cannot be explained by the experimental set-up.

The reference frame of the effector-independent representation was tested in 8 anatomically defined ROIs. Because the informative areas varied between participants, voxels which showed a classification accuracy that belonged to the highest 40% were selected in each anatomical region of each participant. Based on the voxel activity patterns of sequences for each hand, I studied how activity patterns of left hand sequence performance correlated with the

activity patterns of right hand performance. The correlations were estimated with a pattern decomposition method (Section 2.5 Diedrichsen et al., 2011). This means that the correlations were implicitly tested against the baseline correlation (Figure 5.2b). Hence, any positive correlation can be interpreted as common information between voxel patterns of sequences between hands In the right and left hemispheres, the posterior areas of the IPS demonstrated high correlation for both intrinsic and extrinsic pairs of sequences (Figure 5.5). In contrast, a more anterior region in the IPS showed only a significant correlation that indicates an intrinsic representation (Table 5.4). In primary somato-sensory cortex, intrinsic pairs of sequences showed a reliable correlation with each other in both hemispheres. Hence, if a sequence was produced with identical fingers but different hands, similar sensory information was represented in the primary somato-sensory cortex. In the ventral premotor cortex, intrinsic pairs of sequences were significantly correlated with each other for both the left and right hemispheres. As a control region, the same analysis was performed in primary visual cortex. Because the sequences were cued in extrinsic coordinates, I expected to find significant correlation between voxel activity patterns of extrinsic pairs of finger sequences. Indeed, only extrinsic pairs of sequence patterns correlated significantly with each other (Table 5.4). Despite the overlapping left and right hand representations, no reliable correlation pattern could be found in the remaining regions of interest (M1, PMd and SMA). According to the logic laid out in the introduction, it could be concluded that these areas have effector specific representations of the sequences.

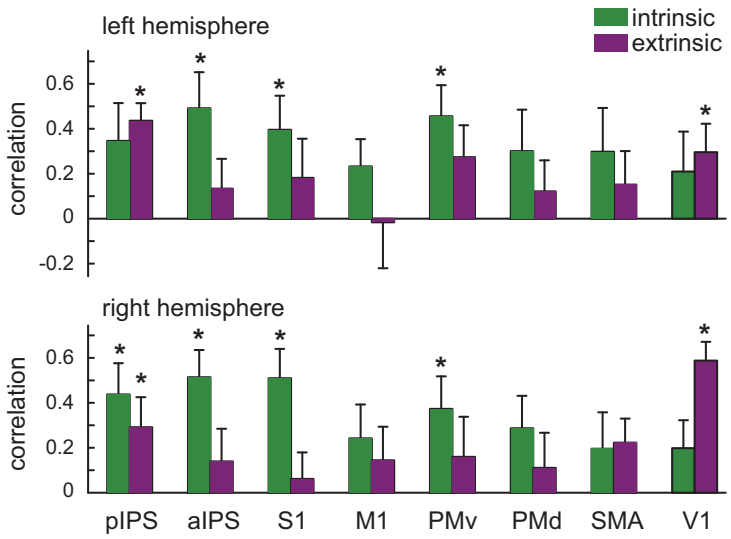

Figure 5.5: *Overlapping regions show intrinsic and extrinsic transfer of information.*
In each anatomical ROIanterior intra-parietal sulcus (aIPS), posterior intra-parietal cortex (pIPS), motorcortex (M1), dorsal premotor cortex (PMd), ventral premotor cortex (PMv), somato-sensory cortex (S1) and supplementary motor area (SMA) –the best 40% voxels (highest averaged accuracy left and right hand) were selected for each participant individually. The correlations were then calculated between the informative patterns of extrinsic and intrinsic sequence pairs. Hence, it was possible to compare these correlations with each other quantitatively (see methods). Although the sequences were cued in extrinsic coordinates, most of the regions showed an intrinsic representation. A significant correlation is indicated with a $*$ (see also Table 5.5 for the full statical report).

5.3.4 Hemispheric asymmetry in the representation

Previous studies have reported that the ipsilateral hemisphere is strongly activated, particularly when the left hand moves (Kawashima et al., 1993; Kim et al., 1993; Singh et al., 1998; Cramer et al., 1999; Nirkko et al., 2001; Kobayashi et al., 2003; Li et al., 1996; Verstynen et al., 2005). When studying the overall BOLD signal changes, visually (Figure 5.6) it appears that the left hemisphere is more active for left hand movements compared to the right hemisphere during right hand movements. To test the asymmetric recruitment of the ipsilateral hemispheres, asymmetry scores were calculated.

Table 5.4: Cortical regions share mainly intrinsic information across hands.

	left hemisphere				**right hemisphere**			
Area	**extrinsic**		**intrinsic**		**extrinsic**		**intrinsic**	
	$t_{(10)}$	p	$t_{(10)}$	p	$t_{(10)}$	p	$t_{(10)}$	p
aIPS	5.5	**<0.05**	2.0	0.06	2.1	**<0.05**	3.1	**<0.05**
pIPS	1.0	0.33	3.0	**<0.05**	0.9	0.3	4.2	**<0.05**
M1	-0.07	0.93	2.9	0.08	0.9	0.3	1.6	0.13
PMv	3.3	0.8	3.3	**<0.05**	0.8	0.3	2.5	**<0.05**
PMd	0.8	0.3	1.6	0.13	0.7	0.4	1.9	0.7
S1	1.0	0.32	2.6	**<0.05**	0.5	0.6	3.9	**<0.05**
SMA	1.0	0.33	1.5	0.15	2.0	0.6	1.2	0.2
V1	2.3	**<0.05**	1.1	0.26	7.0	**<0.05**	1.5	0.14

Two sample t-test for the correlations of intrinsic and extrinsic representations in the anterior intra-parietal sulcus (aIPS), posterior intra-parietal sulcus (pIPS), motor cortex (M1), dorsal premotor cortex (PMd), ventral premotor cortex (PMv), primary somato-sensory cortex (S1), supplementary motor area (SMA) and primary visual cortex (V1).

First, the number of voxels active above a threshold of $t > 2.75$ (movement against rest contrast of left or right hand) were counted. Secondly, because the asymmetry was compared across participants and regions, it needed to be normalised (Verstynen et al., 2005). Thus, the number of active voxels in the ipsilateral cortex (V_{ipsi}) was divided by the added amount of active voxels in the contralateral cortex (V_{contra}) and ipsilateral cortex ($A = V_{ipsi}/(V_{ipsi} + V_{contra})$). This score was calculated for multiple ROIs (see Figure 5.7a), and for each hand separately. If A=0 there is no ipsilateral activation, if A=1 there is all ipsilateral activation and if A<0.5 more voxels were active in the contralateral hemisphere compared to the ipsilateral hemisphere. The hemispheric asymmetry was then studied by contrasting

$A_{right-hand}$ with $A_{left-hand}$ (see Figure 5.7b). The results were consistent with previous findings (Verstynen et al., 2005) and showed that ipsilateral recruitments in the primary motor cortex were more pronounced in the left motor cortex ($t_{(10)} = 3.626$, $p = 0.005$). In addition to the motor cortex, this analysis was extended to five other ROIs (superior and inferior intra-parietal sulcus (IPS), primary sensory cortex (S1) supplementary motor area (SMA)). Similarly, the ipsilateral recruitment in S1 ($t_{(10)} = 5.552$, $p < 0.05$), superior ($t_{(10)} = 2.278$, $p < 0.05$) and inferior IPS ($t_{(10)} = 2.353$, $p < 0.05$), was stronger in the left hemisphere.

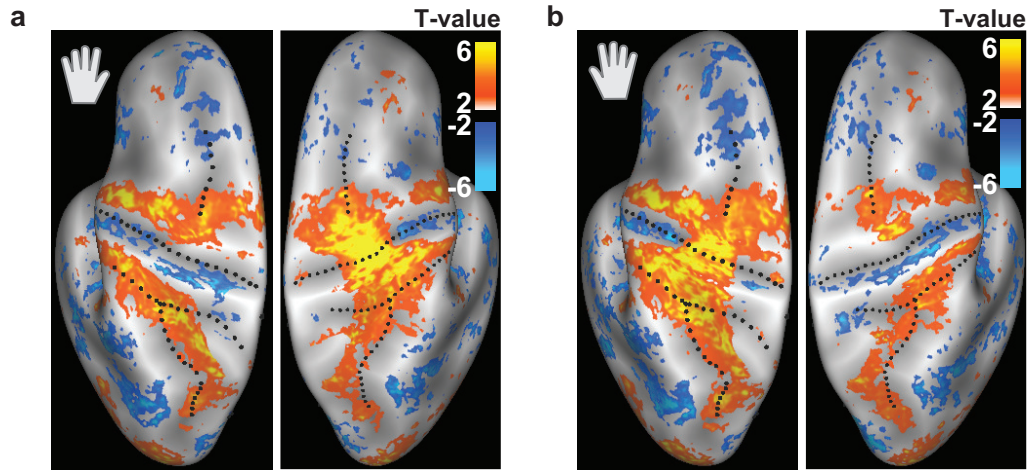

Figure 5.6: *Overall BOLD signal changes during left and right hand sequence performance.*
Traditional mass-univariate contrast of movement vs. rest for the **(a)** left and **(b)** right hand sequence performance shown on an inflated cortical surface.

The same question can also be posed on the basis of classification accuracy. Because the classifier reflects whether a region represents sequences, this measure can provide new neurophysiological insights. It was tested if there is a hemispheric asymmetry in the number of voxels that represent sequences (classification accuracy$>$ 25%). The results (see Figure 5.7) showed that only the superior IPS had a significant asymmetry, with stronger ipsilateral left hemispheric representations in the left compared to the right hemisphere

($t_{(10)} = 2.634$, $p < 0.05$). No hemispheric asymmetry could be found for the remaining regions of interest ($p > 0.2$ for all paired t-tests).

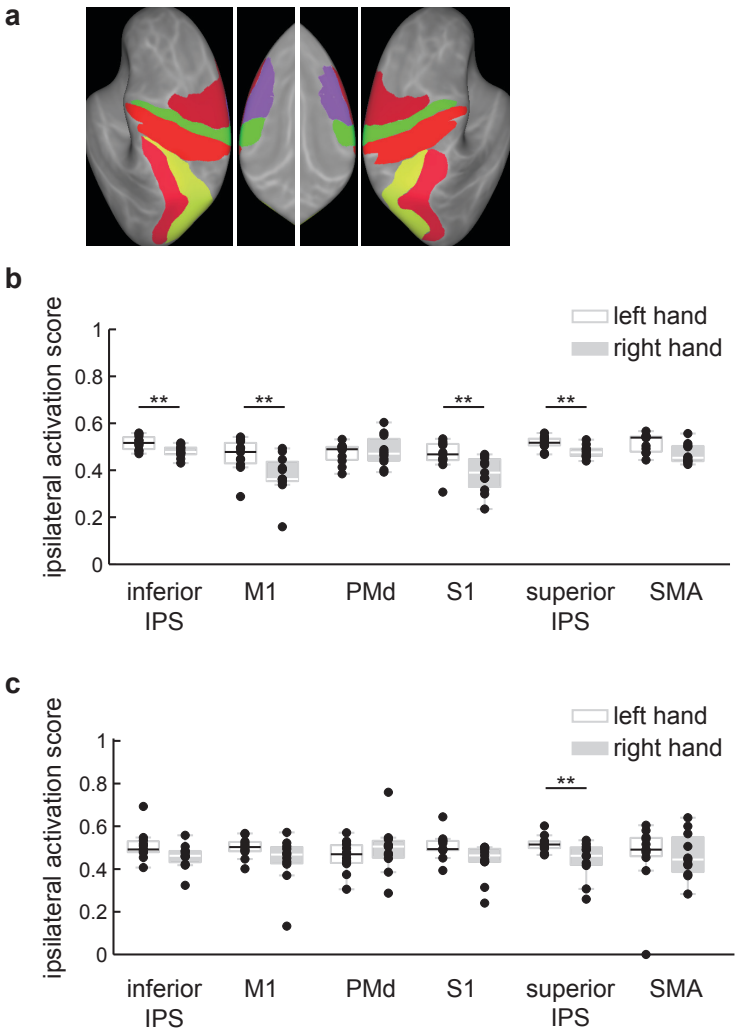

Figure 5.7: *Asymmetric recruitment of the ipsilateral hemispheres* **(a)** Anatomically defined regions of interest, inferior intra-parietal sulcus (magenta), motor cortex (green), dorsal premotor cortex (dark red), somato-sensory cortex, superior intra-parietal sulcus (yellow) and supplementary motor area (lilac). **(b)** Ipsilateral activation score for different ROIs and the left and right hand based on the movement again rest contrast of sequence performance **(c)** Ipsilateral activation score for different ROIs and the left and right hand based on the classification accuracy of sequence.

5.4 Discussion

This experiment tested where in the brain the same information occurs that is shared across hands. The main hypothesis is based on the idea that, in order to exchange information of a left hand motor skill to the right hand, a local brain area must represent this information independently of which hand was used. As in the previous Chapter 4, an explicit finger sequence learning task was used to develop a motor skill for the left hand. To identify brain areas that represented some information about the four trained motor sequences of the left hand, it was tested how well the pattern representing sequences could be distinguished from each other. The identical procedure was performed with voxel activity patterns when the same sequences were executed with the unskilled right hand. If a region shows similar voxel activity patterns between sequence productions of the left and right hands, the area might transfer the information that has been acquired during training of the left hand to the unskilled right hand. The concept of studying representations, and therefore the information of motor behaviour in the brain, stands in sharp contrast to the traditional idea that the behavioural transfer of skill requires an extra dedicated process that leads to increases of overall activity of a region (Grafton et al., 2002; Perez et al., 2007b,a) .

It is well-known that several areas are active for both the left and right hand movements (e.g. Verstynen et al., 2005). Here, it was tested *where* sequence representations of the left and right hand overlap. This was important because regions with such an overlap provide candidate regions for the transfer of information. The results demonstrate that all brain areas, which carry sequential information for trained left hand performance, also represent sequences when the right hand is used. This includes all major motor areas in both hemispheres.

The results show that there is a gradient in the superior IPS from extrinsic in the posterior areas to intrinsic in the more anterior areas. This finding is in line with other studies, which found a similar gradient in the brain (see Filimon, 2010, for a review). For the primary visual cortex, the correlations between the extrinsic sequence pairs were higher. Because sequences are visual cued extrinsically, a sequence A has the identical visual cue for left and right hands, hence it was predicted to find an extrinsic representation in the visual cortex. Note, based on the extrinsic cueing, all intrinsic findings cannot be explained by this experimental design. Overall, most of the areas showed higher correlation between pairs of intrinsic sequences. This means that sequences that involve the same finger independently of the hand elicit similar activity patterns in these regions. There are also regions that do not show any significant correlation between voxel activity patterns of sequences across hands. Following the main hypothesis, it must be argued that these regions do not represent intrinsic or extrinsic information. However, electrophysiology studies of animals (Kakei et al., 1999, 2003) have found extrinsic and intrinsic representations in the primary motor cortex for single movements. These findings could not be confirmed for sequential finger movements, and only a trend for the transfer of extrinsic information could be seen in the primary motor cortex. Alternatively, these areas could transfer other types of information that have not been tested with the current experimental design. Furthermore, the current findings also must be confirmed with right hand training and testing of transfer to the left hand.

The experimental design of the presented study does not allow me to distinguish intrinsic and extrinsic transfer behaviourally. Rather, the design of the study was such that we could determine which neural areas would support the extrinsic and intrinsic transfer, assuming that both happened. Consistent with the stronger transfer in intrinsic coordinates for finger sequences after

prolonged training (Bapi et al., 2000), I found mostly an effector-independent representation of sequence information in intrinsic coordinates. This suggests that, after extended training, a sequence is mostly represented in intrinsic coordinates, thereby replicating the earlier behavioural result.

Hikosaka et al. (2002) proposed that the extrinsic and intrinsic information of sequences is encoded through two different neuronal circuitries. According to this model, the spatial information of sequences has a neocortical representation in prefrontal and parietal cortices. However, my results do not fully support Hikosaka's proposed neuronal circuitry for spatial representation. Our results show no extrinsic sequence representation in the prefrontal cortex, and only the posterior intra-parietal cortex (and not the anterior) shows an extrinsic representation of sequences. Furthermore, Hikosaka proposed that the neocortical intrinsic information of sequences is located in the primary motor cortex. In my results, voxel activity patterns in M1 were more strongly correlated between intrinsic sequences compared to extrinsic sequences, but neither differed significantly from zero, indicating that sequence information is mostly stored here in an effector-dependent manner. Additionally, an intrinsic representation was apparent in the ventral premotor, somatosensory and anterior intra-parietal cortex. Therefore, these areas should be considered to encode intrinsic representations of sequence information, which potentially share information with a contralateral effector.

In this chapter, it was also hypothesised that, through learning, the cortical representations of skilled motor behaviours would become more distinct and could be distinguished better from each other. This hypothesis could be confirmed in the current experiment by comparing the skilled left hand with the unskilled right hand representations. Note that the main finding was an extension of the cortical area that allows differentiation between the voxel activity patterns of sequences. When trained and untrained sequence

representations were compared to each other, a similar effect could be found (Chapter 4). These findings argue against the common intuition that skill is represented in a small, locally-restricted, specialised unit of neurons (Penhune and Doyon, 2005). In contrast, it seems that all motor areas in the cortex represent the skill better and dedicate more cortical area to it.

Previous studies suggested that the left hemisphere plays a special role when complex movements are performed (Kawashima et al., 1993; Kim et al., 1993; Singh et al., 1998; Cramer et al., 1999; Nirkko et al., 2001; Kobayashi et al., 2003; Li et al., 1996; Verstynen et al., 2005). This hypothesis is also supported by patient studies. It was found that patients with lesions in the left hemisphere showed a high chance to develop apraxia, which resulted in poor performance of coordinated and goal-directed movements. In this experiment, previous findings were confirmed, and an asymmetry in the recruitment of ipsilateral cortex could be found in the BOLD activity. Interestingly, such an asymmetry was also present in the superior intra-parietal sulcus when the representation of sequences was studied. When the regions of transfer were studied in the left and right hemispheres, no clear bias for left hemispheric representations was visible. These results show that average BOLD tends to be asymmetric but the representation between hemispheres is relatively symmetric. In sum, the findings suggest that motor skill learning results in an extension of cortical area that represents sequence information. Furthermore, the information that is shared, and possibly transferred between left and right hands, is mainly in intrinsic coordinates.

Chapter 6

General discussion

Methodological innovation

A strong emphasis in my thesis has been to develop multivariate analysis methods to study neuronal correlates of motor representations in the human brain. The methods are primarily based on the concept that local groups of voxels show specific patterns of activity for different finger movements. These voxel patterns are the result of neuronal activity, which is modulated contingent on the movement that is performed. Hence, such areas have information about the movements, i.e. they *represent* the movements.

Similar to previous studies, I employed multi-voxel pattern classification to identify representations (Section 2.1.1). A classifier shows above chance classification accuracy for a local brain area if the voxel activity patterns carry information that enables the classifier to distinguish between classes. As argued before, this can be taken to mean that the area represents the experimental conditions. However during my PhD I have not only applied and implemented existing methods, but also developed and validated novel multi-variate techniques.

A classifier may perform similarly well for pattern differences that are not of interest in a current research question. For instance, a representation could be characterised by an identical and common activity pattern that is systematically scaled through a single factor for each experimental condition - this is a phenomenon referred to as *multiplicative scaling*. The single factor can be caused by differences in the behaviour, such as differences in the overall force or execution time. Although such representations may be of interest for some research questions, it is expected that the representations of finger sequences (Chapter 4) are characterised by independent activity patterns for different experimental conditions. In this thesis, I presented a method that allows the distinction between pattern differences that consist of a multiplicative scaling of a single voxel activity pattern, as opposed to those that are based on independent patterns for each experimental condition (Section 2.4). This method was used to show that the classification accuracy of finger sequence patterns is not explained by a single behavioural factor but by "true" pattern differences of conditions (Chapter 4).

In order to map representations in the neocortex, a novel surface-based searchlight technique was implemented. In comparison to a volume-based searchlight, this approach increased both the performance of the classifier as well as the spatial specificity to locate representations. The improvement was achieved by accounting for the anatomical properties of the subjects brain when selecting local groups of grey matter voxels (Chapter 2.2.2). Hence, it was possible to distinguish representations of primary somato-sensory cortex from those of the motor cortex which lay close together in the volume but are clearly separated anatomically by the central sulcus.

It is not only essential to detect representations, but also to study the characteristics of these representations in greater detail to gain deeper insight in the neurobiological function of different representations in the brain. The

shared information between locally overlapping, but distinct, representations can be measured by correlating their activity patterns (Kriegeskorte et al., 2008a). However, such correlations cannot be compared across different brain areas, because multiple factors – such as scanner noise – can highly influence the correlation value. By decomposing voxel activity patterns into different pattern components, it was possible to estimate the correlation between the informative patterns (Section 2.5 and Diedrichsen et al., 2011). Resultantly, this new method made it possible to compare correlations across different brain regions quantitatively (Chapter 3 and 5).

Furthermore, a statistical framework was developed to test for systematic differences in the spatial activity distribution of conditions within a representation across participants (Section 2.7). This method was subsequently employed to identify and quantify topological arrangements in a statistical manner (Chapter 3).

Additionally, I demonstrated that the size of neuronal patches within a representation can be measured quantitatively (Section 2.6). This was achieved by estimating the correlation between all voxel pairs and their activity changes across conditions within a region. Based on these correlations, a spatial correlation kernel was generated. The smoothness of this kernel can then be expressed as the full-width-half-maximum of a representation. This technique was employed to estimate the size of finger patches quantitatively in the motor cortex, somatosensory cortex and cerebellum (Chapter 3).

New insights through the study of representations

Studying representations is conceptually different from the traditional analysis of overall BOLD signal changes in the brain. This becomes clear in various examples in my empirical work. In Chapter 3, I studied finger representations

in the cerebellum. For tactile stimulation of fingers, two representations were found. This means that voxel activity patterns in these areas are informative about which finger was stimulated. In contrast, when studying the overall activity, no cluster passed the statistical threshold of a group analysis for sensory stimulation. Consequently, informative voxel activity patterns of fingers must be composed of voxels with both increases and decreases in BOLD activity, such that, in summation, the patterns cancel each other out. This demonstrates that representations can be present despite the absence of overall BOLD signal changes and the cerebellum represents slight sensory stimulation as precisely as movements – i.e. the cerebellum is a sensory structure as much as a motor structure (Gao et al., 1996).

Furthermore, this thesis shows that the *strength* of representations can be used as biomarker for motor skill. In Chapter 4, representations of trained and untrained finger sequences were analysed. Before the MRI scan and sequence training, the skill level of the participants was measured in a pre-test. I found that the representational strength of untrained sequences correlated positively with the initial skill level of the participants. In other words, participants who were naturally skilled to perform sequences showed a distinct voxel activity pattern when they performed sequences. Such a correlation could not be seen in the overall signal changes. In summary, the results of my PhD work suggest that the study of representations discloses information that cannot be accessed by traditional analysis methods (Friston et al., 1993).

Neuronal plasticity of motor skill learning was investigated in Chapter 4. Learning processes are difficult to study with fMRI, as it is currently unknown how BOLD signals are altered through motor skill development. The recruitment of additional neuronal units (overall signal increase) or more efficient encoding of the learned behaviour (overall signal decrease) are two common but contradictive hypotheses of how the BOLD signal might

change with learning. This *BOLD dilemma* makes it necessary to study representations instead of overall signal changes. The main hypothesis in Chapter 4 is that voxel activity patterns of sequences become more distinct through learning. This would result in higher classification accuracy of trained compared to untrained finger sequences. In fact, sequence specific increases in the strength of representations were found in the left supplementary motor area. However, the main difference between skilled and unskilled sequence representations is an increase in the extent of cortical areas that decode sequences. Similar results were found in Chapter 5 when participants performed identical sequences with the skilled left hand and the unskilled right hand.

These findings raise the conceptual question of how motor skill is represented in the brain. Usually, it is hypothesised that local areas in the brain represent skill, and through the course of learning, several brain areas are involved but might become unimportant over time (Sakai et al., 1999). In contrast, my research suggests that skilful motor performance is the result of a wide-spread neuronal representation of the skill through all major motor areas in the brain. The current findings provide only the first evidence of how motor skills are represented in the human brain, and additional experiments need to be conducted. For instance, if the extension of representation is the principle mechanism by which motor skills are improved, then highly skilled participants, such as musicians, should show a wide spread representation of a skilled motor behaviour compared to controls, despite an overall reduced BOLD activity (Hund-Georgiadis and von Cramon, 1999; Meister et al., 2005).

Future directions

The current experiments were restricted to healthy participants. Considering my findings and methodological developments, the study of motor representations promise great potential to understand neurological changes in patient groups.

Focal dystonia is the third most common movement disorder and is best known as the degenerative motor disorder that disrupts the professional life of many musicians (see Zoons et al., 2011, for a review). Induced dystonia in animal models showed that receptive fields in the somato-sensory cortex are dedifferentiated and the otherwise fine grain sensory representation disappears (Byl et al., 1996). Based on traditional fMRI analysis, Nelson et al. (2009) found similar changes in the somatosensory cortex of patients when studying topological arrangements of fingers. The multivariate methods developed in this thesis make it possible to measure representational changes, which are beyond a topological arrangement. Additionally, the techniques will allow us to compare representations with each other directly. For instance, the integration of sensory and motor finger representations in the neocortex and cerebellum of musicians dystonia has not been characterised, but understanding this will be essential for a deeper understanding of the disorder.

Stroke patients are another clinical population where the concept of representations carries great potential. Currently, it is unknown what neuronal processes occur when patients recover and gain back lost motor function, such as individuated finger movements (Ward, 2006). Previous work has demonstrated that many brain areas in stroke patients reveal higher activity in a finger tapping task compared to healthy controls (Cao et al., 1998; Chollet et al., 1991; Cramer et al., 1997; Weiller et al., 1992, 1993). This immediately raises the question of whether secondary motor areas, which

have also connections to the spinal cord motorneurons (Strick, 1988), may be important for the recovery of patients. Contrastingly, using a grip force task, (Ward et al., 2003a), it has been found that patients with the most favourable recovery showed no significant increase in the activity compared to controls, whereas patients with increased overall BOLD activity exhibited the worse recovery. In a longitudinal study (Ward et al., 2003b) it was demonstrated that, subsequent to stroke, many motor areas were active in the acute phase, but this task-related increase in activity decreased over time. Interestingly, this task-related reduction in activity correlated with the amount of recovery. It is unclear what the role of this initial activation is and where in the brain motor functions are represented after successful recovery. For instance, encode these regions for the same information more efficiently or do they become unimportant over time? Using multivariate methods, representations of fingers could be identified in the acute phase of stroke and after the patient has recovered. This could allow us to locate areas (e.g. prefrontal cortex) that show an initial teaching signal to develop new motor representations. After successful recovery, the areas that take over the role of lesioned tissue can also be studied using the same approaches. The methods in this thesis offer the possibility to understand the neurological processes that take place *when* patients recover, *why* not all patients are able to achieve full motor function and *how* physiotherapy can support the act of recovery.

Recently it has been shown that *transcranial direct current stimulation* (tDCS) enhances the ability to learn motor tasks (Reis et al., 2009; Waters-Metenier et al., 2012). One hypothesis is that tDCS may be used to bias the location of brain areas that develop the skill representation. This hypothesis is currently being investigated in our research group, implementing the methods that have been presented in this thesis. For instance, in one study, participants learn a motor task with their left hand and receive either anodal or

cathodal stimulation over the ipsilateral hemisphere. Behavioural experiments (Waters-Metenier et al., 2012) show that anodal stimulation increases the motor learning rate dramatically. Based on the core hypothesis of this thesis, such an effect must be reflected in a better representation of the skilled movement in the contralateral hemisphere. By changing the polarity of the stimulation, one could suppose that the representation would not be developed in the contralateral hemisphere, but in the ipsilateral hemisphere. In this way, it might be possible to manipulate the location of skill representations. This manipulation will likely be important for the recovery of stroke patients, as it would trigger the development of new motor representations in the non-lesioned hemisphere of the brain. Furthermore, this technique then could also be used to manipulate misrepresentations of motor behaviours in dystonia patients.

I have argued that the study of representations with multivariate techniques reveals novel insights of how humans control their movements. It will be exiting to see how this field of neuroscience progresses further in the future.

Bibliography

R A Andersen, L H Snyder, C S Li, and B Stricanne. Coordinate transformations in the representation of spatial information. *Curr Opin Neurobiol*, 3(2):171–176, Apr 1993.

R Apps and M Garwicz. Anatomical and physiological foundations of cerebellar information processing. *Nat Rev Neurosci*, 6(4):297–311, 2005.

J Ashburner and K J Friston. Unified segmentation. *Neuroimage*, 26(3):839–51, 2005.

C G Atkeson. Learning arm kinematics and dynamics. *Annu Rev Neurosci*, 12:157–183, 1989.

D Attwell and C Iadecola. The neural basis of functional brain imaging signals. *Trends Neurosci*, 25(12):621–5, 2002.

R S Bapi, K Doya, and A M Harner. Evidence for effector independent and dependent representations and their differential time course of acquisition during motor sequence learning. *Exp Brain Res*, 132(2):149–162, May 2000.

A J Bastian. Learning to predict the future: the cerebellum adapts feedforward movement control. *Curr Opin Neurobiol*, 16(6):645–9, 2006.

S L Bengtsson, Z Nagy, S Skare, L Forsman, H Forssberg, and F Ullén. Extensive piano practicing has regionally specific effects on white matter development. *Nat Neurosci*, 8(9):1148–1150, Sep 2005.

J M Bower and D C Woolston. Congruence of spatial organization of tactile projections to granule cell and purkinje cell layers of cerebellar hemispheres of the albino rat: vertical organization of cerebellar cortex. *J Neurophysiol*, 49(3):745–66, 1983.

N N Byl, M M Merzenich, and W M Jenkins. A primate genesis model of focal dystonia and repetitive strain injury: I. learning-induced dedifferentiation of the representation of the hand in the primary somatosensory cortex in adult monkeys. *Neurology*, 47(2):508–520, Aug 1996.

Y Cao, L D'Olhaberriague, E M Vikingstad, S R Levine, and K M Welch. Pilot study of functional mri to assess cerebral activation of motor function after poststroke hemiparesis. *Stroke*, 29(1):112–122, Jan 1998.

K L Casey, S Minoshima, T J Morrow, and R A Koeppe. Comparison of human cerebral activation pattern during cutaneous warmth, heat pain, and deep cold pain. *J Neurophysiol*, 76(1):571–81, 1996.

M J Catalan, M Honda, R A Weeks, L G Cohen, and M Hallett. The functional neuroanatomy of simple and complex sequential finger movements: a pet study. *Brain*, 121 (Pt 2):253–264, Feb 1998.

F Chollet, V DiPiero, R J Wise, D J Brooks, R J Dolan, and R S Frackowiak. The functional anatomy of motor recovery after stroke in humans: a study with positron emission tomography. *Ann Neurol*, 29(1):63–71, Jan 1991.

B A Clegg, G J Digirolamo, and S W Keele. Sequence learning. *Trends Cogn Sci*, 2(8):275–281, Aug 1998.

K A Coffman and P L Strick. The primary motor cortex is a source of input to the posterior vermis. *In: Society for Neuroscience abstracts*, page 367.326, 2009.

A Collignon, F Maes, D Delaere, D Vandermeulen, P Suetens, and G Marchal. Automated multi-modality image registration based on information theory, June 1995 1995.

D D Cox and R L Savoy. Functional magnetic resonance imaging (fmri) "brain reading": detecting and classifying distributed patterns of fmri activity in human visual cortex. *Neuroimage*, 19(2 Pt 1):261–70, 2003.

S C Cramer, G Nelles, R R Benson, J D Kaplan, R A Parker, K K Kwong, D N Kennedy, S P Finklestein, and B R Rosen. A functional mri study of subjects recovered from hemiparetic stroke. *Stroke*, 28(12):2518–2527, Dec 1997.

S C Cramer, S P Finklestein, J D Schaechter, G Bush, and B R Rosen. Activation of distinct motor cortex regions during ipsilateral and contralateral finger movements. *J Neurophysiol*, 81(1):383–387, Jan 1999.

A M Dale, B Fischl, and M I Sereno. Cortical surface-based analysis. i. segmentation and surface reconstruction. *Neuroimage*, 9(2):179–194, Feb 1999.

E Dayan and L G Cohen. Neuroplasticity subserving motor skill learning. *Neuron*, 72(3):443–454, Nov 2011.

J E Desmond, J D Gabrieli, A D Wagner, B L Ginier, and G H Glover. Lobular patterns of cerebellar activation in verbal working-memory and finger-tapping tasks as revealed by functional mri. *J Neurosci*, 17(24): 9675–85, 1997.

J Diedrichsen. A spatially unbiased atlas template of the human cerebellum. *Neuroimage*, 33(1):127–38, 2006.

J Diedrichsen and R Shadmehr. Detecting and adjusting for artifacts in fmri time series data. *Neuroimage*, 27(3):624–634, Sep 2005.

J Diedrichsen, Y Hashambhoy, T Rane, and R Shadmehr. Neural correlates of reach errors. *J Neurosci*, 25(43):9919–31, 2005a.

J Diedrichsen, T Verstynen, S L Lehman, and R B Ivry. Cerebellar involvement in anticipating the consequences of self-produced actions during bimanual movements. *J Neurophysiol*, 93(2):801–12, 2005b.

J Diedrichsen, J H Balsters, J Flavell, E Cussans, and N Ramnani. A probabilistic mr atlas of the human cerebellum. *Neuroimage*, 46(1):39–46, 2009.

J Diedrichsen, T Verstynen, J Schlerf, and T Wiestler. Advances in functional imaging of the human cerebellum. *Curr Opin Neurol*, 23(4):382–7, 2010.

J Diedrichsen, G R Ridgway, K J Friston, and T Wiestler. Comparing the similarity and spatial structure of neural representations: A pattern-component model. *Neuroimage*, 2011.

B Draganski, J Ashburner, C Hutton, F Kherif, R S Frackowiak, G Helms, and N Weiskopf. Regional specificity of mri contrast parameter changes in normal ageing revealed by voxel-based quantification (vbq). *Neuroimage*, 55 (4):1423–1434, Apr 2011.

J C Eccles, N H Sabah, R F Schmidt, and H Taborikova. Cutaneous mechanoreceptors influencing impulse discharges in cerebellar cortex. i. in mossy fibers. *Exp Brain Res*, 15(3):245–60, 1972.

M Eisenberg, L Shmuelof, E Vaadia, and E Zohary. Functional organization of human motor cortex: directional selectivity for movement. *J Neurosci*, 30(26):8897–8905, Jun 2010.

F Filimon. Human cortical control of hand movements: parietofrontal networks for reaching, grasping, and pointing. *Neuroscientist*, 16(4):388–407, Aug 2010.

B Fischl, M I Sereno, R B Tootell, and A M Dale. High-resolution intersubject averaging and a coordinate system for the cortical surface. *Hum Brain Mapp*, 8(4):272–284, 1999.

A Floyer-Lea and P M Matthews. Distinguishable brain activation networks for short- and long-term motor skill learning. *J Neurophysiol*, 94(1):512–518, Jul 2005.

P T Fox, M E Raichle, and W T Thach. Functional mapping of the human cerebellum with positron emission tomography. *Proc Natl Acad Sci U S A*, 82(21):7462–6, 1985.

K Friston, C Chu, J Mouraomiranda, O Hulme, G Rees, W Penny, and J Ashburner. Bayesian decoding of brain images. *NeuroImage*, 39(1): 181–205, 2008. ISSN 10538119.

K J Friston, K J Worsley, R S J Frackowiak, J C Mazziotta, and A C Evans. Assessing the significance of focal activations using their spatial extent. *Human Brain Mapping*, 1(3):210–220, 1993.

J H Gao, L M Parsons, J M Bower, J Xiong, J Li, and P T Fox. Cerebellum implicated in sensory acquisition and discrimination rather than motor control. *Science*, 272(5261):545–7, 1996.

C Gaser and G Schlaug. Brain structures differ between musicians and non-musicians. *J Neurosci*, 23(27):9240–9245, Oct 2003a.

C Gaser and G Schlaug. Gray matter differences between musicians and nonmusicians. *Ann N Y Acad Sci*, 999:514–517, Nov 2003b.

R Gentner and J Classen. Modular organization of finger movements by the human central nervous system. *Neuron*, 52(4):731–742, Nov 2006.

A P Georgopoulos, J F Kalaska, R Caminiti, and J T Massey. On the relations between the direction of two-dimensional arm movements and cell discharge in primate motor cortex. *J Neurosci*, 2(11):1527–1537, Nov 1982.

A P Georgopoulos, G Pellizzer, A V Poliakov, and M H Schieber. Neural coding of finger and wrist movements. *J Comput Neurosci*, 6(3):279–288, May-Jun 1999.

C Gerloff, B Corwell, R Chen, M Hallett, and L G Cohen. Stimulation over the human supplementary motor area interferes with the organization of future elements in complex motor sequences. *Brain*, 120 (Pt 9):1587–1602, Sep 1997.

S Geyer, A Schleicher, T Schormann, H Mohlberg, A Bodegard, P E Roland, and K Zilles. Integration of microstructural and functional aspects of human somatosensory areas 3a, 3b, and 1 on the basis of a computerized brain atlas. *Anat Embryol (Berl)*, 204(4):351–66, 2001.

S T Grafton, E Hazeltine, and R Ivry. Functional mapping of sequence learning in normal humans. *Journal of Cognitive Neuroscience*, 7(4):497–510, 1995.

S T Grafton, E Hazeltine, and R B Ivry. Motor sequence learning with the nondominant left hand. a pet functional imaging study. *Exp Brain Res*, 146 (3):369–378, Oct 2002.

W Grodd, E Hulsmann, M Lotze, D Wildgruber, and M Erb. Sensorimotor mapping of the human cerebellum: fmri evidence of somatotopic organization. *Hum Brain Mapp*, 13(2):55–73, 2001.

S Grootoonk, C Hutton, J Ashburner, A M Howseman, O Josephs, G Rees, K J Friston, and R Turner. Characterization and correction of interpolation effects in the realignment of fmri time series. *Neuroimage*, 11(1):49–57, 2000.

D L Harrington, S M Rao, K Y Haaland, J A Bobholz, A R Mayer, J R Binderx, and R W Cox. Specialized neural systems underlying representations of sequential movements. *J Cogn Neurosci*, 12(1):56–77, Jan 2000.

J V Haxby, M I Gobbini, M L Furey, A Ishai, J L Schouten, and P Pietrini. Distributed and overlapping representations of faces and objects in ventral temporal cortex. *Science*, 293(5539):2425–30, 2001.

J D Haynes and G Rees. Predicting the orientation of invisible stimuli from activity in human primary visual cortex. *Nat Neurosci*, 8(5):686–91, 2005a.

J D Haynes and G Rees. Predicting the stream of consciousness from activity in human visual cortex. *Curr Biol*, 15(14):1301–7, 2005b.

E Hazeltine, S T Grafton, and R Ivry. Attention and stimulus characteristics determine the locus of motor-sequence encoding. a pet study. *Brain*, 120 (Pt 1):123–40, 1997.

O Hikosaka, M K Rand, S Miyachi, and K Miyashita. Learning of sequential movements in the monkey: process of learning and retention of memory. *J Neurophysiol*, 74(4):1652–1661, Oct 1995.

O Hikosaka, K Sakai, S Miyauchi, R Takino, Y Sasaki, and B Pütz. Activation of human presupplementary motor area in learning of sequential procedures: a functional mri study. *J Neurophysiol*, 76(1):617–621, Jul 1996.

O Hikosaka, K Nakamura, K Sakai, and H Nakahara. Central mechanisms of motor skill learning. *Curr Opin Neurobiol*, 12(2):217–222, Apr 2002.

E Hulsmann, M Erb, and W Grodd. From will to action: sequential cerebellar contributions to voluntary movement. *Neuroimage*, 20(3):1485–92, 2003.

M Hund-Georgiadis and D Y von Cramon. Motor-learning-related changes in piano players and non-musicians revealed by functional magnetic-resonance signals. *Exp Brain Res*, 125(4):417–425, Apr 1999.

C Hutton, A Bork, O Josephs, R Deichmann, J Ashburner, and R Turner. Image distortion correction in fmri: A quantitative evaluation. *Neuroimage*, 16(1):217–240, May 2002.

C Iadecola, G Yang, T J Ebner, and G Chen. Local and propagated vascular responses evoked by focal synaptic activity in cerebellar cortex. *J Neurophysiol*, 78(2):651–9, 1997.

A Imfeld, M S Oechslin, M Meyer, T Loenneker, and L Jancke. White matter plasticity in the corticospinal tract of musicians: a diffusion tensor imaging study. *Neuroimage*, 46(3):600–607, Jul 2009.

I Indovina and J N Sanes. On somatotopic representation centers for finger movements in human primary motor cortex and supplementary motor area. *Neuroimage*, 13(6 Pt 1):1027–34, 2001.

J N Ingram, K P Körding, I S Howard, and D M Wolpert. The statistics of natural hand movements. *Exp Brain Res*, 188(2):223–236, Jun 2008.

I H Jenkins, D J Brooks, P D Nixon, R S Frackowiak, and R E Passingham. Motor sequence learning: a study with positron emission tomography. *The Journal of neuroscience : the official journal of the Society for Neuroscience*, 14(6):3775–90, 1994.

K O Johnson. The roles and functions of cutaneous mechanoreceptors. *Curr Opin Neurobiol*, 11(4):455–61, 2001.

J H Kaas, R J Nelson, M Sur, C S Lin, and M M Merzenich. Multiple representations of the body within the primary somatosensory cortex of primates. *Science*, 204(4392):521–3, 1979.

S Kakei, D S Hoffman, and P L Strick. Muscle and movement representations in the primary motor cortex. *Science*, 285(5436):2136–2139, Sep 1999.

S Kakei, D S Hoffman, and P L Strick. Sensorimotor transformations in cortical motor areas. *Neurosci Res*, 46(1):1–10, May 2003.

Y Kamitani and F Tong. Decoding the visual and subjective contents of the human brain. *Nat Neurosci*, 8(5):679–85, 2005.

Y Kamitani and F Tong. Decoding seen and attended motion directions from activity in the human visual cortex. *Curr Biol*, 16(11):1096–102, 2006.

A Karni, G Meyer, P Jezzard, M M Adams, R Turner, and L G Ungerleider. Functional mri evidence for adult motor cortex plasticity during motor skill learning. *Nature*, 377(6545):155–158, Sep 1995.

A Karni, G Meyer, C Rey-Hipolito, P Jezzard, M M Adams, R Turner, and L G Ungerleider. The acquisition of skilled motor performance: fast and slow experience-driven changes in primary motor cortex. *Proceedings of the National Academy of Sciences of the United States of America*, 95(3):861–8, 1998.

R Kawashima, K Yamada, S Kinomura, T Yamaguchi, H Matsui, S Yoshioka, and H Fukuda. Regional cerebral blood flow changes of cortical motor areas and prefrontal areas in humans related to ipsilateral and contralateral hand movement. *Brain Res*, 623(1):33–40, Sep 1993.

M Kawato, M Isobe, Y Maeda, and R Suzuki. Coordinates transformation and learning control for visually-guided voluntary movement with iteration: a newton-like method in a function space. *Biol Cybern*, 59(3):161–177, 1988.

K N Kay, S V David, R J Prenger, K A Hansen, and J L Gallant. Modeling low-frequency fluctuation and hemodynamic response timecourse in event-related fmri. *Hum Brain Mapp*, 29(2):142–56, 2008.

R M Kelly and P L Strick. Cerebellar loops with motor cortex and prefrontal cortex of a nonhuman primate. *J Neurosci*, 23(23):8432–44, 2003.

S W Kennerley, K Sakai, and M F Rushworth. Organization of action sequences and the role of the pre-sma. *J Neurophysiol*, 91(2):978–993, Feb 2004.

S G Kim, J Ashe, K Hendrich, J M Ellermann, H Merkle, K Uğurbil, and A P Georgopoulos. Functional magnetic resonance imaging of motor cortex: hemispheric asymmetry and handedness. *Science*, 261(5121):615–617, Jul 1993.

M Kobayashi, S Hutchinson, G Schlaug, and A Pascual-Leone. Ipsilateral motor cortex activation on functional magnetic resonance imaging during unilateral hand movements is related to interhemispheric interactions. *Neuroimage*, 20(4):2259–2270, Dec 2003.

I Koch and J Hoffmann. Patterns, chunks, and hierarchies in serial reaction-time tasks. *Psychol Res*, 63(1):22–35, 2000.

A J Kovacs, D W Han, and C H Shea. Representation of movement sequences is related to task characteristics. *Acta Psychol (Amst)*, 132(1):54–61, Sep 2009a.

A J Kovacs, T Mühlbauer, and C H Shea. The coding and effector transfer of movement sequences. *J Exp Psychol Hum Percept Perform*, 35(2):390–407, Apr 2009b.

N Kriegeskorte, R Goebel, and P Bandettini. Information-based functional brain mapping. *Proc Natl Acad Sci U S A*, 103(10):3863–8, 2006.

N Kriegeskorte, M Mur, and P Bandettini. Representational similarity analysis - connecting the branches of systems neuroscience. *Front Syst Neurosci*, 2: 4, 2008a.

N Kriegeskorte, M Mur, D A Ruff, R Kiani, J Bodurka, H Esteky, K Tanaka, and P A Bandettini. Matching categorical object representations in inferior temporal cortex of man and monkey. *Neuron*, 60(6):1126–41, 2008b.

N Kriegeskorte, W K Simmons, P S Bellgowan, and C I Baker. Circular analysis in systems neuroscience: the dangers of double dipping. *Nat Neurosci*, 12(5):535–540, May 2009.

Nikolaus Kriegeskorte, Elia Formisano, Bettina Sorger, and Rainer Goebel. Individual faces elicit distinct response patterns in human anterior temporal cortex. *Proceedings of the National Academy of Sciences*, 104(51): 20600–20605, 2007. ISSN 1091-6490.

Nan Laird, Nicolas Lange, and Daniel Stram. Maximum liklihood computations with repeated measures: application of the em algorithm. *Journal of the American Statistical Association*, 82(397):97–105, 1987.

S Lehericy, H Benali, P F Van de Moortele, M Pelegrini-Issac, T Waechter, K Ugurbil, and J Doyon. Distinct basal ganglia territories are engaged in early and advanced motor sequence learning. *Proc Natl Acad Sci U S A*, 102(35):12566–71, 2005.

A Li, F Z Yetkin, R Cox, and V M Haughton. Ipsilateral hemisphere activation during motor and sensory tasks. *AJNR Am J Neuroradiol*, 17(4):651–655, Apr 1996.

L Ma, B Wang, S Narayana, E Hazeltine, X Chen, D A Robin, P T Fox, and J Xiong. Changes in regional activity are accompanied with changes in inter-regional connectivity during 4 weeks motor learning. *Brain Res*, 1318: 64–76, Mar 2010.

Y Matsuzaka, N Picard, and P L Strick. Skill representation in the primary motor cortex after long-term practice. *J Neurophysiol*, 97(2):1819–1832, Feb 2007.

I Meister, T Krings, H Foltys, B Boroojerdi, M Müller, R Töpper, and A Thron. Effects of long-term practice and task complexity in musicians and nonmusicians performing simple and complex motor tasks: implications for cortical motor organization. *Hum Brain Mapp*, 25(3):345–352, Jul 2005.

M M Merzenich, R J Nelson, J H Kaas, M P Stryker, W M Jenkins, J M Zook, M S Cynader, and A Schoppmann. Variability in hand surface representations in areas 3b and 1 in adult owl and squirrel monkeys. *J Comp Neurol*, 258(2):281–96, 1987.

T Mima, N Sadato, S Yazawa, T Hanakawa, H Fukuyama, Y Yonekura, and H Shibasaki. Brain structures related to active and passive finger movements in man. *Brain*, 122 (Pt 10):1989–97, 1999.

Mark Mintun, Brian Lundstrom, Abraham Snyder, Andrei Vlassenko, Gordon Shulman, and Marcus Raichle. Blood flow and oxygen delivery to human brain during functional activity: Theoretical modeling and experimental data. *PNAS*, 98(12):6859–6864, 2001.

M Misaki, Y Kim, P A Bandettini, and N Kriegeskorte. Comparison of multivariate classifiers and response normalizations for pattern-information fmri. *Neuroimage*, 2010.

M Mur, P A Bandettini, and N Kriegeskorte. Revealing representational content with pattern-information fmri–an introductory guide. *Soc Cogn Affect Neurosci*, 4(1):101–9, 2009.

A J Nelson and R Chen. Digit somatotopy within cortical areas of the postcentral gyrus in humans. *Cereb Cortex*, 18(10):2341–51, 2008.

A J Nelson, D T Blake, and R Chen. Digit-specific aberrations in the primary somatosensory cortex in writer's cramp. *Ann Neurol*, 66(2):146–154, Aug 2009.

D F Nichols, L R Betts, and H R Wilson. Decoding of faces and face components in face-sensitive human visual cortex. *Front Psychol*, 1:28–28, 2010.

A C Nirkko, C Ozdoba, S M Redmond, M Bürki, G Schroth, C W Hess, and M Wiesendanger. Different ipsilateral representations for distal and proximal movements in the sensorimotor cortex: activation and deactivation patterns. *Neuroimage*, 13(5):825–835, May 2001.

K A Norman, S M Polyn, G J Detre, and J V Haxby. Beyond mind-reading: multi-voxel pattern analysis of fmri data. *Trends Cogn Sci*, 10(9):424–30, 2006.

N N Oosterhof, T Wiestler, P E Downing, and J Diedrichsen. A comparison of volume-based and surface-based multi-voxel pattern analysis. *Neuroimage*, 2010.

E S Pearson and H O Hartley. *Biometrika Tables for Statisticians*. Cambridge University Press, 1976.

V B Penhune and J Doyon. Dynamic cortical and subcortical networks in learning and delayed recall of timed motor sequences. *The Journal of neuroscience : the official journal of the Society for Neuroscience*, 22(4): 1397–406, 2002.

V B Penhune and J Doyon. Cerebellum and m1 interaction during early learning of timed motor sequences. *Neuroimage*, 26(3):801–12, 2005.

V B Penhune and C J Steele. Parallel contributions of cerebellar, striatal and m1 mechanisms to motor sequence learning. *Behav Brain Res*, 226(2): 579–591, Jan 2012.

F Pereira, T Mitchell, and M Botvinick. Machine learning classifiers and fmri: a tutorial overview. *Neuroimage*, 45(1 Suppl):S199–209, 2009.

M A Perez, S Tanaka, S P Wise, N Sadato, H C Tanabe, D T Willingham, and L G Cohen. Neural substrates of intermanual transfer of a newly acquired motor skill. *Curr Biol*, 17(21):1896–1902, Nov 2007a.

M A Perez, S P Wise, D T Willingham, and L G Cohen. Neurophysiological mechanisms involved in transfer of procedural knowledge. *J Neurosci*, 27 (5):1045–1053, Jan 2007b.

G Peyre. Toolbox fast marching - a toolbox for fast marching and level sets computations. 2008.

R A Poldrack. Imaging brain plasticity: conceptual and methodological issues–a theoretical review. *Neuroimage*, 12(1):1–13, Jul 2000.

R A Poldrack, F W Sabb, K Foerde, S M Tom, R F Asarnow, S Y Bookheimer, and B J Knowlton. The neural correlates of motor skill automaticity. *J Neurosci*, 25(22):5356–64, 2005.

K P Pruessmann, M Weiger, M B Scheidegger, and P Boesiger. Sense: sensitivity encoding for fast mri. *Magn Reson Med*, 42(5):952–62, 1999.

Rajeev R and N Kriegeskorte. Pattern-information fmri: New questions which it opens up and challenges which face it. *Int. J. Imaging Syst. Technol.*, 20: 31–41, 2010. ISSN 0899-9457.

J A Rathelot and P L Strick. Muscle representation in the macaque motor cortex: an anatomical perspective. *Proc Natl Acad Sci U S A*, 103(21): 8257–62, 2006.

J Reis, H M Schambra, L G Cohen, E R Buch, B Fritsch, E Zarahn, P A Celnik, and J W Krakauer. Noninvasive cortical stimulation enhances motor skill acquisition over multiple days through an effect on consolidation. *Proc Natl Acad Sci U S A*, 106(5):1590–1595, Feb 2009.

M Rijntjes, C Buechel, S Kiebel, and C Weiller. Multiple somatotopic representations in the human cerebellum. *Neuroreport*, 10(17):3653–8, 1999.

V Romei, G Thut, C Ramos-Estebanez, and A Pascual-Leone. M1 contributes to the intrinsic but not the extrinsic components of motor-skills. *Cortex*, 45 (9):1058–1064, Oct 2009.

K Sakai, O Hikosaka, S Miyauchi, R Takino, Y Sasaki, and B Pütz. Transition of brain activation from frontal to parietal areas in visuomotor sequence learning. *J Neurosci*, 18(5):1827–1840, Mar 1998.

K Sakai, O Hikosaka, S Miyauchi, Y Sasaki, N Fujimaki, and B Putz. Presupplementary motor area activation during sequence learning reflects visuo-motor association. *J Neurosci*, 19(10):RC1, 1999.

R M Sanchez-Panchuelo, S Francis, R Bowtell, and D Schluppeck. Mapping human somatosensory cortex in individual subjects with 7t functional mri. *J Neurophysiol*, 103(5):2544–56, 2010.

M H Schieber. Motor cortex and the distributed anatomy of finger movements. *Adv Exp Med Biol*, 508:411–6, 2002.

M H Schieber and L S Hibbard. How somatotopic is the motor cortex hand area? *Science*, 261(5120):489–92, 1993.

J E Schlerf, T D Verstynen, R B Ivry, and R M Spencer. Evidence of a novel somatopic map in the human neocerebellum during complex actions. *J Neurophysiol*, 103(6):3330–6, 2010.

D Schluppeck, C E Curtis, P W Glimcher, and D J Heeger. Sustained activity in topographic areas of human posterior parietal cortex during memory-guided saccades. *J Neurosci*, 26(19):5098–5108, May 2006.

C H Shea, A J Kovacs, and S Panzer. The coding and inter-manual transfer of movement sequences. *Front Psychol*, 2:52–52, 2011.

K Shima and J Tanji. Both supplementary and presupplementary motor areas are crucial for the temporal organization of multiple movements. *J Neurophysiol*, 80(6):3247–3260, Dec 1998.

L N Singh, S Higano, S Takahashi, N Kurihara, S Furuta, H Tamura, Y Shimanuki, S Mugikura, T Fujii, A Yamadori, M Sakamoto, and S Yamada. Comparison of ipsilateral activation between right and left handers: a functional mr imaging study. *Neuroreport*, 9(8):1861–1866, Jun 1998.

M A Smith and R Shadmehr. Intact ability to learn internal models of arm dynamics in huntington's disease but not cerebellar degeneration. *J Neurophysiol*, 93(5):2809–21, 2005.

J F Soechting and M Flanders. Moving in three-dimensional space: frames of reference, vectors, and coordinate systems. *Annu Rev Neurosci*, 15:167–191, 1992.

C J Steele and V B Penhune. Specific increases within global decreases: a functional magnetic resonance imaging investigation of five days of motor sequence learning. *J Neurosci*, 30(24):8332–8341, Jun 2010.

P L Strick. Anatomical organization of multiple motor areas in the frontal lobe: implications for recovery of function. *Adv Neurol*, 47:293–312, 1988.

M Sur, R J Nelson, and J H Kaas. Representations of the body surface in cortical areas 3b and 1 of squirrel monkeys: comparisons with other primates. *J Comp Neurol*, 211(2):177–92, 1982.

J D Swisher, J C Gatenby, J C Gore, B A Wolfe, C H Moon, S G Kim, and F Tong. Multiscale pattern analysis of orientation-selective activity in the primary visual cortex. *J Neurosci*, 30(1):325–30, 2010.

J Tanji and K Shima. Role for supplementary motor area cells in planning several movements ahead. *Nature*, 371(6496):413–416, Sep 1994.

L W Tempel and J S Perlmutter. Vibration-induced regional cerebral blood flow responses in normal aging. *J Cereb Blood Flow Metab*, 12(4):554–61, 1992.

G W Thickbroom, M L Byrnes, and F L Mastaglia. Dual representation of the hand in the cerebellum: activation with voluntary and passive finger movement. *Neuroimage*, 18(3):670–4, 2003.

I Toni, M Krams, R Turner, and R E Passingham. The time course of changes during motor sequence learning: a whole-brain fmri study. *Neuroimage*, 8 (1):50–61, 1998.

L G Ungerleider, J Doyon, and A Karni. Imaging brain plasticity during motor skill learning. *Neurobiol Learn Mem*, 78(3):553–64, 2002.

D C Van Essen and D L Dierker. Surface-based and probabilistic atlases of primate cerebral cortex. *Neuron*, 56(2):209–225, Oct 2007.

D C Van Essen and H A Drury. Structural and functional analyses of human cerebral cortex using a surface-based atlas. *J Neurosci*, 17(18):7079–7102, Sep 1997.

D C Van Essen, J W Lewis, H A Drury, N Hadjikhani, R B Tootell, M Bakircioglu, and M I Miller. Mapping visual cortex in monkeys and humans using surface-based atlases. *Vision Res*, 41(10-11):1359–1378, 2001.

T Verstynen, J Diedrichsen, N Albert, P Aparicio, and R B Ivry. Ipsilateral motor cortex activity during unimanual hand movements relates to task complexity. *J Neurophysiol*, 93(3):1209–22, 2005.

N S Ward. The neural substrates of motor recovery after focal damage to the central nervous system. *Arch Phys Med Rehabil*, 87(12 Suppl 2):30–35, Dec 2006.

N S Ward, M M Brown, A J Thompson, and R S Frackowiak. Neural correlates of outcome after stroke: a cross-sectional fmri study. *Brain*, 126(Pt 6): 1430–1448, Jun 2003a.

N S Ward, M M Brown, A J Thompson, and R S Frackowiak. Neural correlates of motor recovery after stroke: a longitudinal fmri study. *Brain*, 126(Pt 11): 2476–2496, Nov 2003b.

S Waters-Metenier, M Husain, T Wiestler, and J Diedrichsen. Bihemispheric transcranial direct current stimulation enhances skill learning and transfer to the untrained hand. *Neural Control of Movement, 22nd annual meeting, Venice*, 2012.

C Weiller, F Chollet, K J Friston, R J Wise, and R S Frackowiak. Functional reorganization of the brain in recovery from striatocapsular infarction in man. *Ann Neurol*, 31(5):463–472, May 1992.

C Weiller, S C Ramsay, R J Wise, K J Friston, and R S Frackowiak. Individual patterns of functional reorganization in the human cerebral cortex after capsular infarction. *Ann Neurol*, 33(2):181–189, Feb 1993.

D M Wolpert, R C Miall, and M Kawato. Internal models in the cerebellum. *Trends in Cognitive Science*, 2(9):313–321, 1998.

C N Woolsey, T C Erickson, and W E Gilson. Localization in somatic sensory and motor areas of human cerebral cortex as determined by direct recording of evoked potentials and electrical stimulation. *J Neurosurg*, 51(4):476–506, 1979.

K J Worsley, S Marrett, P Neelin, A C Vandal, K J Friston, and A C Evans. A unified statistical approach for determining significant voxels in images of cerebral activation. *Human Brain Mapping*, 12:900–918, 1996.

T Wu, K Kansaku, and M Hallett. How self-initiated memorized movements become automatic: a functional mri study. *J Neurophysiol*, 91(4):1690–1698, Apr 2004.

J Xiong, L Ma, B Wang, S Narayana, E P Duff, G F Egan, and P T Fox. Long-term motor training induced changes in regional cerebral blood flow in both task and resting states. *Neuroimage*, 45(1):75–82, Mar 2009.

T A Yousry, U D Schmid, H Alkadhi, D Schmidt, A Peraud, A Buettner, and P Winkler. Localization of the motor hand area to a knob on the precentral gyrus. a new landmark. *Brain*, 120 (Pt 1):141–57, 1997.

Y Zhang, C Forster, T A Milner, and C Iadecola. Attenuation of activity-induced increases in cerebellar blood flow by lesion of the inferior olive. *Am J Physiol Heart Circ Physiol*, 285(3):H1177–82, 2003.

E Zoons, J Booij, A J Nederveen, J M Dijk, and M A Tijssen. Structural, functional and molecular imaging of the brain in primary focal dystonia–a review. *Neuroimage*, 56(3):1011–1020, Jun 2011.